

Mining Science and Technology

Горные науки
и технологии

Vol. 9 №1
2024



<https://mst.misis.ru/>

<https://t.me/MinSciTech>



Activities of the *Mining Science and Technology (Russia) (Gornye nauki i tekhnologii)* international journal are aimed at developing international scientific and professional cooperation in the field of mining.

The journal target audience comprises researchers, specialists in the field of mining, representatives of academic and professional communities.

The journal publishes original papers describing research findings, experience in the implementation of projects in mining industry, review publications.

The journal seeks to develop interdisciplinary areas that contribute to progress in mining, for example, technological and environmental safety, project organization and management in mining industry, development of territories, legal aspects of natural resource use, and other areas studied by researchers and practitioners. The journal always welcomes new developments. Papers are accepted in English or Russian.

EDITOR-IN-CHIEF

Vadim L. Petrov, Prof., Dr.Sci.(Eng.), University of Science and Technology MISIS, Moscow, Russian Federation

DEPUTIES EDITOR-IN-CHIEF

Oleg I. Kazanin, Prof., Dr.Sci.(Eng.), Saint Petersburg Mining University, St. Petersburg, Russian Federation

Svetlana A. Epshtein, Dr.Sci.(Eng.), University of Science and Technology MISIS, Moscow, Russian Federation

EDITORIAL BOARD

Zach Agioutantis, Prof., Ph.D., University of Kentucky, Lexington, Kentucky, USA

Maksim A. Bogdasarou, Prof., Dr.Sci.(Geol. and Min.), Brest State A. S. Pushkin University, Brest, Belarus

Grigory Yu. Boyarko, Prof. Dr. Sci. (Econ.), Cand. Sci. (Geol. and Miner.), National Research Tomsk Polytechnic University, Tomsk, Russian Federation

Xuan Nam Bui, Prof., Dr.Sci., Hanoi University of Mining and Geology, Duc Thang – Bac Tu Liem, Hanoi, Vietnam

Carsten Drenstedt, Prof., Ph.D., Freiberg University of Mining and Technology, Freiberg, Germany

Faramarz Doulati Ardejani, Prof., Ph.D., Colledge of Engineering, University of Tehran, Tehran, Iran

Mikhail S. Ershov, Prof., Dr.Sci.(Eng.), National University of Oil and Gas “Gubkin University”, Moscow, Russian Federation

Akper A. Feyzullaev, Prof., Dr.Sci.(Geol. and Min.), Institute of Geology and Geophysics of the National Academy of Sciences of Azerbaijan, Baku, Azerbaijan

Ochir Gerel, Prof., Dr.Sci.(Geol. and Min.), Geoscience Center, the Mongolian University of Science and Technology, Ulaanbaatar, Mongolia

Zoran Gligorić, Prof., Dr.Sci. (Mining-Underground Mining), University of Belgrade, Belgrade, Republic of Serbia

Monika Hardygora, Prof., Ph.D., Wroclaw University of Technology, Wroclaw, Poland

Nikolae Ilias, Prof., Dr.Sci.(Eng.), University of Petrosani, Petrosani, Romania

Vladislav Kecojevic, Prof., Ph.D., Benjamin M. Statler College of Engineering and Mineral Resources, West Virginia University, Morgantown, West Virginia, USA

Aleksey A. Khoreshok, Prof., Dr.Sci.(Eng.), Gorbachev Kuzbass State Technical University, Kemerovo, Russian Federation

Vladimir I. Klishin, Prof., Dr.Sci.(Eng.), Institute of Coal, Siberian Branch, Russian Academy of Sciences, Kemerovo, Russian Federation

Vladimir N. Koshelev, Prof., Dr.Sci.(Chem.), National University of Oil and Gas “Gubkin University” (Gubkin University), Moscow, Russian Federation

Jyant Kumar, Prof., Ph.D-Geotech.Eng., Indian Institute of Science, Bengaluru, India

Vladimir A. Makarov, Prof., Dr.Sci.(Geol. and Min.), Siberian Federal University, Krasnoyarsk, Russian Federation

Sergey I. Malafeev, Prof., Dr.Sci.(Eng.), Vladimir State University named after Alexander and Nikolay Stoletovs, Vladimir, Russia

Oleg S. Misnikov, Prof., Dr.Sci.(Eng.), Tver State Technical University, Tver, Russian Federation

Valery V. Morozov, Prof., Dr.Sci.(Eng.), University of Science and Technology MISIS, Moscow, Russian Federation

Igor M. Petrov, Dr.Sci.(Eng.), Infomine Research Group LLC, Moscow, Russian Federation

Bakhadirzhan R. Raimzhanov, Prof., Dr.Sci.(Eng.), University of Science and Technology MISIS (branch), Almalyk, Uzbekistan

Bayan R. Rakishev, Prof., Dr.Sci.(Eng.), Kazakh National Research Technical University named after K.I. Satpayev, Alma-Ata, Kazakhstan

Oscar Jaime Restrepo Baena, Prof., Ph.D., National University of Colombia, Medellín, Colombia

Alexander N. Shashenko, Prof., Dr.Sci.(Eng.), National Mining University, Dnipro, Ukraine

Vadim P. Tarasov, Prof., Dr.Sci.(Eng.), University of Science and Technology MISIS, Moscow, Russian Federation

Denis P. Tibilov, Prof., Dr.Sci.(Econ.), Moscow State Institute of International Affairs (University) under the Ministry of Foreign Affairs of Russia, Moscow, Russian Federation

Niyaz G. Valiev, Prof., Dr.Sci.(Eng.), The Ural State Mining University, Ekaterinburg, Russian Federation

Natalia Zhuravleva, Prof., Dr.Sci.(Eng.), West Siberian Testing Center JSC (WSTCenter JSC), Novokuznetsk, Russian Federation

Vera V. Yurak, Assoc. Prof., Dr. Sci. (Econ.), Ural State Mining University, Yekaterinburg; Institute of Economics, Ural Branch of the Russian Academy of Sciences, Yekaterinburg, Russian Federation

EDITORIAL COUNCIL

Yuri G. Agafonov, Assoc. Prof., Cand.Sci.(Eng.), University of Science and Technology MISIS, Moscow, Russian Federation

Michael R. Filonov, Prof., Dr.Sci.(Eng.), University of Science and Technology MISIS, Moscow, Russian Federation

Leonid A. Plaschansky, Prof., Cand.Sci.(Eng.), University of Science and Technology MISIS, Moscow, Russian Federation

Yuri I. Razorenov, Prof., Dr.Sci.(Eng.), Platov South-Russian State Polytechnic University, Novocherkassk, Russian Federation

EXECUTIVE SECRETARY

Daria P. Galushka, University of Science and Technology MISIS, Moscow, Russian Federation

QUARTERLY

FOUNDED in 2016

REGISTRATION

The journal science and applied research journal is registered by the Federal Service for Communication, IT and Mass Communication Control on August 10, 2015. Registration Certificate E-No. ФС77-62652

INDEXATION

Scopus, CAS, EBSCO, DOAJ, РИНЦ, ВИНТИ РАН, Dimensions, BASE, J-Gate, Jisc Library Hub Discover.

FOUNDER AND PUBLISHER



UNIVERSITY MISIS
University of Science and Technology
MISIS

CONTACT

4 Leninsky Prospect, Moscow 119049, Russian Federation

Phone: +7 (495) 955-00-77

e-mail: send@misis.ru



This work is licensed under a
[Creative Commons Attribution 4.0 License](https://creativecommons.org/licenses/by/4.0/).



Деятельность научно-практического журнала «Горные науки и технологии» (Mining Science and Technology (Russia)) направлена на развитие международного научного и профессионального сотрудничества в области горного дела.

Целевая аудитория журнала – исследователи, специалисты в области горного дела, представители академического и профессионального сообществ.

В журнале публикуются оригинальные статьи, описывающие результаты исследований, опыт реализации проектов в горнопромышленном комплексе, обзорные публикации.

Журнал стремится развивать такие междисциплинарные направления, как технологическая и экологическая безопасность, организация и управление проектами в горной промышленности, развитие территорий, правовые аспекты использования природных ресурсов и другие, которые способствуют прогрессу в горном деле и реализуются исследователями и практиками.

ГЛАВНЫЙ РЕДАКТОР

Петров Вадим Леонидович, проф., д.т.н., Университет науки и технологий МИСИС, г. Москва, Российская Федерация

ЗАМЕСТИТЕЛИ ГЛАВНОГО РЕДАКТОРА

Казанин Олег Иванович, проф., д.т.н., Санкт-Петербургский горный университет, г. Санкт-Петербург, Российская Федерация

Эпштейн Светлана Абрамовна, д.т.н., Университет науки и технологий МИСИС, г. Москва, Российская Федерация

РЕДАКЦИОННАЯ КОЛЛЕГИЯ

Агиутантис Зак, проф., д-р наук, Университет Кентукки, г. Лексингтон, Кентукки, США

Богдасаров Максим Альбертович, проф., д.г.-м.н., Брестский государственный университет им. А.С. Пушкина, г. Брест, Беларусь

Боярко Григорий Юрьевич – проф., д.э.н., к.г.-м.н., Национальный исследовательский Томский политехнический университет, г. Томск, Российская Федерация

Буи Суан Нам, проф., д-р наук, Ханойский университет горного дела и технологии, г. Ханой, Вьетнам

Валиев Нияз Гадым оглы, проф., д.т.н., Уральский государственный горный университет, г. Екатеринбург, Российская Федерация

Герел Очир, проф., д.г.-м.н., Центр геолого-геофизических исследований, Монгольский университет науки и технологии, г. Улан-Батор, Монголия

Глигорич Зоран, проф., д-р наук, Белградский университет, г. Белград, Республика Сербия

Дребенштедт Карстен, проф., д-р наук, Технический университет Фрайбургская горная академия, г. Фрайберг, Германия

Дулати Ардежани Фарамарз, проф., д-р наук, Инженерный колледж, Тегеранский университет, г. Тегеран, Иран

Ершов Михаил Сергеевич, проф., д.т.н., Российский государственный университет нефти и газа (национальный исследовательский университет) им. И.М. Губкина, г. Москва, Российская Федерация

Журавлева Наталья Викторовна, проф., д.т.н., АО «Западно-Сибирский испытательный центр» (АО «ЗСИЦентр»), г. Новокузнецк, Российская Федерация

Илиаш Николае, проф., д.т.н., Университет Петрошани, г. Петрошани, Румыния

Кецоджевич Владислав, проф., д-р наук, Институт инженерного дела и минеральных ресурсов им. Бенджамина М. Статлера Университета Западной Вирджинии, г. Моргантаун, Западная Вирджиния, США

Клишин Владимир Иванович, проф., д.т.н., Институт угля Сибирского отделения Российской академии наук, г. Кемерово, Российская Федерация

Кошелев Владимир Николаевич, проф., д.х.н., Российский государственный университет нефти и газа им. И.М. Губкина, г. Москва, Российская Федерация

Кумар Джьянт, проф., д-р наук (геотехнический инжиниринг), Индийский институт науки (Indian Institute of Science), г. Бангалор, Индия

Макаров Владимир Александрович, проф., д.г.-м.н., Сибирский федеральный университет, г. Красноярск, Российская Федерация

Малафеев Сергей Иванович, проф., д.т.н., Владимирский государственный университет имени А.Г. и Н.Г. Столетовых, г. Владимир, Российская Федерация

Мисников Олег Степанович, проф., д.т.н., Тверской государственный технический университет, г. Тверь, Российская Федерация

Морозов Валерий Валентинович, проф., д.т.н., Университет науки и технологий МИСИС, г. Москва, Российская Федерация

Петров Игорь Михайлович, д.т.н., ООО «Исследовательская группа «Инфолайн»», г. Москва, Российская Федерация

Раимжанов Бахадиржан Раимжанович, проф., д.т.н., филиал Университета науки и технологий МИСИС, г. Алмалык, Узбекистан

Ракишев Баян Ракишевич, проф., д.т.н., Казахский национальный исследовательский технический университет им. К.И. Сатпаева, г. Алма-Ата, Казахстан

Рестрепо Баэна Оскар Хайме, проф., д-р наук, Национальный университет Колумбии, г. Медельин, Колумбия

Тарасов Вадим Петрович, проф., д.т.н., НИТУ «МИСиС», г. Москва, Российская Федерация

Тибилов Денис Петрович, проф., д.э.н., Московский государственный институт международных отношений (Университет) Министерства иностранных дел России, г. Москва, Российская Федерация

Фейзуллаев Акпер Акпер оглы, проф., д.г.-м.н., Институт геологии и геофизики (ИГГ) Национальной Академии Наук Азербайджана, г. Баку, Азербайджан

Хорешок Алексей Алексеевич, проф., д.т.н., Кузбасский государственный технический университет им. М.С. Горбачева, г. Кемерово, Российская Федерация

Шашенко Александр Николаевич, проф., д.т.н., Национальный горный университет, г. Днепр, Украина

Хардигора Моника, проф., д-р наук, Вроцлавский технологический университет, г. Вроцлав, Польша

Юрак Вера Васильевна, доц., д.э.н., Уральский государственный горный университет, г. Екатеринбург; старший научный сотрудник, Институт экономики Уральского отделения Российской академии наук (ИЭ УрО РАН), г. Екатеринбург, Российская Федерация

РЕДАКЦИОННЫЙ СОВЕТ

Агафонов Юрий Григорьевич, доц., к.т.н., Университет науки и технологий МИСИС, г. Москва, Российская Федерация

Плащанский Леонид Александрович, проф., к.т.н., Университет науки и технологий МИСИС, г. Москва, Российская Федерация

Разоренов Юрий Иванович, проф., д.т.н., Южно-Российский государственный политехнический университет (НПИ) им. М.И. Платова, г. Новочеркасск, Российская Федерация

Филонов Михаил Рудольфович, проф., д.т.н., Университет науки и технологий МИСИС, г. Москва, Российская Федерация

ОТВЕТСТВЕННЫЙ СЕКРЕТАРЬ

Галушка Дарья Петровна, Университет науки и технологий МИСИС, г. Москва, Российская Федерация

ПЕРИОДИЧНОСТЬ 4 раза в год

ОСНОВАН в 2016 году

РЕГИСТРАЦИЯ

Зарегистрирован Федеральной службой по надзору в сфере связи, информационных технологий и массовых коммуникаций 10 августа 2015 года.

Свидетельство о регистрации Эл № ФС77-62652.

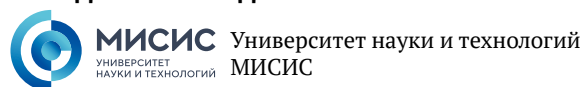
ИНДЕКСИРОВАНИЕ

Scopus, CAS, EBSCO, DOAJ, РИНЦ, ВИНТИ РАН, Dimensions, BASE, J-Gate, Jisc Library Hub Discover.



Журнал открытого доступа.

УЧРЕДИТЕЛЬ И ИЗДАТЕЛЬ



АДРЕС УЧРЕДИТЕЛЯ И ИЗДАТЕЛЯ

119049, г. Москва, Ленинский проспект, д. 4

КОНТАКТЫ РЕДАКЦИИ

Адрес: 119049, г. Москва, Ленинский проспект, д. 4

Телефон: +7 (495) 955-00-77

e-mail: send@misis.ru



Контент доступен под лицензией
Creative Commons Attribution 4.0 License.



CONTENTS

BENEFICIATION AND PROCESSING OF NATURAL AND TECHNOGENIC RAW MATERIALS

Investigation of old waste dump composition of lean gold-bearing ores
from the Golden Pride Project (GPP) mining operation in Nzega district, Tanzania 5
J. Shirima, A. Wikedzi, A. V. Rasskazova

Assessing viability of processing ash and slag dumps for energy-efficient ash beneficiation
at Magadan CPP 12
L. V. Shipunov, M. A. Kuzmenkov, N. K. Gaidai

Electrochemical action on the flotation beneficiation of ordinary iron ore concentrate 21
Kh. K. Rakhimov, E. L. Chanturiya, D. V. Shekhirev

Characterization and thermal behavior of some types of kaolin of different origin
from Northern Vietnam 30
T. T. T. Nguyen, H. B. Bui

SAFETY IN MINING AND PROCESSING INDUSTRY AND ENVIRONMENTAL PROTECTION

Experimental study on forced ventilation in dead-end mine working with various setbacks
of the ventilation pipeline from the working face 41
A. A. Kamenskikh, G. Z. Faynburg, M. A. Semin, A. V. Tatsiy

Determining airflow requirements in mine workings based on field measurements
of actual emissions from internal combustion engine equipment 53
V. A. Senatorov

POWER ENGINEERING, AUTOMATION, AND ENERGY PERFORMANCE

Assessing the efficiency of measures to enhance electric power quality
in variable-frequency drive for scraper conveyors 60
V. L. Petrov, A. V. Pichuev



СОДЕРЖАНИЕ

ОБОГАЩЕНИЕ, ПЕРЕРАБОТКА МИНЕРАЛЬНОГО И ТЕХНОГЕННОГО СЫРЬЯ

Исследование лежалых отвалов бедной золотосодержащей руды
горнодобывающего предприятия Golden Pride Project (GPP) в районе Нзегга, Танзания 5
Дж. Ширима, А. Викедзи, А.В. Рассказова

Оценка целесообразности переработки золошлаковых отвалов
Магаданской теплоэлектростанции 12
Л.В. Шипунов, М.А. Кузьменков, Н.К. Гайдай

Использование электрохимических воздействий в процессе флотационного дообогащения
рядового железорудного концентрата 21
Х.К. Рахимов, Е.Л. Чантурия, Д.В. Шехирев

Характеристика и термическое поведение некоторых видов каолина
различного происхождения из Северного Вьетнама 30
Т.Т.Т. Нгуен, Х.Б. Буи

ТЕХНОЛОГИЧЕСКАЯ БЕЗОПАСНОСТЬ В МИНЕРАЛЬНО-СЫРЬЕВОМ КОМПЛЕКСЕ И ОХРАНА ОКРУЖАЮЩЕЙ СРЕДЫ

Экспериментальные исследования проветривания тупиковой выработки
нагнетательным способом при различном отставании вентиляционного трубопровода
от груди забоя 41
А.А. Каменских, Г.З. Файнбург, М.А. Семин, А.В. Тацкий

Определение расхода воздуха в горных выработках на основе натуральных измерений
фактической газовойности оборудования с двигателями внутреннего сгорания 53
В.А. Сенаторов

ЭНЕРГЕТИКА, АВТОМАТИЗАЦИЯ И ЭНЕРГОЭФФЕКТИВНОСТЬ

Оценка эффективности средств повышения качества электроэнергии
в системе частотно-регулируемого электропривода скребковых конвейеров 60
В.Л. Петров, А.В. Пичуев



BENEFICIATION AND PROCESSING OF NATURAL AND TECHNOGENIC RAW MATERIALS

Research paper

<https://doi.org/10.17073/2500-0632-2023-07-130>

UDC 622.7.1

**Investigation of old waste dump composition of lean gold-bearing ores from the Golden Pride Project (GPP) mining operation in Nzega district, Tanzania**J. Shirima¹ , A. Wikedzi¹  , A. V. Rasskazova²   ¹ University of Dar es Salaam, Dar es Salaam Region, Tanzania² Mining Institute, Separate Division of Khabarovsk Federal research center of the Far Eastern branch, Russian Academy of Sciences, Khabarovsk, Russian Federation annbot87@mail.ru**Abstract**

The search for alternative sources of useful minerals is a pressing issue. One such possible source is the processing of lean gold-bearing ores, which previously did not seem feasible to exploit for subsoil users, leading to their disposal in off-balance ore dumps. Processing these resources becomes economically viable as gold prices rise and processing technologies improve over time. This paper presents the elemental and mineralogical composition of lean gold-bearing ore dumps from the Golden Pride Project (GPP) mining operation in Tanzania's Lihendo district. This area contains an old dump of lean gold-bearing ores, weighing approximately 1.4 million tons. Extracting valuable components from lean mineral raw materials is a current priority. Sampling was conducted to study the dumps. Boreholes were drilled to a depth of 1 m, covering a total sampling area of 20 ha; 18 samples, each averaging 3 kg in weight, were collected. The results of X-ray fluorescence analysis (XRF) indicated the presence of Fe, S, Si, Ca, Mn, Cu, Al, Cr, Ti, As, and Ag in the collected samples. X-ray diffraction (XRD) analysis revealed that the main minerals in the dumps are muscovite, kaolinite, quartz, montmorillonite, and goethite. The average gold grade in the selected samples is 0.72 g/t. Studies of the grain-size distribution and gold distribution by grain-size classes after ore grinding demonstrated that the majority of gold (74%) is in the -75 µm class. In the initial mineral material of the dumps, the share of the +30-50 mm grain-size class is 81%. The paper proposes potential methods for processing lean dumps of gold-bearing ores. One such method involves crushing the dump material, separating the -75 µm class, and subjecting it to direct leaching or leaching using "carbon-in-pulp" technique. Heap leaching appears to be the most promising method for extracting gold from such dumps in terms of technical and economic feasibility. Positive experience has been reported in applying this process to ores of similar mineralogical type.

Keywords

Golden Pride Project (GPP), X-ray phase analysis, X-ray fluorescence analysis, lean gold-bearing ore, ore characterization, processing methods

For citationShirima J., Wikedzi A., Rasskazova A.V. Investigation of old waste dump composition of lean gold-bearing ores from the Golden Pride Project (GPP) mining operation in Nzega district, Tanzania. *Mining Science and Technology (Russia)*. 2024;9(1):5–11. <https://doi.org/10.17073/2500-0632-2023-07-130>

ОБОГАЩЕНИЕ, ПЕРЕРАБОТКА МИНЕРАЛЬНОГО И ТЕХНОГЕННОГО СЫРЬЯ

Научная статья

Исследование лежалых отвалов бедной золотосодержащей руды горнодобывающего предприятия Golden Pride Project (GPP) в районе Нзегга, ТанзанияДж. Шири́ма¹ , А. Вики́дзи¹  , А. В. Рассказова²   ¹ Университет Дар-эс-Салама, регион Дар-эс-Салам, Танзания² Институт горного дела, обособленное подразделение Хабаровского федерального исследовательского центра Дальневосточного отделения Российской академии наук, г. Хабаровск, Российская Федерация annbot87@mail.ru**Аннотация**

Поиск альтернативных источников полезных минералов является достаточно актуальной проблемой. Одним из таких возможных источников является переработка бедных золотосодержащих руд, переработка которых ранее не представлялась привлекательной для недропользователей, вследствие чего



из них формировались отвалы забалансовой руды. Переработка этих ресурсов становится востребованной на фоне роста цен и уровня технологий с течением времени. В данной статье представлен элементный и минералогический состав бедных золотосодержащих отвалов горного предприятия Golden Pride Project (GPP) в Танзании, в районе «Лихендо». В данном районе находится старый отвал бедной золотосодержащей руды (масса составляет примерно 1,4 млн т). Извлечение ценных компонентов из бедного минерального сырья является актуальным направлением в настоящее время. Для опробования отвалов был произведен отбор проб. Глубина бурения скважин составила 1 м, общая площадь опробования – 20 га; было отобрано 18 проб средней массой 3 кг. Результаты рентгенофлуоресцентного анализа (РФА/XRF) показали, что в отобранных пробах присутствуют такие элементы, как Fe, S, Si, Ca, Mn, Cu, Al, Cr, Ti, As, Ag. Результаты рентгенофазового анализа (XRD) показали, что основными минералами в отвалах являются мусковит, каолинит, кварц, монтмориллонит и гетит. Среднее содержание золота в отобранных пробах составляет 0,72 г/т. Исследования гранулометрического состава и распределения золота по классам крупности после измельчения руды показали, что большая часть золота (74 %) находится в классе –75 мкм. В исходной минеральной массе отвалов доля класса крупности +30–50 мм составляет 81 %. В статье предложены возможные методы переработки бедных отвалов золотосодержащих руд. Одним из возможных методов переработки отвалов является измельчение минерального сырья, отделение класса –75 мкм и его прямое выщелачивание либо выщелачивание по технологии «уголь в пульпе». Наиболее перспективным с точки зрения технико-экономических показателей представляется метод кучного выщелачивания. Имеется положительный опыт применения данной технологии в отношении руд аналогичного минерального типа.

Ключевые слова

Golden Pride Project (GPP), рентгенофазовый анализ, рентгенофлуоресцентный анализ, бедная золотосодержащая руда, характеристика руды, методы переработки

Для цитирования

Shirima J., Wikedzi A., Rasskazova A.V. Investigation of old waste dump composition of lean gold-bearing ores from the Golden Pride Project (GPP) mining operation in Nzega district, Tanzania. *Mining Science and Technology (Russia)*. 2024;9(1):5–11. <https://doi.org/10.17073/2500-0632-2023-07-130>

Introduction

In today's world, the industrial revolution has led to an increased demand for minerals such as gold, cobalt, nickel, rare earth elements, and platinum group elements like rhodium, osmium, palladium, ruthenium, and iridium [1, 2]. However, primary reserves of these minerals worldwide are limited. The search for alternative sources of minerals is a pertinent issue [3]. One such potential source is the processing of lean gold-bearing ores, which were previously deemed unprofitable by subsoil users and consequently sent to off-balance ore dumps. The relevance of processing these resources becomes more pronounced as gold prices rise and processing technologies improve over time. Currently, the costs of processing lean ores are justified [1]. It is imperative to employ methods for assessing the cut-off grade of valuable components and the economic feasibility of projects to make informed operational and economic decisions [4].

The extraction of gold from lean mineral raw materials is relevant in many regions worldwide, driven by a decline in the gold grade of currently extracted ores due to the preferential extraction of richer and more easily processable ores [5]. Examples include the Ridgway mine in the United States, as well as Simmergo, Ergo, and Crown Sand in South Africa [6].

Despite the utilization of low-grade ore in processing at various plants globally, each deposit pre-

sents its unique challenges necessitating specific feasibility studies [7]. Key to such studies is understanding the properties of the ore itself, as they dictate the selection of a processing method, thereby directly influencing the economics of mineral mining, such as gold [8, 9].

This paper aims to investigate elemental and mineralogical composition and grain-size distribution of the lean gold-bearing ore dumps from the Golden Pride Project (GPP). Additionally, recommendations on possible methods of processing lean mineral raw materials from the dumps are provided.

The Golden Pride Project (GPP) was a gold mining project in the Nzega district of Tanzania, 25 km from the town of Nzega. The open pit operated from 1998 until its closure in 2013¹, extracting 2.589 million tons of ore and produced 169 thousand ounces of gold. The deposit reserves are estimated at 5.79 million tons of ore (2.04 million tons in category A and 3.75 million tons in category B, with an average grade of 2 g/t). The deposit was developed using an open-pit method, with the primary method of gold extraction being sorption leaching via activated carbon (carbon-in-pulp (CIP) process).

¹ Report of the Presidential Mining Review Committee to Advise the Government on Oversight of the Mining Sector. 2008. URL: https://www.policyforum-tz.org/sites/default/files/BomaniReport-English_0.pdf [Accessed: January 2023].

The ore district comprises layers of basic volcanites, volcanoclastic rocks, banded ferruginous formations, and intrusive porphyries intruded by late granites. The complex structure includes thick north-striking structures emphasized by late dolerite dykes and thinner structures of northwestern and northeastern strike. Exploration identified two main types of mineralization: gold-quartz vein mineralization with high gold grade and extensive carbonate-siliceous alteration and pyrite veinlets, and extensive low-grade impregnated gold mineralization located in the northeastern Kanegele shear system.

The Golden Pride Project (GPP) ores belong to the latter type of mineralization.

Throughout the mine's operational life, the cut-off grade was approximately 2 g/t gold². Materials with a gold grade below this threshold were either stockpiled for blending or transported to the waste rock dump, as their processing was deemed unprofitable [10–12]. However, with rising gold prices and advancements in processing techniques, this material may become expedient for processing. Of particular interest are the dumps in Lihendo County, where an earlier estimation indicated approximately 1.4 million tons of gold-bearing ore at a grade of 1.37 g/t gold, necessitating further evaluation of the ore processing potential.

² Developing the golden opportunity, GPP Annual Report. 2004. URL: https://www.annualreports.com/HostedData/AnnualReportArchive/R/ASX_RSG_2004.pdf [Accessed: January 2023].

Materials and Methods

1. Materials

At the first stage of sampling preparation, the whole Lihendo district in Tanzania (130 ha) was subdivided using Expert GPS Pro version 7. Samples were then collected at the intersections of the vertical and horizontal grid lines within an area of 20 ha (inside the area circled by the line in Figure 1 using a Germin GPS, Montana 680t navigator).

A total of 18 samples were procured from boreholes drilled to a depth of 1 m, amounting to approximately 54 kg of samples (Table 1). The coordinates of the sampling points (longitude and latitude in Arc1960 format) are provided in Table 1.

2. Techniques

2.1. Sample Preparation

Initially, the samples underwent drying in a desiccator at 105 °C for 1 h to eliminate moisture. Three samples were combined into a single metallurgical sample, ground to a fineness of $-2\ \mu\text{m}$, and then divided into 6 samples using a rotary splitter (Sepor 040J-001 24), each weighing approximately 9 kg each. The rotary splitter operated at a rotation speed of 0.5 rps. From each of the these 9-kg samples, a 0.5-kg subsample was extracted for X-ray diffraction analysis. Additionally, 1-kilogram samples were set aside for X-ray diffraction and X-ray fluorescence analyses.

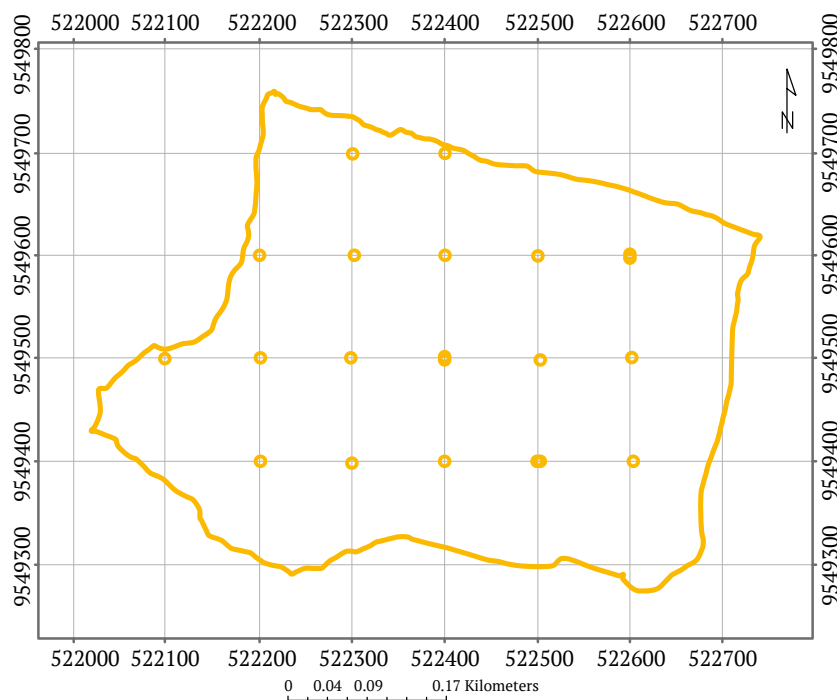


Fig. 1. Diagram of sampling points in the Lihendo district (UTM)



Table 1

Coordinates of sampling points (in Arc1960 format)

Point No.	Latitude	Longitude	Point No.	Latitude	Longitude
1	4°4'31"	33°12'0"	10	4°4'24"	33°11'57"
2	4°4'28"	33°12'0"	11	4°4'21"	33°11'57"
3	4°4'24"	33°12'0"	12	4°4'41"	33°11'54"
4	4°4'21"	33°12'0"	13	4°4'38"	33°11'54"
5	4°4'41"	33°11'57"	14	4°4'34"	33°11'54"
6	4°4'38"	33°11'57"	15	4°4'31"	33°11'54"
7	4°4'34"	33°11'57"	16	4°4'28"	33°11'54"
8	4°4'31"	33°11'57"	17	4°4'24"	33°11'54"
9	4°4'28"	33°11'57"	18	4°4'21"	33°11'54"

2.2. Chemical and Mineralogical Analysis

It is important to conduct elemental and mineralogical analysis prior to selecting any mineral processing method, as these analyses directly influence the economics of a project. In this study, the elemental composition was determined using X-ray fluorescence analysis (XRF, HITACHI-X MET 8000 instrument). The MINING LE mode was employed to measure Si, P, Al and Mg, while the MINING MODE was used for determining the other elements. Each analysis had a duration of 120 s per sample.

Mineral phases were identified using a Bruker AXS D2 PHASER XRD instrument manufactured in Germany (model A26-X1-A2B0D2C). To identify these phases, the XRD generator operated at 30 kV and 10 mA current using a copper anode.

2.3. Grain-Size Analysis

Researchers have discovered that the majority of gold particles are liberated when an ore is milled to approximately 50–80% of –75 µm size class [13, 14]. In this study a similar methodology was adopted. A sample weighing approximately 1 kg was pulverized to 50% of –75 µm class [14]. The dry sample was screened for approximately 15 min, after which the gold content of each mesh-screen size (oversize) was analyzed using an atomic absorption spectrometer (AAS).

Findings

The XRF analysis results of six samples revealed a relatively uniform elemental composition of the dumps (Fig. 2). The elemental composition observed in the studied samples is statistically representative, with a confidence level of 95%. The results of the elemental composition of the dumps are: Fe – 7.61, S – 0.22, Si – 10.74, Ca – 0.61, Mn – 0.04, Cu – 0.01, Al – 2.69, Cr – 0.025, Ti – 0.49, As – 0.04% (wt), Au – 0.72 g/t, Ag – 0.06 g/t. Among the valuable metals

identified, Ag and Au are notable, while Si predominates as the major nonmetal. The samples exhibit low concentrations of sulfur and arsenic, as well as calcium, manganese, copper, chromium, and titanium.

X-ray diffraction (phase) analysis revealed the presence of the following mineral phases in the samples: quartz, biotite, kaolinite, montmorillonite, goethite, cuprite, and muscovite (Fig. 2).

The primary minerals, each constituting more than 10% of the composition, include muscovite, kaolinite, and quartz. Biotite, montmorillonite, and goethite are categorized as minor phases, with their respective weight share amounting to less than 10% (Table 2).

Gold distribution was investigated through mesh-screen analysis using mesh sizes of 75 µm, 106 µm, 125 µm, and 150 µm. The results of this analysis revealed a unimodal distribution of gold in the ore, with the majority of gold present in the –75 µm fine fraction, as outlined in Table 3.

To determine the grain-size distribution of the initial material from the lean gold-bearing ore dumps, mesh-screen analysis of the materials was performed. Screens with mesh sizes ranging from 15 to 50 mm were employed for this analysis. The resultant grain-size distribution (Fig. 3) indicated that only 0.4% of the material exhibited a grain size smaller than 20 mm, while the predominant portion (81%) possessed a grain size falling within the range of +30–50 mm.

Discussion

Based on the results of X-ray phase analysis, the lean gold-bearing dumps predominantly consist of oxides and silicates. Mineralogical analysis suggests that the dump material corresponds to the gold-quartz type, with indication of metasomatism in-

ferred from the muscovite content. Minor sulfide minerals present have negligible influence on potential leaching processes [15, 16]. The XRF results indicate copper and sulfur contents below 0.05% and 0.5%, respectively. Copper acts as a cyanicide, interfering with cyanide during gold leaching processes, leading to increased consumption. However, adverse effects

from copper are not anticipated in the examined minerals. The material contains approximately 28% kaolinite, which may exhibit sorption properties toward gold-cyanide complexes formed during leaching. The high kaolinite content may also adversely affect filtration properties, which are crucial in heap and in-situ leaching processes.

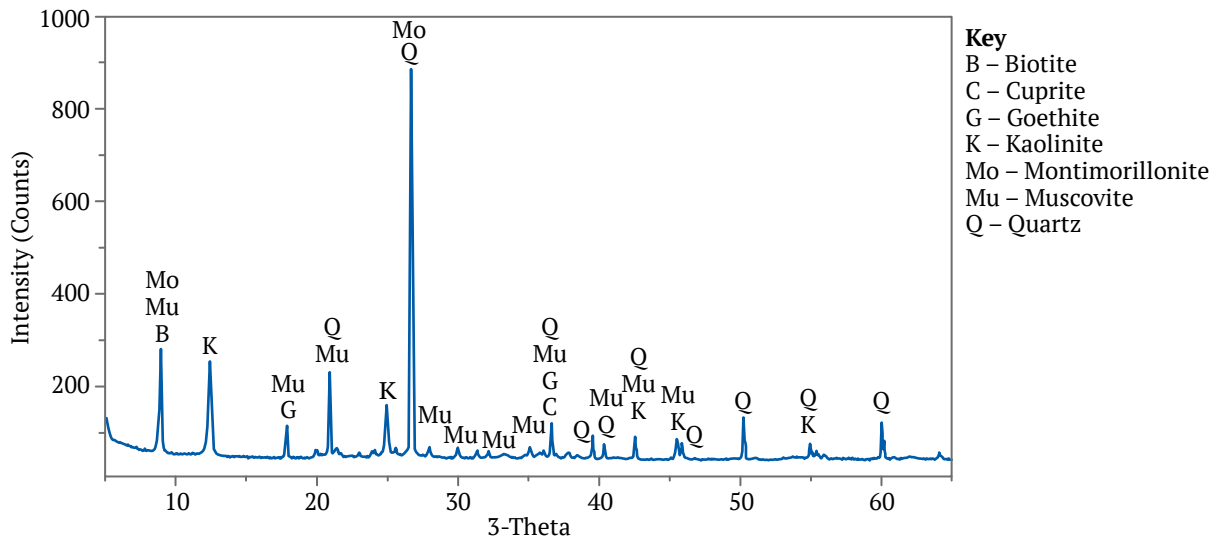


Fig. 2. X-ray phase analysis (XRD) and major mineral phases

Table 2

Basic mineralogical composition of the sample

Mineral	Weight fraction, %
Muscovite	37.66
Quartz	28.03
Kaolinite	27.77
Biotite	3.89
Goethite	1.44
Montmorillonite	0.89
Other minerals	0.32
Total	100

Table 3

Gold grain size distribution

Grain-size class, μm	Grain-size class yield, %	Gold grade in grain-size class, g/t	Gold distribution, %
+150	11.49	0.07	3.39
+125-150	23.41	0.05	4.93
+106-125	44.21	0.08	14.91
+75-106	6.61	0.10	2.79
-75	14.27	1.23	73.99
Total	100.00	0.24	100.00

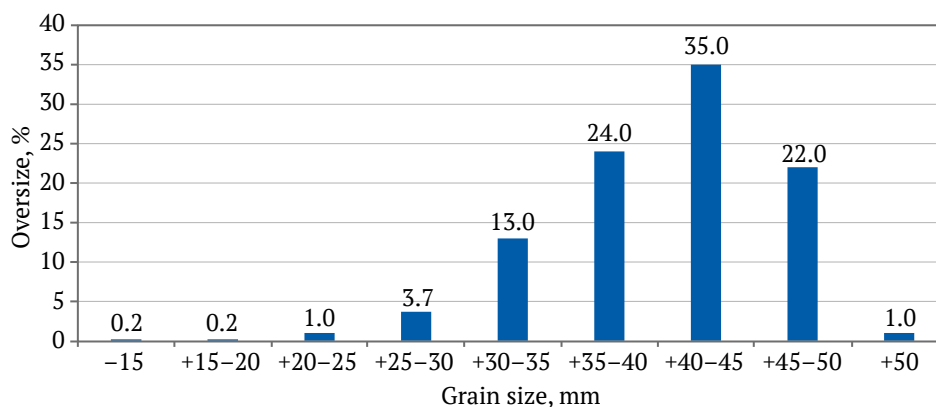


Fig. 3. Grain-size distribution of lean gold-bearing ore dump material



Moreover, the average gold grade was determined to be 0.72 g/t, contrasting with a higher grade of 1.37 g/t³ reported in a historical study. The disparity could be attributed to the limited sampling points (7) in the historical study, alongside potential variations in a sampling depths, which can influence gold grades⁴.

The heap leaching process emerges as a promising method for processing this mineralized material, given the low gold grades (0.72 g/t) necessitating lower capital and operating costs for extracting valuable components [17]. The profitability from gold sales generated by heap leaching may significantly surpass that of processing plant methods. The grain size of the dump material (+25 mm) meets heap leaching requirements, although additional pelletizing operations may be necessary, necessitating further metallurgical studies.

Positive experience from heap leaching of gold-quartz ores at the Mayskoe deposit (Khakassia, Russian Federation) is documented, achieving recoveries of 73–86%. The process involved crushing the ores to –10 mm, pelletized, heaped, and cyanide solution spraying, followed by gold precipitation from the pregnant solutions through electrolytic precipitation on zinc chips. Subsequent acid treatment of the precipitates and roasting led to the production of base billion [18].

³ Developing the golden opportunity, GPP Annual Report. 2004. URL: https://www.annualreports.com/HostedData/AnnualReportArchive/R/ASX_RSG_2004.pdf [Accessed: January 2023].

⁴ Ibid.

Conclusion

This study examined lean gold-bearing dumps from the Lihendo area in the Nzega District, Tanzania. The presence of clay minerals, such as kaolinite, poses challenges to filtration processes in heap leaching method and may also exhibit sorption activity towards extracted gold cyanide complexes resulting from leaching.

The minimum required grain size for mineral raw material in agitation leaching processes is typically 80% of the –75 µm size class. However, various design solutions exist where the grain size of leachable material is smaller [19]. Based on the mineralogical and elemental analysis findings, agitation leaching, including the carbon-in-pulp mode, appears to be the likely hydrometallurgical treatment method. It was established that in the minerals from the dump, where the grain size was reduced to meet the requirements agitation leaching, 74 % of the gold was found in the –75 µm fraction. Therefore, crushing, pulverization, and separation of fine fraction using hydrocyclones could be a viable approach for material processing. The –75 µm fraction could be processed via direct leaching or in the coal-in-pulp mode, reducing the portion of ore subjected to leaching. This approach is practical as 74% of the gold is contained in the –75 µm fraction, yielding approximately 14.27%. Despite the technical feasibility of agitation leaching, heap leaching of the studied material emerges as a practically applicable method in terms of economic indicators. Similar gold-quartz ores have demonstrated gold recovery rates of about 70–80%.

References

1. Araya N., Kraslawski A., Cisternas L.A. Towards mine tailings valorization: Recovery of critical materials from Chilean mine tailings. *Journal of Cleaner Production*. 2020;263:121555. <https://doi.org/10.1016/j.jclepro.2020.121555>
2. Hlabangana N., Bhebhe S., Mguni N.G., et al. Optimisation of the leaching parameters of a gold ore in sodium cyanide solution. *International Journal of Engineering Research and Reviews*. 2018;6(1):1–10.
3. Tilton J.E. Is mineral depletion a threat to sustainable mining? *SEG Newsletter*. 2010. URL: http://inside.mines.edu/UserFiles/File/economicsBusiness/Tilton/Sustainable_Mining_Paper.pdf [Accessed: January 2023].
4. Nieto A., Muncher B. An applied economic assessment and value maximization of a mining operation based on an iterative cut-off grade optimization algorithm. *International Journal of Mining and Mineral Engineering*. 2021;12(4):309–326. <https://doi.org/10.1504/IJMME.2021.121330>
5. Aleksandrova T.N. Complex and deep processing of mineral raw materials of natural and technogenic origin: state and prospects. *Journal of Mining Institute*. 2022;256:503–504.
6. Marsden J.O. Overview of gold processing techniques around the world. *Mining, Metallurgy & Exploration*. 2006;23(3):121–125. <https://doi.org/10.1007/BF03403198>
7. Gorain B., Lakshmanan V.I., Ojaghi A. Ore body knowledge. In: Lakshmanan V., Gorain B. (eds.) *Innovations and Breakthroughs in the Gold and Silver Industries: Concepts, Applications and Future Trends*. NY: Springer International Publishing; 2019. https://doi.org/10.1007/978-3-030-32549-7_2
8. Baum W. Ore characterization, process mineralogy and lab automation a roadmap for future mining. *Minerals Engineering*. 2014;60:69–73. <https://doi.org/10.1016/j.mineng.2013.11.008>



9. Nayak A., Ashrit S., Jena M. S., et al. Mineralogical characterization for selection of possible beneficiation route for low-grade lead-zinc ore of Rampura Agucha, India. *Transactions of the Indian Institute of Metals*. 2020;73(3):775–784. <https://doi.org/10.1007/s12666-020-01887-y>
10. Asad M. W. A. Cutoff grade optimization algorithm with stockpiling option for open pit mining operations of two economic minerals. *International Journal of Surface Mining, Reclamation and Environment*. 2005;19(3):176–187. <https://doi.org/10.1080/13895260500258661>
11. Azimi Y., Osanloo M., Esfahanipour A. An uncertainty based multi-criteria ranking system for open pit mining cut-off grade strategy selection. *Resources Policy*. 2013;38(2):212–223. <https://doi.org/10.1016/j.resourpol.2013.01.004>
12. Kalitenge D. Cut-off Grade Optimization in Open-pit Mines Considering Two Processing Streams and Rehabilitation Cost. [Master of Science Thesis]. 2021. URL: <https://era.library.ualberta.ca/items/0edd2e0d-a615-4243-9cbc-f8e1b2dde87e/download/601fca24-42e9-4b65-8215-320d35dd8695> [Accessed: October 2023]
13. Kondos P. D., Deschênes G., Morrison R. M. Process optimization studies in gold cyanidation. *Hydrometallurgy*. 1995;39(1–3):235–250. [https://doi.org/10.1016/0304-386x\(95\)00032-c](https://doi.org/10.1016/0304-386x(95)00032-c)
14. Coetzee L. L., Theron S. J., Martin G. J., et al. Modern gold departments and its application to industry. *Minerals Engineering*. 2011;24(6):565–575. <https://doi.org/10.1016/j.mineng.2010.09.001>
15. Dadgar A. Refractory concentrate gold leaching: Cyanide vs. bromine. *The Journal of the Minerals, Metals & Materials Society*. 1989;41(12):37–41. <https://doi.org/10.1007/BF03220846>
16. Mwanga A. *The design of a mobile concentrator plant for gold extraction from Tailings in Tanzania*. 2010. URL: https://www.academia.edu/en/71531220/The_design_of_a_mobile_concentrator_plant_for_gold_extraction_form_tailings_in_Tanzania [Accessed: January 2023].
17. Rasskazova A. V. Leaching of base gold-bearing ore with chloride-hypochlorite solutions. In: *IMPC 2018 – 29th International Mineral Processing Congress*. Moscow, September 17–21, 2018. Canadian Institute of Mining, Metallurgy and Petroleum; 2019. Pp. 4093–4098.
18. Gudkov S. S., Dementyev V. E., Druzhina G. Ya. *Heap leaching of gold and silver*. Irkutsk: JSC Irgiredmet; 2004. 352 p. (In Russ.)
19. Marsen J. O., House C. I. *The chemistry of gold extraction*. House Ellis-Horwood: Chichester; 1992.

Information about the authors

Jackson Shirima – PhD-Student, University of Dar es Salaam, Dar es Salaam Region, Tanzania; ORCID [0000-0001-6206-0306](https://orcid.org/0000-0001-6206-0306); e-mail jackson1rustus@gmail.com

Alphonse Wikedzi – Cand. Sci. (Eng.), Leading Researcher, University of Dar es Salaam, Dar es Salaam Region, Tanzania; ORCID [0000-0003-3063-8550](https://orcid.org/0000-0003-3063-8550), Scopus ID [57189371148](https://scopus.com/authid/detail.url?authorID=57189371148); e-mail alpho20012001@gmail.com

Anna V. Rasskazova – Cand. Sci. (Eng.), Leading Researcher, Mining Institute, Separate Division of Khabarovsk Federal Research Center of the Far Eastern Branch of the Russian Academy of Sciences, Khabarovsk, Russian Federation; ORCID [0000-0002-6998-8120](https://orcid.org/0000-0002-6998-8120), Scopus ID [36661516800](https://scopus.com/authid/detail.url?authorID=36661516800), ResearcherID [K-6384-2015](https://orcid.org/K-6384-2015); e-mail annbot87@mail.ru

Received 05.07.2023

Revised 17.11.2023

Accepted 20.11.2023



BENEFICIATION AND PROCESSING OF NATURAL AND TECHNOGENIC RAW MATERIALS

Research paper

<https://doi.org/10.17073/2500-0632-2023-05-116>

UDC 622

**Assessing viability of processing ash and slag dumps for energy-efficient ash beneficiation at Magadan CPP**L. V. Shipunov¹ , M. A. Kuzmenkov¹  , N. K. Gaidai^{1,2}   ¹North-Eastern State University, Magadan, Russian Federation²North-Eastern Integrated Research Institute named after N.A. Shilo of Far Eastern Branch of the Russian Academy of Sciences, Magadan, Russian Federation nataly_mag@rambler.ru**Abstract**

Complex processing of ash and slag waste is a supported directions for the development of environmental friendliness and performance in power engineering. The rational use of this waste in large-scale production processes has now been realized in the construction field. The development of up-to-date beneficiation technologies raises the possibility of extracting various useful components from ash and slag wastes. This study aims to investigate the potential for using energy-efficient ash beneficiation to produce a heavy metal-containing fraction and separate the magnetic fraction. To assess the feasibility of ash beneficiation and its rational use, the technical documentation of ash and slag dumps of PJSC “Magadanenergo” was studied, and semi-quantitative analyses of samples collected from these dumps were carried out. The data on the content of useful components and quantities of ash and slag enabled us to develop complex beneficiation flow sheets, assess their process efficiency, and evaluate their potential financial viability. The estimated volume of metals to be recovered includes 785 tons of Ti (me-1), 183 tons of Sr (me-2), and 4,867 tons of Fe (me-3). The performance indicators of the beneficiation and aggregated values of economic indicators for this project implementation on an industrial scale were calculated. The economic feasibility of the ash processing project showed good values for two out of three models over a ten-year planning horizon. Implementing the project also effectively improves the environmental situation by potentially processing up to 10% of the total volume of ash dumps, fulfilling one-fifth of the Energy Strategy of the Russian Federation’s requirements until 2035. While investigations of ash from the Magadan Cogeneration Power Plant (MCP) are not new, they were not previously carried out within the framework of studying integrated processing of ash to obtain various useful components.

Keywords

ash, Magadan Cogeneration Power Plant, waste, beneficiation, samples, cost efficiency, ecology, Magadan

For citationShipunov L. V., Kuzmenkov M. A., Gaidai N. K. Assessing viability of processing ash and slag dumps for energy-efficient ash beneficiation at Magadan CPP. *Mining Science and Technology (Russia)*. 2024;9(1):12–20. <https://doi.org/10.17073/2500-0632-2023-05-116>

ОБОГАЩЕНИЕ, ПЕРЕРАБОТКА МИНЕРАЛЬНОГО И ТЕХНОГЕННОГО СЫРЬЯ

Научная статья

Оценка целесообразности переработки золошлаковых отвалов Магаданской теплоэлектростанцииЛ. В. Шипунов¹ , М. А. Кузьменков¹  , Н. К. Гайдай^{1,2}   ¹Северо-Восточный государственный университет, г. Магадан, Российская Федерация²Северо-Восточный комплексный научно-исследовательский институт им. Н. А. Шило Дальневосточного отделения Российской академии наук, г. Магадан, Российская Федерация nataly_mag@rambler.ru**Аннотация**

Комплексная переработка золошлаковых отходов является одним из поддержанных направлений развития экологичности и эффективности производства энергетики. Рациональное использование их в массовом производстве в настоящее время реализовано в области строительства. Развитие современных технологий обогащения позволяет ставить вопрос о получении из золошлаковых отхо-



дов различных полезных компонентов. Цель данного исследования – изучение возможности применения энергоэффективного обогащения золы с целью производства тяжелой металлосоодержащей фракции и отделения магнитной фракции. Для оценки возможности обогащения золы и ее рационального использования была исследована техническая документация золошлаковых отвалов ПАО «Магаданэнерго» и проведены полуколичественные анализы отобранных проб с золошлакового отвала. Полученные данные по содержаниям полезных компонентов и количеству золошлаков позволили разработать комплексные обогатительные схемы с оценкой их технологической эффективности и произвести оценку потенциальной экономической эффективности. Объем металлов, планируемых к извлечению, по оценкам, составил: для Ti(me-1) – 785 т, для Sr(me-2) – 183 т и для Fe(me-3) – 4867 т. Рассчитаны технологические показатели обогащения и укрупненные значения экономических показателей для реализации данного проекта в промышленных масштабах. Экономическая целесообразность проекта по переработке золы в двух моделях из трех показывает хорошие значения в десятилетнем горизонте. Реализация проекта эффективна и с точки зрения улучшения экологической ситуации, т.к. позволяет вовлечь в переработку до 10 % всего объема золоотвалов, что на пятую часть выполняет требования Энергетической стратегии Российской Федерации до 2035 года. Исследования золы Магаданской теплоэлектростанции (МТЭЦ) не являются новыми, но в рамках исследования комплексной переработки золы с целью получения различных полезных компонентов ранее работы не проводились.

Ключевые слова

зола, МТЭЦ, отходы, обогащение, пробы, экономическая эффективность, экология, Магадан

Для цитирования

Shipunov L. V., Kuzmenkov M. A., Gaidai N. K. Assessing viability of processing ash and slag dumps for energy-efficient ash beneficiation at Magadan CPP. *Mining Science and Technology (Russia)*. 2024;9(1):12–20. <https://doi.org/10.17073/2500-0632-2023-05-116>

Introduction

Ash and slag waste has plagued mankind since the industrial revolution, posing significant environmental challenges. The complex processing of ash and slag waste is recognized as a vital approach to enhancing the environmental friendliness and efficiency of power engineering¹.

So far, the rational use of such waste in large-scale production has been limited to various construction processes [1–3]. However, the development of up-to-date beneficiation technologies has opened up opportunities to explore new sources of minerals. One such research avenue is the beneficiation of ash to extract valuable components, including precious and rare metals, underburnt coal, and the potential for producing sorbent [4]. Numerous studies have focused on recovering magnetite [5, 6], precious and rare metals [7–9], and aluminosilicates [10, 11]. The economic outcomes of these projects have varied across different periods of the Russian market's development, with profitability largely depending on the success in marketing the extracted products.

To date, no extensive research has been conducted on processing ash and slag waste for the purpose of extracting titanium concentrate, nor has the economic efficiency of such projects been assessed. This gap may be attributed to the challenges associated with the material composition of ash and underburnt

coal pellets. The effectiveness of beneficiation varies significantly with the composition and ratio of these materials.

The authors have previously studied and reported on the compositions and types of coals supplied to the MCPP over the last 20 years [12]. Briefly, the coal from the Talda deposit (Kuzbass) is characterized as a typical long-flame steam low-ash coal, rich in limestone within the mineral particles. Coals from different mining areas of the deposit were washed together, resulting in a final blended fraction delivered to MCPP.

Annually, PJSC Magadanenergo supplies about 300 000 tons of coal from the aforementioned deposit (Kemerovo coal basin, Kuzbass)². Concurrently, during the autumn-spring heating season and the maintenance of boiler units in the summer, about 33 000 m³ of ash and slag waste are generated. With a density of 1.2–1.3 t/m³, this amounts to about 41 000 t of ash and slag waste per year.

Problem definition

To date, there is no cost-effective, proven technology for processing ash and slag wastes from the Magadan Cogeneration Power Plant (MCPP), as required by the Energy Strategy of the Russian Federation.

¹ “Round table” on the topic “Legislative regulation” regulation of the use of ash and slag waste from coal TPP”. Ministry of Energy of the Russian Federation. URL: <https://minenergo.gov.ru/node/140114> (accessed date: 20.11.22).

² Batakova O.G. Magadanenergo will bring more than 300 kt of coal for the heating season of 2021–2022. Website of PJSC Magadanenergo. 2021; URL: <http://www.magadanenergo.ru/content/magadanenergo-zavezet-bolee-300-tysyach-tonn-uglya-dlya-otopitelnogo-sezona-2021-2022> (accessed date: 03.05.2021).



Studies on the use of MCPP ash as a component of clinkers in cement mixtures for concrete production have proved unsuccessful due to the high content of calcium oxide, which adversely affects the strength properties of the resulting concrete. The grade of the concrete decreases from B30 to B10, which is unacceptable for the construction of critical buildings and structures of the energy industry. Meanwhile, research on the application of ash and slag wastes in small-scale construction products (bricks, blocks, plates) has not been in demand due to the limited volume of residential construction in Magadan from 2010 to 2022.

On the other hand, the Energy Strategy of the Russian Federation for the period up to 2035 requires all energy companies using coal in their energy generation to develop measures to reduce the environmental impact on the areas where thermal power plants are located, including taking into account the involvement of ash and slag waste in processing. According to this strategy's provisions, 15% of all generated ash and slag waste should be utilized and neutralized by 2024, and 50% by 2035⁵.

Based on our previous studies and the studies of other authors in similar areas, we have focused on the ash and slag dumps of MCPP with the aim of obtaining a heavy fraction (extremely saturated with various metal oxides, such as those of titanium, zirconium, strontium, rubidium, and sulfides of zinc and copper), which could be subsequently processed by various methods to obtain metal concentrates. For titanium and zirconium oxides, we intended to apply a technique of alternating magnetic and electric separation with a successive increase in the magnetic field induction of separators, aiming to obtain a separate magnetic concentrate with a grade of about 53–62 wt. % (as indicated by preliminary studies), and selective concentrates of ilmenite, rutile, monazite, and zircon. For the extraction of strontium and rubidium, we propose to use a sequential scheme of electric separators with final acidic dissolution and concentrate separation in an electrolysis unit.

Research techniques

The primary objective of this work is to study the yield of the heavy fraction from ash and slag waste by applying traditional methods of gravity, magnetic, and electric beneficiation, as well as to calculate the economic feasibility of this process. The expected metal concentrates comprising the heavy fraction

from the initial gravity beneficiation, which are considered in further calculations, are listed as previously mentioned.

To achieve this goal, the following tasks were undertaken:

1) *Estimation of ash volumes accumulated in the ash and slag dumps of MCPP.* This analysis was performed by processing and compiling the statistical information provided by MCPP along with field observations of the ash and slag waste generation and storage processes, including pouring into the ash dump [13].

2) *Sampling and semi-quantitative analysis of useful components in the ash and slag wastes of MCPP.* This analysis was performed using the energy-dispersive X-ray fluorescent spectrometer EDX-800HS2 manufactured by “Shimadzu” (Japan), utilizing semi-quantitative of energy-dispersive X-ray fluorescent spectroscopy method. Measurement conditions were as follows: Rh anode tube (50-watt power), voltage settings of 50 kV and 15 kV, a current of 100 μ A (auto), in a helium medium, with a measurement diameter of 5 mm and a measurement time of 100 s. The samples were measured in the Ti-U (0.00–40.00 keV), Na-Sc (0.00–4.40 keV), and S-K (2.1–3.4 keV) bands [13].

The samples were collected at MCPP's ash and slag dump, located near Rechnaya Street. The sampling technique involved first identifying the main zones of the ash disposal area (dump): the safety berm, hydrotransport outflow zones, ash mixing zones, net ash hydraulic deposition zones. Samples were taken from the net ash hydraulic deposition zones at a depth of about four meters, after removing the overlaying layers of ash and slag waste, which were then moved to another dump by PJSC “Magadanenergo” machinery according to the schedule of ash and slag relocation. The samples were taken along the flank using the handful method. Approximately eight handfuls of material, each weighing just over 1 kg, constituted one flank sample. These samples were subsequently mixed in the mineral processing laboratory of SVSU Polytechnic Institute using the coning and quartering method three times, then dried and quartered mechanically at a classical splitter. One-eighth of the sample was sent for semi-quantitative analysis [13]. In total, eight flank samples were collected, amounting to 72.4 kg of initial ash before drying. The weight of the samples decreased to 58.2 kg after drying.

3) *Development and basic calculation of rational beneficiation process flow sheets.* The development of the flow sheets was based on the classical flow sheets for the beneficiation of titanium-zirconium sands from alluvial deposits, with subsequent

⁵ Energy Strategy of the Russian Federation for the period up to 2035. Ministry of Energy of the Russian Federation; 2020. URL: <https://minenergo.gov.ru/node/1026> (accessed date: 20.11.22).



magnetic-electric concentration on the appropriate separators. The recovery of strontium was also calculated [14]. The flow sheets took into account the equipment fleet in the SVSU beneficiation laboratory, which consists mainly of gravity beneficiation units (high-frequency jigging machine MOL2.5, concentration tables SKO-1 and RP-4, screw separator, fine filling sluice with rubber high-profile stencil, centrifugal separator) and magnetic and electric beneficiation units (drum-type magnetic separator, liquid magnetic separator, dry high-gradient field magnetic separator, drum-type electric separator). The classical method of beneficiation theory calculation was used: product yields and recoveries were calculated from the grades in the feed, concentrate, and tailings. From the yields and recoveries, the expected concentrate volumes were calculated [15].

4) Calculation of basic economic indicators for the selected process flow sheets to determine feasibility of further development of the ash processing project. Economic indicators were calculated using the refined NPV method as outlined by Atkinson, 2005 [16]. The basic rigid model was built based on these calculations, and additional scenarios were defined according to it: pessimistic, realistic, and optimistic (each of which took into account the possibilities of achieving the preset values of productivity, recovery, and sale of marketable products at the preset prices, according to the scenarios).

Research Findings

The ash volumes were obtained by processing the total dataset of field observations, which took the form of statistical information on the ash dumps of

M CPP, provided by PJSC “Magadanenergo”. The main values used in further calculations are summarized in Table 1. Maps of the dumps and the sampling locations have been given in the previously published materials by the authors [17].

Semi-quantitative analyses of the ash composition were conducted on samples collected in July 2022 using the method described above to estimate the quantities of metals in the M CPP ash. Sampling was performed on the flanks of the net ash hydraulic deposition zones to reduce the probability of sample contamination by surrounding rocks [13, 14].

The semi-quantitative analyses of the ash composition were carried out by the specialists from the Institute of Organic and Physical Chemistry named after A. E. Arbuzov, which is a separate structural subdivision of the FITs Kazan Scientific Center of RAS. The determined percentages of components in M CPP ash are summarized in Table 2.

Mineralogical studies showed that the composition of the samples corresponds to the typical composition of ash and slag waste. They contain quartz, silicates, iron oxides, pyrite, carbonate, silicon, pyrrhotite, pure iron, brass (Cu + Zn), as well as iron alloys of various compositions: Fe-Ni-Cr alloy, ferrochromite (Cr + Fe), and iron with chromium and manganese (Fe + Cr and Fe + Mn with manganese content up to 0.78%), celestine, and traces of carnallite.

The main operational parameters established in the course of the analysis of rational beneficiation flow sheets were calculated by analogy with similar projects for the processing of alluvial titanium-zirconium deposits material [15], and for magnetite, based on the studies of L. N. Adeeva and V. F. Borbat [18].

Table 1

Brief technical characteristics of ash dumps at M CPP

Designation	1 quarter of 2021	2 quarter of 2021	3 quarter of 2021	4 quarter of 2021
Total disposal, thousand m ³ (by quarter)	13.38	3.50	1.94	11.25
ZShO-1*, section 1	13.38	0.00	0.00	0.00
ZShO-1, section 2	0.00	3.50	1.94	11.25
Accumulated total at ZShO-1, thousand m ³	2,713.20	2,704.70	2,706.70	2,708.10
Accumulated total at ZShO-1, kt	3,255.90	3,245.70	3,248.10	3,249.70
Accumulated total at section 1 of ZShO-1, thousand m ³	2,108.50	2,111.50	2,111.50	2,101.70
Accumulated total at section 2 of ZShO-1, thousand m ³	604.70	593.30	595.20	606.50
Accumulated total at ZShO-2**, thousand m ³	1,781.80	1,796.80	1,796.80	1,806.60
Accumulated total at ZShO-2, kt	2,138.10	2,156.10	2,156.10	2,167.90

* ZShO-1 is ash and slag dump 1, located in the immediate vicinity of Rechnaya Street near Pionerny and Solnechny urban districts.

** ZShO-2 is ash-and-slag dump 2, located over a distance from Rechnaya Street, in the valley of the Balakhapchan River, is connected by a dirt road with ash-and-slag dump 1.



The operational parameters of the MCPP ash-and-slag waste beneficiation, as calculated [19], are given in Table 3. The initial percentages were taken to be equal to the median average values from Table 2 for the corresponding components.

Based on the values obtained according to formula 1, the quantities of useful components (metals to be extracted) were calculated:

$$V_{Me} = V_{ZShO-1} \cdot a_{Me}, \quad (1)$$

where V_{Me} is the calculated metal quantity, t, V_{ZSho-1} is the ash dump volume, t, and a_{Me} is the initial metal percentage.

From the total metal quantities obtained, the extractable quantity is determined, taking into account process losses. To account for losses, a correction coefficient $K_{ben.}$ was introduced, which took into account the total losses (its value ranges from 0.75 to 0.95; for further calculations, taking into account

the gravity flow sheet, it was taken to be equal to 0.90) [20]:

$$Q_{Me} = V_{Me} \cdot E_{Me} \cdot k_{ben.}, \quad (2)$$

where Q_{Me} is the quantity of extractable metal, t, E_{Me} is the metal recovery into concentrate, %.

The annual flow of metals P , coming with newly disposed ash continuously generated by MCPP, which can also be involved in beneficiation, were separately calculated:

$$P_{Me} = Z_{ZShO-1} \cdot a_{Me} \cdot E_{ME} \cdot k_{ben.}, \quad (3)$$

where P_{Me} is the flow of extracted metal, t; Z_{ZSho-1} is the annual volume of “new” ash and slag disposed in dumps, t; a_{Me} is the initial metal grade, %; E_{Me} is the metal recovery into concentrate, %; $K_{ben.}$ is the coefficient taking into account total losses.

The values of the quantities of metals planned for recovery, calculated using the formulas above, are summarized in Table 4.

Table 2

Component composition percentages in MCPP ash

Sample	Si	Al	Fe	Sa	K	Ti	Mg	P	Sr	Mn	Zr	Cu	Zn	Rb	S
%															
1	52.30	20.20	15.30	4.20	3.50	1.60	1.10	0.70	0.50	0.20	0.10	0.10	0.04	0.03	–
2	55.00	20.10	10.80	4.70	4.60	1.80	1.30	0.60	0.30	0.10	0.10	0.10	0.03	0.03	0.40
3	54.40	20.30	13.20	3.40	3.90	1.80	1.20	0.80	0.60	0.20	0.20	0.10	0.04	0.04	–
4	56.30	21.20	10.10	3.40	4.30	2.00	0.90	0.70	0.50	0.10	0.20	0.05	0.04	0.03	0.20
5	40.20	18.20	23.00	8.10	3.30	2.30	1.80	0.50	0.80	0.30	0.30	0.10	0.10	0.05	1.00
6	51.30	17.70	17.90	0.21	3.80	1.70	1.20	0.50	0.40	0.30	0.20	0.10	0.03	0.04	0.10
7	55.00	20.80	10.60	4.20	4.40	2.10	1.30	0.60	0.40	0.20	0.20	0.10	0.05	0.04	–
8	51.50	20.20	11.70	5.00	0.10	3.10	0.90	0.05	0.20	0.20	0.20	0.10	0.04	0.10	0.90

Table 3

Operational parameters for beneficiation of MCPP ash-and-slag waste

Metal	Initial percentage a	Marketable concentrate percentage b	Tailings percentage o	Concentrate yield $y_{conc.}$	Tailings yield $y_{tail.}$	Total recovery $E, \%$
Ti + Zr	2.20	45.00	0.50	3.82	96.18	78.14
Sr	0.50	25.00	0.10	1.61	98.39	80.32
Fe	14.00	65.00	4.00	16.40	83.61	76.11

Table 4

Quantities of metals to be extracted

Metal	Quantity at Ash-and-Slag Dump-1 (ZShO-1) $V_{Me},$ tons	Extractable quantity $Q_{Me},$ tons	Annual incoming quantity $P_{Me},$ tons	Planned quantity to be extracted $P_{Me} + 3\% Q_{Me},$ tons
Ti (me-1)	71,493.40	50,279.07	634.35	785.19
Sr (me-2)	16,248.50	11,745.90	148.19	183.43
Fe (me-3)	454,958.00	311,651.56	3,931.97	4,866.92



Taking into account the obtained values, the annual productivity by ash was calculated, and on this basis, the equipment and machinery were selected to provide the processing process:

$$U_{ash} = \frac{\sum_{Me-1}^{Me-3} P_{Me} + 3\%Q_{Me}}{AVG_{y_{c-t}}} \cdot AVG_{y_{t-n}}, \quad (4)$$

where U_{ash} is the annual productivity by ash, tpy, $AVG_{y_{c-t}}$ is the arithmetic mean of concentrate yield, % (7.32%), and $AVG_{y_{t-n}}$ is the arithmetic mean of tailings yield, % (92.72%).

The obtained value is 63 000 tons of ash processing per year, or 24 tons per hour. Selecting equipment and machinery based on these indicators is a straightforward task and does not require additional consideration.

The last task of calculating basic economic indicators was solved using analytical and computational methods for assessing the economic efficiency of innovation projects. Capital investments and operating costs were evaluated by analogy with similar technical projects for the mining and processing of alluvial rare metal material, with a discount rate of about 12%. Furthermore, based on the volumes of potential shipments of metal concentrates, the following indicators were calculated: NPV for a period of ten years and IRR for the same period. In the calculated rigid model, straight-line depreciation was used.

Input total expenditures amount to 188.50 mln rubles (CAPEX category – capital expenditures), and operating expenditures amount to 128.31 mln rubles per year (OPEX category – operating expenditures). The OPEX structure is as follows: 23.00% for the salary fund (the headcount is twenty-seven persons); 77.00% for material and operational maintenance costs, depreciation, and debenture interests.

The planned supply is based on the annual flow of a recoverable metal and the involvement of an

additional 3% of accumulated recoverable metal in processing. In monetary terms, this amounts to 177.84 mln rubles. In this scenario, categorized as realistic, the accounting for the strontium metal yield is greatly underestimated due to the expected difficulties in extracting 183.43 tons of strontium per year. Only half of this quantity, i.e. 91.5 tons of strontium, was included in the model. The selling price of the shipped titanium concentrate was taken from open internet sources, at 66.00 thousand rubles per ton of concentrate (as of November 2022). The strontium concentrate’s selling price is 96.00 thousand rubles per ton, and that of magnetite concentrate is 6.75 thousand rubles per ton⁴.

The purchase of equipment and machinery is planned to be financed through borrowing from large financial organizations. Loan terms and conditions are 18.00% p.a. in rubles for a period of five years for fixed assets, and a second credit line for ensuring production activities at 12.0% p.a. in rubles for a period of three years. The structure of the borrowed capital is 54.0% for the main credit line, 42.0% for the second credit line, and 4.0% for attracted external financing.

The discount rate is 12% p.a. in rubles, given the current economic situation. Cash flows are presented in real terms. Only the final cash flow used to calculate NPV was adjusted for the inflation rate forecasted by the Ministry of Economic Development of the Russian Federation.

For the sake of illustrating the model, the assumption that the taxable base is formed exclusively in the period in which the settlement with budgets of various levels takes place was introduced. The model used the following tax rates: VAT at 20.0%, profit tax at 15.5%, and corporate property tax at 2.2%.

The model obtained based on the calculations results is shown in Table 5.

⁴ Titanium concentrate. Starov & Co. URL: <https://www.iodine.ru/> (accessed date: 20.11.22).

Table 5

Flexibility within a rigid model

Item	Indicator value, realistic model	Indicator value, pessimistic model	Indicator value, optimistic model
NPV, mln rubles	424.31	-31.40	657.65
IRR, %	42.00	9.00	66.00
ROS, %	29.00	7.00	39.00
PB, years	4.00	N/A	2.00
DPB	Does not exceed the forecasting time-frame	Exceeds the forecasting time-frame	Does not exceed the forecasting time-frame



The models were formed mainly depending on the changes in the selling prices of metals and the actual strontium sales indicator. In the pessimistic model, strontium is completely excluded from the calculation, and the selling prices for titanium and magnetite are underestimated by 10% compared to the current prices.

Practical application

Justifying economic efficiency is a mandatory stage in developing a rational flow sheet for ash and slag waste processing. One promising area for using the obtained results is the separation of the metal-bearing fraction and subsequent additional beneficiation to obtain concentrates of rare metals. These results will be presented to PJSC Magadanenergo as part of the investment proposal for the project of ash and slag waste processing at MCPP.

Another application of the performed economic efficiency substantiation is the planning by the university of the loading of its own laboratory for mineral beneficiation within the framework of a tolling agreement (an agreement on rendering services on processing of basic raw materials with transfer of finished bulk or selective concentrates to the customer) with PJSC Magadanenergo, should a decision be made on processing the ash and slag wastes to extract rare metals into a separate concentrate.

Findings Discussion

In the course of the study, the performance of the beneficiation process and the aggregated values of economic indicators for the implementation of this project on an industrial scale were calculated. Despite modest performance and low capital costs, the economic effect in two of the three scenarios (optimistic and realistic) appears attractive. However, the high risk of the results obtained due to some assumptions made in the study should be noted.

The first assumption relates to the limited accessibility of the region in relation to the central traffic arteries of the Russian Federation. This results in logistical complexity and a high final price for the consumer, making it difficult to find a buyer at the realizable cost mentioned above. The market saturation with ilmenite concentrate also decreases the attractiveness of the distant Magadan titanium dioxide and magnetite for potential buyers.

The second assumption concerns the effectiveness of strontium extraction technology gravity in the gravity beneficiation processes, which, due to the specific chemical compounds of strontium, also introduces certain risks.

Moreover, if the question of complete processing of the entire ash and slag dump of MCPP at the current site or a second site arises, there will be certain difficulties. These are directly related to the instability of coal deliveries to MCPP from the same producer, affecting both scheduled and off-schedule indicators governing the economics of the beneficiation process. The problem can be addressed by answering two questions, but this is only possible after the commencement of the MCPP ash beneficiation project and full-fledged exploration works:

1) Was the content of titanium dioxide in the ash of coal supplied to MCPP in previous years the same as currently?

2) Will the content of titanium dioxide in the ash of coal to be supplied to MCPP in the future be the same as currently?

The final assumption made concerns the confidence that the metals are distributed in such minerals and fraction from which they will be relatively easily extracted into an intermediate concentrate by gravity beneficiation and further upgraded in small volumes in the SVSU beneficiation laboratory. This question also requires further study.

Conclusion

The information obtained from various sources, along with the primary process design and semi-quantitative analysis of performance, appears to demonstrate the cost-effectiveness of the proposed process solutions. The beneficiation process flow sheet can be implemented not only as a stationary complex within a separate building but also as an open modular installation, which would allow for relocation to a second ash dump site in the future.

Meanwhile, the economic feasibility of the ash processing project in two of the three models showed good economic performance over a ten-year horizon. The project's implementation can also be effective in terms of improving the environmental situation, as it allows for the processing of up to 10% of the total volume of the ash dumps. This ensures fulfillment of one-fifth of the requirements of the Energy Strategy of the Russian Federation up to 2035⁵.

The research is planned to continue with an additional study of the elemental and mineralogical composition of the ashes to determine the main minerals hosting the useful components planned for extraction.

⁵ Energy Strategy of the Russian Federation for the period up to 2035. Ministry of Energy of the Russian Federation; 2020. URL: <https://minenergo.gov.ru/node/1026> (accessed date: 20.11.22).



References

1. Bazhenov Y.M., Shchebenkin P.F., Dvorkin L.I. *Application of industrial waste in the production of construction materials*. Moscow: Stroyizdat Publ.; 1986. 120 p. (In Russ.)
2. Borisenko L.F., Deltsin L.M., Vlasov A.S. *Prospects of utilization of ash from coal-fired thermal power plants*. Moscow: CJSC Geoinformmark Publ.; 2001. 68 p. (In Russ.)
3. Liu H., Banerji Sh.K., Burkett W.J., VanEngele J. Environment properties of fly ash bricks. In: *World of Coal Ash (WOCA) Conference*. Lexington, KY, USA, May 4–7, 2019.
4. Vereshchagina T.A., Kutikhina E.A., Buyko O.V., Anshits A.G. Hydrothermal synthesis and sorption performance to Cs(I) and Sr(II) of zirconia-analcime composites derived from coal fly ash cenospheres. *Chimica Techno Acta*. 2022;9(4):20229418. <https://doi.org/10.15826/chimtech.2022.9.4.18>
5. Lanzerstorfer C. Pre-processing of coal combustion fly ash by classification for enrichment of rare earth elements. *Energy Reports*. 2018;4:660–663. <https://doi.org/10.1016/j.egy.2018.10.010>
6. Leonov S.B., Nikolskaya N.I.I., Vlasova V.V. CPP ashes – a possible raw material for obtaining iron concentrates. In: *Collection of Scientific Papers “Knowledge into Practice”*. Irkutsk: IrSTU Publ.; 1999. Pp. 6–9. (In Russ.)
7. Cherepanov A.A. Precious metals in the ash-cinder waste of Far Eastern heat-and-power stations. *Tikhookeanskaya Geologiya*. 2008;27(2):16–28. (In Russ.)
8. Cherepanov A.A., Kardash V.T. Complex processing of ash and slag wastes from CPPs (results of laboratory and semi-industrial tests). *Geology and Mineral Resources of World Ocean*. 2009;(2):98–115. (In Russ.)
9. Bakunin Y.N., Cherepanov A.A. Gold and platinum in ash and slag wastes of Khabarovsk CPP. In: *Ore Processing. Collection of Scientific Papers*. Irkutsk: IrSTU Publ.; 2003. Pp. 65–80. (In Russ.)
10. Karnaukhov Yu. P., Sharsva V.V., Podvolskaya E.N. Binders on the basis of waste ash-and-slag mixture and liquid glass from microsilica. *Stroitel'nye Materialy*. 1998;(5):12–13. (In Russ.)
11. Kizilstein L. Ya., Shpitsgluz A. L., Rylov V. G. Aluminosilicate microspheres of pulverized coal combustion ash. *Khimiya Tverdogo Topliva*. 1987;(6):122–124. (In Russ.)
12. Gayday N.K., Kuzmenkov M.A., Shipunov L.V. Analysis of coals and ashes of the Magadan CHPP. *Aktual'nyye Nauchnyye Issledovaniya v Sovremennom Mire*. 2021;12–11(80):253–261. (In Russ.)
13. Shipunov L.V., Kuz'menkov M.A., Gaiday N.K. Characteristics of ash and ash dumps of Magadan TPP. In: *Ideas, hypotheses, search... Materials of the XXVII Regional Scientific Conference of Postgraduate Students, Degree-Seeking Students, and Young Researchers*. Magadan, April 21, 2022. Moscow: Znanie-M Publ.; 2022. Pp. 223–232. (In Russ.) <https://doi.org/10.38006/00187-196-5.2022.223.232>
14. Shipunov L.V., Kuzmenkov M.A., Gaiday N.K. Estimation of rare metal content distribution in an ash dump of Magadan CPP. In: *At the Crossroads of the North and the East (Methodologies and Practices of Regional Development): Proceedings of the IV International Scientific and Practical Conference*. Magadan, November 17–18, 2022. Magadan: SVSU Publ.; 2022. Pp. 214–220 (In Russ.)
15. Polkin S.I. *Ores and placers of rare and precious metals beneficiation*. 2nd ed., reprint and additional. Moscow: Nedra Publ.; 1987. Pp. 123–169. (In Russ.)
16. Egorov V. N. *Mineral Processing*. Moscow: Nedra Publ.; 1987. Pp. 28–56. (In Russ.)
17. Shipunov L.V., Kuzmenkov M.A., Gaidai N.K. Mapping of ash and slag dumps of Magadanskaya TPP. In: *Innovative trajectory of modern science development: collection of papers*. Petrozavodsk: “New Science” International Center for Science Partnerships; 2022. Pp. 125–131. (In Russ.)
18. Adeeva L.N., Borbat V.F. Ashes of heating and power plant – perspective raw material for industry. *Herald of Omsk University*. 2009;(2):141–151. (In Russ.)
19. Atkinson A.A., Banker R.D., Kaplan R.S., Yuong S.M. *Management accounting*. 3rd ed. New Jersey: Pearson College Div; 2000. (Trans. ver.: Atkinson A.A., Banker R.D., Kaplan R.S., Yuong S.M. *Management accounting*. 3rd ed.: trans. from English. Moscow: Williams; 2005. Pp. 321–457. (In Russ.))
20. *Ore processing plant design handbook*. In 2 Books, Book 1. Compiled by: Baranov V.F. et al.; editors: Prof. Tikhonov O.N. et al. Moscow: Nedra Publ.; 1988. Pp. 194–209. (In Russ.)



Information about the authors

Lev V. Shipunov – Senior Lecturer at the Department of Digital Engineering, North-Eastern State University, Magadan, Russian Federation; ORCID [0000-0002-0840-8209](https://orcid.org/0000-0002-0840-8209); e-mail Eazey2308@gmail.com

Maxim A. Kuzmenkov – Senior Lecturer at the Department of Digital Engineering, North-Eastern State University, Magadan, Russian Federation; ORCID [0000-0002-6375-9693](https://orcid.org/0000-0002-6375-9693), Scopus ID [58286501200](https://scopus.com/authorid/58286501200); e-mail Snowfallandtea@mail.ru

Nataliya K. Gaidai – Cand. Sci. (Eng.), Associate Professor, Director of the Polytechnic Institute, North-Eastern State University, Magadan, Russian Federation; Senior Researcher at the Laboratory of regional Geology and Geophysics, North-Eastern Integrated Research Institute named after N.A. Shilo of Far Eastern Branch of the Russian Academy of Sciences, Magadan, Russian Federation; ORCID [0000-0002-2679-4967](https://orcid.org/0000-0002-2679-4967), Scopus ID [6603868070](https://scopus.com/authorid/6603868070); e-mail nataly_mag@rambler.ru

Received 07.05.2023

Revised 06.10.2023

Accepted 01.11.2023



BENEFICIATION AND PROCESSING OF NATURAL AND TECHNOGENIC RAW MATERIALS

Research paper

<https://doi.org/10.17073/2500-0632-2023-12-196>

UDC 622.765.4



Electrochemical action on the flotation beneficiation of ordinary iron ore concentrate

Kh. K. Rakhimov¹ , E. L. Chanturiya^{1,2}   , D. V. Shekhirev¹  ¹ University of Science and Technology MISIS, Moscow, Russian Federation² N. V. Melnikov Institute for the Problems of Integrated Subsoil Development, Russian Academy of Sciences (IPKON RAS), Moscow, Russian Federation elenachan@mail.ru

Abstract

One of the main challenges in processing fresh ferruginous quartzites is to obtain high-quality iron ore concentrates containing more than 70% total iron and less than 1.8% silica to produce DR pellets and hot Briquetted Iron (HBI). Currently, it is widely recognized that the most effective methods to achieve high-quality iron ore concentrates is through reverse flotation using cationic amine collectors in an alkaline medium. However, due to the very fine impregnation of magnetite in quartz, the insufficiently complete release of magnetite even with fine grinding, and the proximity of the flotation (surface) behavior of the separated minerals, high-quality concentrates are not always achievable in the flotation process. Consequently, exploring methods to enhance the efficiency of flotation separation of minerals and improve concentrate quality remains a pertinent issue. Historical studies have shown that electrochemical treatment can adjust the properties of reagents, enhance their effect on specific minerals, and thus control the flotation process. The efficiency of quartz and other silicates flotation by amines significantly depends on the ratio of ionic and molecular forms of the reagent in aqueous solutions of the collector and in the flotation pulp. Altering this ratio can impact the outcomes of reverse cationic flotation of iron ores. It is feasible to change the ratio of the amine forms through electrochemical oxidation or reduction of the reagent solution. Moreover, the electrochemical treatment facilitates the dispersion of the amine in the aqueous medium and its physical adsorption on minerals. Therefore, electrochemical pretreatment of amines can be considered a promising method for intensifying the reverse flotation of iron ore. This paper presents research results aimed at improving the quality of the oversize of the fine screening of ordinary magnetite concentrate from Mikhailovsky GOK, named after A. V. Varichev, through the use of electrochemically treated solutions of cationic amine class collectors in the process of reverse cationic flotation. The research findings confirmed the feasibility of using preliminary diaphragmless electrochemical treatment of reagents Tomamine RA-14 and Lilafлот 811M (esters of monoamine of different composition) for the targeted modification of their properties and for increasing the efficiency of reverse flotation. Consequently, the silica content in the flotation cell product decreased from 1.66–1.7% to 1.51–1.56, with the grade of total iron exceeding 70%.

Keywords

fresh ferruginous quartzites, magnetite concentrate, reverse cationic flotation, amines, electrochemical treatment

For citation

Rakhimov Kh.K., Chanturiya E.L., Shekhirev D.V. Electrochemical action on the flotation beneficiation of ordinary iron ore concentrate. *Mining Science and Technology (Russia)*. 2024;9(1):21–29. <https://doi.org/10.17073/2500-0632-2023-12-196>

ОБОГАЩЕНИЕ, ПЕРЕРАБОТКА МИНЕРАЛЬНОГО И ТЕХНОГЕННОГО СЫРЬЯ

Научная статья

Использование электрохимических воздействий в процессе флотационного дообогащения рядового железорудного концентрата

Х. К. Рахимов¹ , Е. Л. Чантурия^{1,2}   , Д. В. Шехирев¹  ¹ Университет науки и технологий МИСИС, г. Москва, Российская Федерация² Институт проблем комплексного освоения недр им. академика Н.В. Мельникова Российской академии наук (ИПКОН РАН), г. Москва, Российская Федерация elenachan@mail.ru

Аннотация

Одной из основных задач при переработке неокисленных железистых кварцитов является получение высококачественных железорудных концентратов, содержащих более 70 % железа общего и менее 1,8 % кремнезема для получения DR-окатышей и горячебрикетированного железа.



В настоящее время общепризнано, что наиболее эффективным способом получения высококачественных железорудных концентратов является обратная флотация катионными собирателями аминами в щелочной среде, однако из-за тончайшей вкрапленности магнетита в кварц, недостаточно полного раскрытия магнетита даже при тонком измельчении, а также из-за близости флотационных (поверхностных) свойств разделяемых минералов даже в процессе флотации не всегда возможно выделить высококачественные концентраты. В этой связи остается актуальным поиск способов повышения эффективности флотационного разделения минералов и повышения качества концентрата.

Ранее проведенными исследованиями показано, что с помощью электрохимической обработки можно регулировать свойства реагентов, усиливать их воздействие на определенные минералы и таким образом управлять процессом флотации. Поскольку эффективность флотации кварца и других силикатов аминами в существенной мере зависит от соотношения ионной и молекулярных форм реагента в водных растворах собирателя и во флотационной пульпе, изменение этого соотношения может влиять на результаты обратной катионной флотации железных руд. Изменение соотношения форм амина возможно при электрохимическом окислении или восстановлении раствора реагента. Кроме того, электрохимическая обработка способствует диспергации амина в водной среде и его физической адсорбции на минералах. Соответственно, предварительная электрохимическая обработка аминов может рассматриваться как одно из перспективных направлений интенсификации обратной флотации железных руд.

В статье представлены результаты поисковых исследований по улучшению качества концентрата, полученного флотацией мелкого грохочения рядового магнетитового концентрата Михайловского ГОКа им. А.В. Варичева за счет использования в процессе обратной катионной флотации электрохимически обработанных растворов катионных собирателей класса аминов.

Результаты поисковых исследований подтвердили возможность применения предварительной бездисафрагментной электрохимической обработки реагентов Tomamine PA-14 и Lilafлот 811M (эфиров моноамина различного состава) для направленного модифицирования их свойств и повышения эффективности обратной флотации надрешетного продукта: содержание кремнезема в камерном продукте снизилось с 1,66–1,7 % до 1,51–1,56 при содержании железа общего более 70 %.

Ключевые слова

неокисленные железистые кварциты, магнетитовый концентрат, обратная катионная флотация, амины, электрохимическая обработка

Для цитирования

Rakhimov Kh.K., Chanturiya E.L., Shekhirev D.V. Electrochemical action on the flotation beneficiation of ordinary iron ore concentrate. *Mining Science and Technology (Russia)*. 2024;9(1):21–29. <https://doi.org/10.17073/2500-0632-2023-12-196>

Introduction

One of the primary challenges in the processing of fresh ferruginous quartzites is obtaining high-quality iron ore concentrates with over 70% total iron and less than 1.8% silica for the production of DR pellets and direct reduction iron. Recent studies [1, 2] explore the potential of enhancing the efficiency of ferruginous quartzite processing, including improving the quality of ordinary magnetite concentrate through fine screening. The unique texture and structure of these ores, characterized by the finest unreleased impregnation of quartz in magnetite and vice versa, along with complex intergrowths of magnetite, quartz, and other silicates, make it challenging to achieve the desired quality of magnetic separation concentrates, even with fine grinding. Therefore, fine screening of ordinary magnetite concentrates separated by magnetic separation, additional grinding of the oversize, and further finishing by flotation are required to improve the magnetite concentrate quality. Studies [3, 4], analyzing the material composition of the fine screening over-

size from ordinary magnetite concentrate of magnetic separation, reveal that a significant part of all mineral phases in the initial oversize are intergrown with each other. Grinding the material to a grain size of 80% – 30 microns leads to a more complete release of lean magnetite intergrowths, increasing the proportion of magnetite in the form of rich intergrowths while maintaining the proportion of magnetite as released grains. Moreover, inclusions of quartz and celadonite in magnetite, indiscernible as separate mineral phases and identified only through average elemental composition, remain unreleased even with fine grinding, leading to a decreased quality of the magnetite concentrate. Study [3] presents theoretical performance predictions, while studies [5, 6] provide experimental results of reverse cationic flotation of the oversize.

It is now widely acknowledged that reverse flotation using cationic amine collectors in an alkaline medium is the most effective method for iron ores and concentrate flotation [7–9]. Study [7] offers a comprehensive review of collectors, depressors,



and medium regulators globally utilized in iron ore flotation. Publications [8, 9] detail the characteristics of amine cationic collectors, explore various amines, and present the results of their application in iron ore flotation based on pulp pH and quartz grain size distribution. The superiority of cationic reverse flotation over anionic flotation of iron ores has been established through comparison [10], and the study on the role of starch consumption as a depressor of iron minerals in reverse flotation by amines in an alkaline medium showed the potential to increase iron recovery into the cell product [11]. Reviews [12, 13] also highlight the efficiency of reverse cationic flotation of iron ores by amines in an alkaline medium. However, achieving high-quality concentrates through reverse flotation with amines is sometimes hindered by the insufficient release of magnetite even with fine grinding, the presence of magnetite intergrowths with quartz and other silicates, and the proximity of flotation (surface) behavior of the separated minerals. Attempts to enhance the selectivity of silicates and Ca – containing mineral flotation to separate magnetite using a mixture of collectors, however have been explored in [14, 15], but finding ways to improve mineral separation efficiency and magnetite concentrate quality remains a crucial pursuit.

Historical studies have shown that electrochemical treatment can modify the properties of reagents, amplify their effect on certain minerals, and thereby control the flotation process [16, 17].

The reagent’s form in aqueous solution significantly influences the structure and composition of the mineral particles’ surface hydrophobic layer, affecting their flotation behavior. The aqueous medium may contain ionic, molecular, polymeric, and micellar forms of amine in ratios that depend on reagent concentrations and medium conditions [18]. Since the flotation efficiency of quartz and other silicates by amines largely relies on the ratio of ionic and molecular forms of the reagent in collector solutions and the flotation pulp, changing this ratio can impact the results of reverse cationic flotation of iron ores [18]. Modifying the amine forms ratio is possible through electrochemical oxidation or reduction of the reagent in an aqueous solution. Furthermore, electrochemical treatment aids in the dispersion of the amine in the aqueous medium and its physical adsorption on minerals.

Given the foregoing, and based on literature data, the potential for intensifying the reverse flotation of iron ores with amines after their preliminary electrochemical treatment is considered promising.

This paper presents research findings on improving the quality of the oversize of fine screening of ordinary magnetite concentrate through the use of electrochemically treated solutions of cationic amine class collectors in the process of reverse cationic flotation i.e., the application of additional flotation beneficiation of the oversize.

Research Subjects and Methods

The research focused on the oversize from fine screening of the ordinary magnetite concentrate from the A.V. Varichev Mikhailovsky GOK (sample ND). The mineral and chemical compositions of this sample are detailed in Tables 1 and 2, respectively.

For the flotation beneficiation process, cationic reagents produced on an industrial scale by Nouryon Surface Chemistry AB Akzo Nobel and Clariant, TOMAH PRODUCTS ING, were used as collectors (Table 3).

Table 1

Chemical composition of ND sample, %

ND sample	Fe _{total}	SiO ₂
ND, according to MGOK data	61.7	12.6
ND, according to X-ray fluorescence analysis data, direct analysis	62.22	11.78
ND, according to X-ray fluorescence analysis data, estimated, weighted average	61.32	11.80

Table 2

Mineral composition of the oversize by mineral group (according to MLA data)

Mineral group	Minerals included in the group	Mineral group share, %
Magnetite	“Pure” magnetite, magnetite with fine quartz inclusions, magnetite with fine quartz and celadonite inclusions	84.77
Hematite	Hematite, goethite	3.82
Carbonates:	Ankerite, siderite, calcite	0.89
Quartz	Quartz, quartz with fine inclusions of magnetite	7.73
Aegirine	Aegirine	0.71
Celadonite	Celadonite	1.73
Aluminosilicates	Minerals of aluminosilicate group	0.07
Other	Other	0.20
Iron scrap	Iron scrap	0.08
Total	Sum of minerals	100.00

The electrochemical treatment (ECT) of a 1% aqueous solution (using recycled water from MGOK) of the reagents Lilafлот 811 M (mixture of monoamine esters (alkoxypropylamines) alkene $C_{13}H_{29}NO$ (isomer) (50–70%) + alkane $C_{15}H_{33}NO_3$ (30–50%), degree of neutralization of 20–40%) and Tomamine PA-14 (monoamine ester $R-O-CH_2CH_2CH_2-NH_2$; [3-(isodecyloxy) propylamine-1] 95%, degree of neutralization of 30% + iso-alcohols C_9-C_{11} 5%; iso-C10 saturated) was carried out in laboratory setting. The ECT was performed using direct electric current in a diaphragmless glass electrochemical cell of 150 ml capacity (Fig. 1). For electrodes, insoluble titanium drop-forged mesh coated with ruthenium oxide coating was employed, maintaining a working areas ratio of 1 : 2 between the anode and cathode. The reagent solution's treatment involved applying electric current concentrations of 0.28, 0.4, and 0.6 Ah/L in both “cathode” and “anode” modes, where the electrode with the larger area functioned as the cathode in cathode mode and as the anode in anode mode. The electric current was supplied to the electrodes through a rectifier, and the solution was agitated using a magnetic stirrer throughout the treatment process.

The electrochemical treatment (ECT) of the reagent solution lasted for 10 min. Before and after the treatment, the pH and Eh of the reagent solution were measured.

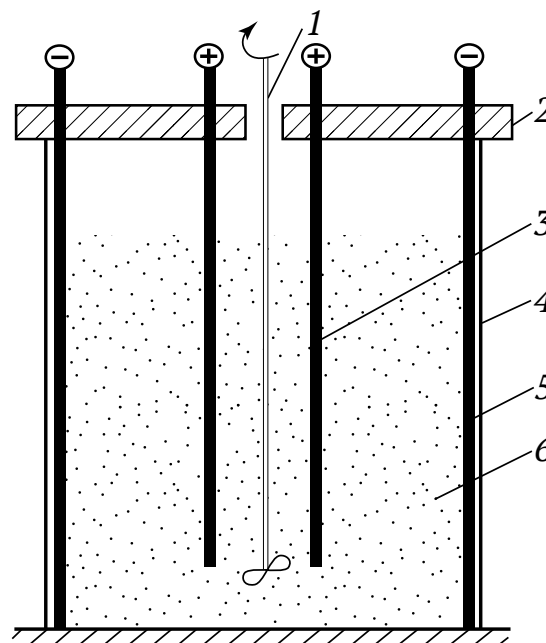


Fig. 1. Apparatus for diaphragmless treatment of a reagent solution:
 1 – mechanical stirrer; 2 – removable cover made of non-conductive material with an opening for the mechanical stirrer; 3 – cylindrical anode (insoluble titanium drop-forged mesh with ruthenium oxide coating); 4 – beaker made of non-conductive material (glass); 5 – cylindrical cathode (insoluble titanium drop-forged mesh with ruthenium oxide coating); 6 – reagent solution

Table 3

Conditions for electrochemical treatment of recycled water and reagent solutions

Treatment conditions	Current concentration, Ah/L	Treatment time, min	Initial pH	Initial Eh	Final pH	Final Eh
Recycled water						
Anode	0.28	10	7.784	+176.1	8.77	-243.2
Anode	0.4	10	7.784	+176.1	8.11	-72.2
Anode	0.6	10	7.784	+176.1	7.926	+142
Cathode	0.28	10	7.784	+176.1	8.34	+86.7
Cathode	0.4	10	7.784	+176.1	7.87	+134.8
Cathode	0.6	10	7.784	+176.1	8.06	-276
Tomamine						
Anode	0.28	10	9.18	+60.5	9.06	+112
Anode	0.4	10	9.18	+60.5	9.152	+125
Anode	0.6	10	9.18	+60.5	9.23	+148.6
Cathode	0.28	10	9.18	+60.5	9.1	+32.3
Cathode	0.4	10	9.18	+60.5	9.33	+40.4
Cathode	0.6	10	9.18	+60.5	9.24	-302.3
Lilafлот 811M						
Cathode	0.28	10	7.91	+84	9.195	-360
Cathode	0.4	10	7.91	+84	9.0	-308.6
Cathode	0.6	10	7.91	+84	8.8	-330



Reverse cationic flotation was conducted on the ground oversize (a 294 g subsample) of fine screening from the ordinary magnetite concentrate using the Tomamine PA-14 reagent and recycled water from Mikhailovsky GOK. The process followed a flow sheet that included preliminary magnetic consolidation of the oversize, rougher reverse flotation of the magnetic fraction, and recleaner reverse flotation of the cell product [3]. Similarly, the Lilafлот 811M reagent was used according to an analogous flow sheet but without preliminary magnetic consolidation. In both

cases, the grinding time was set at 15 min. The collector’s consumption rate was 240 g/t for the rougher flotation and 100 g/t for the cleaner flotation. Dextrin, used as a magnetite depressor, was added during the rougher flotation at a rate of 600 g/t. The pH level was maintained at 10–10.5 using caustic soda.

Research Findings and Discussion

The conditions for electrochemical treatment and the results from the flotation experiments are presented in Tables 3–5 and Figs. 2 and 3.

Table 4

Results of reverse cationic flotation with preliminary magnetic consolidation using electrochemically treated Tomamine reagent

Treatment conditions	Current concentration, Ah/L	Product	Yield, %	Percentage		Recovery, %	
				Fe	SiO ₂	Fe	SiO ₂
No treatment	–	n/m	6.3	16.32	67.13	1.65	35.42
		Flotation froth (product) 1	29.2	53.71	21.93	25.29	53.87
		Flotation froth (product) 2	7.4	67.47	4.07	8.02	2.52
		Cell flotation product	57.2	70.39	1.70	65.04	8.19
		Initial	100.0	61.9285	11.870	100.00	100.00
Anode	0.28	n/m	4.5	15.85	67.82	1.17	24.81
		Flotation froth (product) 1	33.6	51.9	23.88	28.36	64.83
		Flotation froth (product) 2	8.2	66.29	4.49	8.81	2.96
		Cell flotation product	53.7	70.51	1.7	61.67	7.39
		Initial	100.0	61.445	12.365	100.00	100.00
Anode	0.4	n/m	5.8	15.56	67.7	1.47	31.62
		Flotation froth (product) 1	31.5	52.51	23.16	27.04	58.92
		Flotation froth (product) 2	7.4	66.71	4.17	8.05	2.49
		Cell flotation product	55.4	70.06	1.56	63.43	6.98
		Initial	100.0	61.137	12.377	100.00	100.00
Anode	0.6	n/m	5.6	15.8	67.71	1.45	30.39
		Flotation froth (product) 1	32.1	52.44	23.23	27.55	59.58
		Flotation froth (product) 2	7.7	66.81	4.45	8.45	2.75
		Cell flotation product	54.6	69.99	1.67	62.55	7.29
		Initial	100.0	61.071	12.510	100.00	100.00
Cathode	0.28	n/m	5.4	15.06	68.73	1.33	29.54
		Flotation froth (product) 1	34.3	53.14	22.06	29.99	60.48
		Flotation froth (product) 2	6.3	66.25	4.73	6.90	2.39
		Cell flotation product	54.0	69.62	1.76	61.78	7.59
		Initial	100.0	60.815	12.518	100.00	100.00
Cathode	0.4	n/m	6.1	19.47	63.02	1.96	31.36
		Flotation froth (product) 1	31.3	52.18	22.99	26.74	58.34
		Flotation froth (product) 2	6.7	66.19	4.4	7.32	2.41
		Cell flotation product	55.9	69.9	1.74	63.99	7.89
		Initial	100.0	61.018	12.321	100.00	100.00
Cathode	0.6	n/m	5.4	16.29	66.48	1.44	29.71
		Flotation froth (product) 1	33.2	53.01	22.27	28.78	60.95
		Flotation froth (product) 2	8.1	66.8	3.83	8.81	2.55
		Cell flotation product	53.3	70.1	1.55	60.97	6.80
		Initial	100.0	61.232	12.146	100.00	100.00

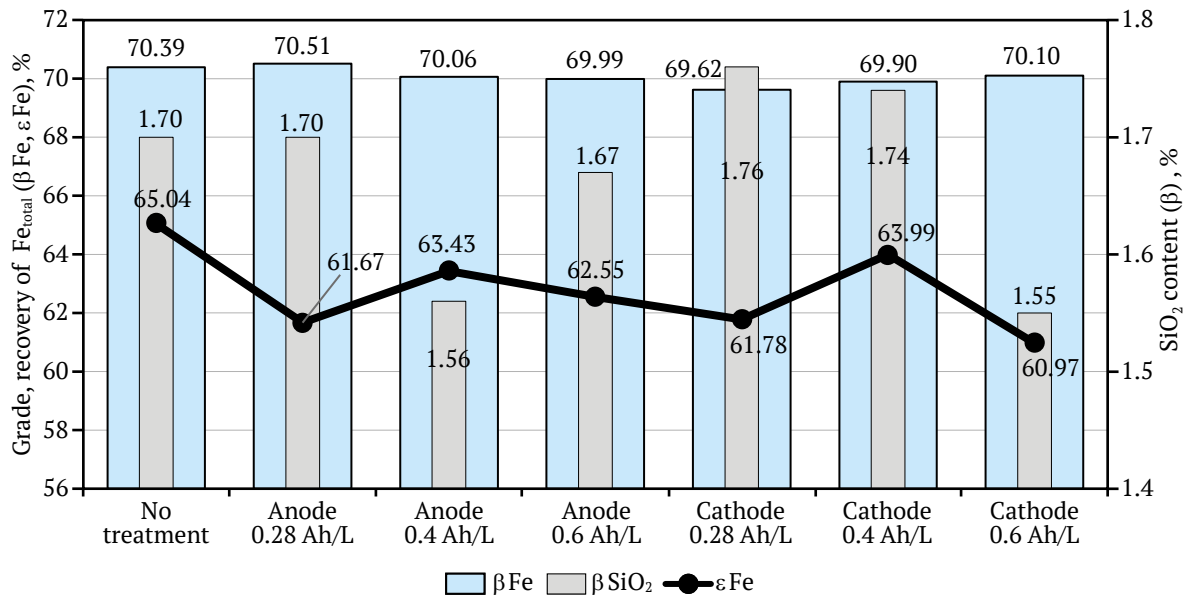


Fig. 2. Results of reverse cationic flotation with preliminary magnetic consolidation using electrochemically treated Tomamine reagent

Table 5

Results of reverse cationic flotation without preliminary magnetic consolidation using electrochemically treated Lilafлот 811 M amine reagent

Treatment conditions	Current concentration, Ah/L	Product	Yield, %	Percentage, %		Recovery, %	
				Fe	SiO ₂	Fe	SiO ₂
No treatment	-	Flotation froth (product) 1	41.28	50.24	25.27	33.61	82.79
		Flotation froth (product) 2	9.26	67.92	14.57	10.20	10.71
		Cell flotation product	49.46	70.10	1.66	56.19	6.50
		Initial	100.00	61.70	12.60	100.00	100.00
Cathode	0.28	Flotation froth (product) 1	40.98	49.55	26.99	32.91	87.79
		Flotation froth (product) 2	8.42	68.08	9.19	9.29	6.14
		Cell flotation product	50.59	70.48	1.51	57.79	6.06
		Initial	100.00	61.70	12.60	100	100.00
Cathode	0.4	Flotation froth (product) 1	38.54	47.15	29.50	29.45	90.23
		Flotation froth (product) 2	7.10	68.30	5.58	7.86	3.15
		Cell flotation product	54.36	71.15	1.54	62.69	6.63
		Initial	100.00	61.70	12.60	100.00	100.00
Cathode	0.6	Flotation froth (product) 1	31.44	45.10	34.55	22.98	86.21
		Flotation froth (product) 2	5.64	65.36	9.62	5.97	4.30
		Cell flotation product	62.92	69.67	1.90	71.05	9.49
		Initial	100.00	61.70	12.60	100.00	100.00

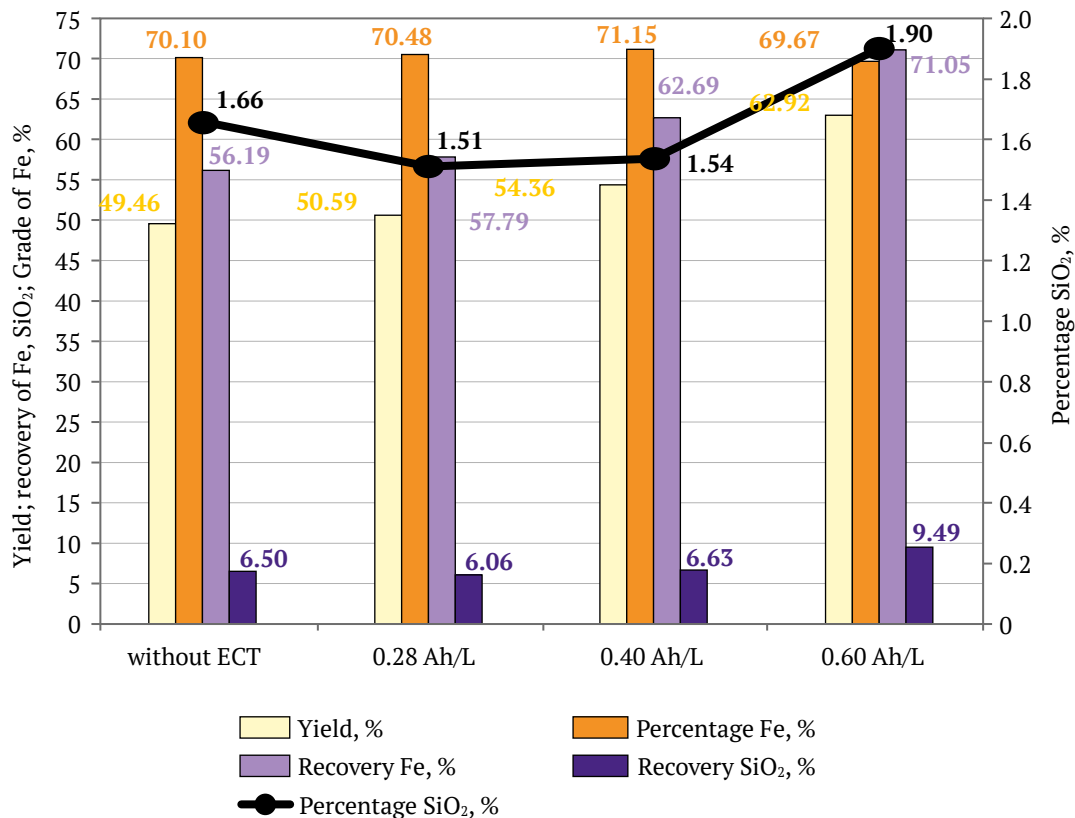


Fig. 3. Results of reverse cationic flotation without preliminary magnetic consolidation using electrochemically treated Lilafлот 811 M amine reagent

The analysis of the obtained results indicates that the anode mode of diaphragmless electrochemical treatment using Tomamine PA-14 reagent at a current concentration of 0.4 Ah/l had a noticeable effect. It allowed for a reduction in silica content from 1.7 to 1.56% while maintaining the required quality of total iron grade at 70.06 %, albeit with a slight decrease in Fe recovery from 65.04% to 63.43% compared to the reference test without ECT. Somolarly, the cathode mode at 0.6 Ah/L yielded a high-quality concentrate containing 70.1 % total iron with a recovery of 60.97%, versus 65.04% total iron in the test without ECT, and a silica content of 1.55 % (refer to Table 4, Fig. 2).

Therefore, the electrochemical treatment of the Tomamine PA-14 reagent positively influenced the concentrate's quality in terms of silica content, significantly reducing its while maintaining the iron grade at over 70%.

The electrochemical diaphragmless treatment of the Lilafлот 811 M reagent yielded positively results in the cathode mode. Without ECT, the flotation product contained 70.10% Fetotal and 1.66% SiO₂, with recoveries of 56.19 and 6.50%, respectively. Treating the reagent at a current concentration of 0.28 Ah/l increased the total iron grade in the concentrate to

70.48% and reduced the silica content to 1.51%, with recoveries of 57.79% for iron and 6.06% for silica, respectively. Treating the reagent at a current concentration of 0.4 Ah/L improved performance, resulting in a high-quality concentrate with a total iron grade of 71.15% and a silica content of 1.54%, with recoveries of 62.69% for total iron and 6.63% SiO₂ for silica (refer to Table 5, Fig. 3). Further increasing the current concentration to 0.6 Ah/L compromised the process's selectivity, decreasing the quality of the iron ore concentrate produced while increasing the recovery of total iron into the concentrate.

The electrooxidation and electroreduction reactions of amine are highly complex and, despite numerous studies, the mechanisms of these reactions remain unclear. At the anode, typically, the removal of an electron from the electron pair of a nitrogen atom usually occurs, initiating of sequence of complex transformations. Meanwhile, at the cathode, the reagent gains an additional electron. It is important to consider that, in the case of amines used as flotation reagents, they are often complex mixtures composed of monoamines, mono- and diamine esters, and others, further complicating the determination of the electrooxidation or electroreduction mechanisms.



Conclusions

The research findings suggest that preliminary diaphragmless electrochemical treatment of reagents such as Tomamine RA-14 and Lilaflot 811M (esters of monoamine with varying composition) could be used to purposefully modify their properties and enhance the efficiency of reverse flotation of the oversize. This could lead to a decrease in silica content in the cell flotation product and an increase

in the grade and recovery of total iron in the flotation concentrate.

It should be noted that since all cationic amine collectors (including monoamines, diamines, and their esters) have diverse compositions and are often initially mixtures, varying effects of electrochemical treatment can be anticipated for each reagent. Consequently, it is necessary to test each collector under different ECT conditions on a case-by-case basis.

References

1. Varichev A. V., Kretov S. I., Kuzin V. F. *Large-scale iron ore production in the Russian Federation*. Under the scientific ed. of B. F. Kuzin. Moscow: MGGU Publishing House; 2010. 395 p. (In Russ.)
2. Ismagilov R. I., Kozub A. V., Gridasov I. N., Shelepov E. V. Case study: advanced solutions applied by JSC Andrei Varichev Mikhailovsky GOK to improve ferruginous quartzite concentration performance. *Russian Mining Industry*. 2020;(4):98–103. (In Russ.) <https://doi.org/10.30686/1609-9192-2020-4-98-103>
3. Ismagilov R. I., Chanturiya E. L., Shekhirev D. V. Prognostical assessment of technological indicators of ferruginous quartzites enrichment. *Sustainable Development of Mountain Territories*. 2022;14(4):529–545. (In Russ.) <https://doi.org/10.21177/1998-4502-2022-14-4-529-545>
4. Ismagilov R. I., Chanturiya E. L., Shelepov E. V. et al. Innovative technology of magnetite concentrate processing for DRI pellets production at JSC “Mikhailovsky GOK named after A.V. Varichev”. In: *Proceedings of the international conference “Current problems of complex and deep processing of mineral raw materials of natural and anthropogenic origin” Readings from Plaksin-2022*. Vladivostok: DFU Publ; 2022. Pp. 5–14. (In Russ.)
5. Nikolaeva N. V., Aleksandrova T. N., Afanasova A., Chanturiya E. L. Mineral and technological features of magnetite-hematite ores and their influence on the choice of processing technology. *ACS Omega*. 2021;6(13):9077–9085. <https://doi.org/10.1021/acsomega.1c00129>
6. Ismagilov R. I., Chanturiya E. L., Shekhirev D. V., Rakhimov Kh. K. Experimental evaluation of the efficiency of cationic collectors in reverse flotation of the oversize of fine screening of ordinary magnetite concentrate from Named after A.V. Varichev Mikhailovsky GOK. In: *Current problems of complex and deep processing of natural and non-traditional mineral raw materials. Proceedings of the International Conference (Readings from Plaksin – 2023)*. Moscow: Sputnik+ Publishing House; 2023. Pp. 251–254. (In Russ.)
7. Araujo A. C., Vianna P. R. M., Peres A. E. C. Reagents in iron ores flotation. *Minerals Engineering*. 2005;18(2):219–224. <https://doi.org/10.1016/j.mineng.2004.08.023>
8. Papini R. M., Brandão P. R. G., Peres A. E. C. Cationic flotation of iron ores: amine characterisation and performance. *Minerals & Metallurgical Processing*. 2001;18:5–9. <https://doi.org/10.1007/BF03402863>
9. Vieira A. M., Peres A. E. C. The effect of amine type, pH, and size range in the flotation of quartz. *Minerals Engineering*. 2007;20(10):1008–1013. <https://doi.org/10.1016/j.mineng.2007.03.013>
10. Ma X., Marques M., Gontijo C. Comparative studies of reverse cationic/anionic flotation of Vale iron ore. *International Journal of Mineral Processing*. 2011;100(3–4):179–183. <https://doi.org/10.1016/j.minpro.2011.07.001>
11. Lima N. P., Valadão G. E. S., Peres A. E. C. Effect of amine and starch dosages on the reverse cationic flotation of an iron ore. *Minerals Engineering*. 2013;45:180–184. <https://doi.org/10.1016/j.mineng.2013.03.001>
12. Filippov L. O., Severov V. V., Filippova I. V. An overview of the beneficiation of iron ores via reverse cationic flotation. *International Journal of Mineral Processing*. 2014;127:62–69. <https://doi.org/10.1016/j.minpro.2014.01.002>
13. Nakhaei F., Irannajad M. Reagent types in flotation of iron oxide minerals: A review. *Mineral Processing and Extractive Metallurgy Review*. 2018;39(2):89–124. <https://doi.org/10.1080/08827508.2017.1391245>
14. Filippov L. O., Filippova I. V., Severov V. V. The use of collector’s mixture in the reverse cationic flotation of magnetite ore: the role of Fe-bearing silicates. *Minerals Engineering*. 2010;23(2):91–98. <https://doi.org/10.1016/j.mineng.2009.10.007>



15. Filippov L. O., Duverger A., Filippova I. V., Kasaini H., Thiry J. Selective flotation of silicates and Ca-bearing minerals: the role of non-ionic reagent on cationic flotation. *Minerals Engineering*. 2012;36–38:314–323. <https://doi.org/10.1016/j.mineng.2012.07.013>
16. Chanturiya V. A., Nazarova G. N. *Electrochemical technology in hydrometallurgical beneficiation processes*. Moscow: Nauka Publ.; 1977. 160 p. (In Russ.)
17. Chanturiya V. A., Dmitrieva G. M., Trofimova E. A. *Intensification of beneficiation of iron ores of complex material composition*. Moscow: Nauka Publ.; 1988. 206 p. (In Russ.)
18. Ryaboy V. I. Cationic reagents. In: *Physico-chemical fundamentals of flotation theory*. Moscow: Nauka Publ.; 1983. Pp. 167–181. (In Russ.)

Information about the authors

Khusrav K. Rakhimov – PhD-Student of the Department of Enrichment and Processing of Mineral Resources and Technogenic Raw Materials, University of Science and Technology MISIS, Moscow, Russian Federation; ORCID [0009-0007-8644-7055](https://orcid.org/0009-0007-8644-7055); e-mail rakhimov.khusrav@mail.ru

Elena L. Chanturiya – Dr. Sci. (Eng.), Professor, Professor of the Department of Enrichment and Processing of Mineral Resources and Technogenic Raw Materials, University of Science and Technology MISIS, Moscow, Russian Federation; Research Institute of Comprehensive Exploitation of Mineral Resources of the Russian Academy of Sciences, Moscow, Russian Federation; ORCID [0000-0002-5757-4799](https://orcid.org/0000-0002-5757-4799), Scopus ID [57196009376](https://scopus.com/authid/detail.url?authorID=57196009376), ResearcherID [J-4214-2014](https://orcid.org/J-4214-2014), AuthorID [67982](https://orcid.org/67982); e-mail elenachan@mail.ru

Dmitry V. Shekhirev – Cand. Sci. (Eng.), Senior Researcher, Associate Professor of the Department of Enrichment and Processing of Minerals and Technogenic Raw Materials, University of Science and Technology MISIS, Moscow, Russian Federation; ORCID [0000-0002-9668-9716](https://orcid.org/0000-0002-9668-9716), Scopus ID [57170910700](https://scopus.com/authid/detail.url?authorID=57170910700), AuthorID [589402](https://orcid.org/589402); e-mail shekhirev@list.ru

Received 27.12.2023

Revised 19.01.2024

Accepted 20.01.2024



BENEFICIATION AND PROCESSING OF NATURAL AND TECHNOGENIC RAW MATERIALS

Research paper

<https://doi.org/10.17073/2500-0632-2023-12-189>

UDC 622:666.3

**Characterization and thermal behavior of some types of kaolin of different origin from Northern Vietnam**

T. T. T. Nguyen , H. B. Bui

Hanoi University of Mining and Geology, Hanoi, Vietnam nguyenthithanhthao@humg.edu.vn**Abstract**

Kaolin (mainly composed of kaolinite, whose chemical formula is $\text{Al}_2\text{Si}_2\text{O}_5(\text{OH})_4$), serves as a versatile raw material widely used in various industries including production of ceramics, paper, paints, cosmetics, pneumatics, building materials, and hazardous waste storage. In the northern part of Vietnam, due to favorable geological conditions, there are diverse deposits of high quality kaolin of different origin and scale. Decades of research indicate the diversity of kaolin sources in the region, with special attention paid to hydrothermally altered and exchange types of kaolin, the formation of which is associated with complex processes of weathering, hydrothermal alteration and reprecipitation. The aim of this study was to characterize three different types of kaolin derived from different sources in Northern Vietnam (from weathered pegmatites, weathered felsic effusives, and hydrothermal-metasomatic altered rocks). The main focus was to analyze the thermal behavior of these samples during calcination in the temperature range from 300 °C to 1,100 °C. The comprehensive characterization was performed by X-ray diffraction (XRD), FT-IR spectroscopy (FT-IR), thermal analysis (thermogravimetry/differential thermogravimetry (TG/DTG)) and scanning electron microscopy with energy dispersive X-ray spectroscopy (SEM-EDS). The results showed that kaolinite with particle size less than 2 μm was identified in all samples. Minor amounts of muscovite and montmorillonite are present in some samples, and pyrophyllite is present in a sample from the hydrothermally altered rocks. Kaolinite morphology in all the samples showed typical forms including hexagonal and pseudohexagonal. The main chemical constituents of the samples are SiO_2 and Al_2O_3 ; in addition to these, $\text{K}_2\text{O} + \text{Na}_2\text{O}$, TiO_2 and iron are present in smaller quantities. Thermal analysis allowed to reveal the formation of metakaolinite phase at temperatures around 494 °C and 507 °C in the two studied samples from weathered rocks, while the pyrophyllite-bearing sample undergoes this transition at a higher temperature of 653.8 °C. The onset of metakaolinitization was observed at about 500 °C for the weathered rock samples and about 700 °C for the pyrophyllite-bearing sample. In addition, mullitization leading to the formation of mullite was evident at 1,100 °C. The study findings allow concluding that the studied kaolins can be used in traditional ceramics production.

Keywordskaolin, $\text{Al}_2\text{Si}_2\text{O}_5(\text{OH})_4$, pyrophyllite, mullite, thermal analysis, metakaolinite, mullitization, pegmatite, Northern Vietnam**For citation**Nguyen T.T.T., Bui H.B. Characterization and thermal behavior of some types of kaolin of different origin from Northern Vietnam. *Mining Science and Technology (Russia)*. 2024;9(1). <https://doi.org/10.17073/2500-0632-2023-12-189>

ОБОГАЩЕНИЕ, ПЕРЕРАБОТКА МИНЕРАЛЬНОГО И ТЕХНОГЕННОГО СЫРЬЯ

Научная статья

Характеристика и термическое поведение некоторых видов каолина различного происхождения из Северного Вьетнама

Т.Т.Т. Нгуен , Х.Б. Буи

Ханойский университет горного дела и геологии, г. Ханой, Вьетнам nguyenthithanhthao@humg.edu.vn**Аннотация**

Каолин (состоящий в основном из каолинита, химическая формула которого $\text{Al}_2\text{Si}_2\text{O}_5(\text{OH})_4$) служит универсальным сырьем, широко используется в различных отраслях промышленности, включая производство керамики, бумаги, красок, косметики, пневматики, строительных материалов и хранение



опасных отходов. В северной части Вьетнама благодаря благоприятным геологическим условиям находятся разнообразные месторождения высококачественного каолина различного происхождения и масштаба. Хотя в ряде работ изучены качество, потенциал, распространение и происхождение типов каолина в Северном Вьетнаме, исследования различий между каолинами из разных источников весьма ограничены. Целью данного исследования было определение характеристик трех различных типов каолина, полученных из различных источников в Северном Вьетнаме (из выветренных пегматитов, выветренных изверженных магматических пород кислого состава и гидротермально-метасоматических измененных пород). Основное внимание было уделено анализу термического поведения этих проб в ходе прокалывания в диапазоне температур от 300 до 1100 °С. Всесторонняя характеристика проводилась методами рентгеноструктурного анализа (XRD), Фурье-ИК-спектроскопии (FT-IR), термического анализа (термогравиметрия/дифференциальная термогравиметрия (TG/DTG)) и сканирующей электронной микроскопии с энергодисперсионной рентгеновской спектроскопией (SEM-EDS). Результаты показали, что во всех пробах был обнаружен каолинит с размером частиц менее 2 мкм. В отдельных пробах присутствуют незначительные количества мусковита и монтмориллонита, а в пробе из гидротермально измененных пород – пиррофиллита. Морфология каолинита во всех пробах проявлялась в типичных формах, включая гексагональную и псевдогексагональную. Основными химическими компонентами являются SiO_2 и Al_2O_3 ; помимо них, в меньших количествах присутствуют $\text{K}_2\text{O} + \text{Na}_2\text{O}$, TiO_2 и общее железо. Термический анализ выявил образование метакаолиновой фазы при температурах около 494 и 507 °С в двух изученных пробах из выветренных пород, а пиррофиллитсодержащая проба претерпевает этот переход при более высокой температуре – 653,8 °С. Начало метакаолинизации наблюдалось при температуре около 500 °С для проб из выветренных пород и около 700 °С – для пиррофиллитсодержащей пробы. Кроме того, при 1100 °С проявилась муллитизация, приводящая к образованию муллита. Полученные результаты позволяют сделать вывод о возможности применения этих проб каолина в традиционном производстве керамики.

Ключевые слова

каолин, $\text{Al}_2\text{Si}_2\text{O}_5(\text{OH})_4$, пиррофиллит, муллит, термический анализ, метакаолинит, муллитизация, пегматит, Северный Вьетнам

Для цитирования

Nguyen T. T. T., Bui H. B. Characterization and thermal behavior of some types of kaolin of different origin from Northern Vietnam. *Mining Science and Technology (Russia)*. 2024;9(1). <https://doi.org/10.17073/2500-0632-2023-12-189>

Introduction

Kaolin (mainly composed of kaolinite, whose chemical formula is $\text{Al}_2\text{Si}_2\text{O}_5(\text{OH})_4$), serves as a versatile raw material widely used in various industries including production of ceramics, paper, paints, cosmetics, pneumatics, building materials, and hazardous waste storage [1–3]. The quality and applicability of kaolin depends on factors such as its chemical composition, physical properties, mineralogical composition and structural morphology. For example, Maja (2017) showed that clay from Slatina deposit in Serbia has composition and other characteristics suitable for ceramic and construction industries, especially for the production of tiles, thin-walled hollow bricks, and roof tiles/lightweight blocks [4]. Further studies aimed at investigating properties such as purity, mineralogical composition, color and texture by researchers such as Hernández et al. (2019) identified the characteristics of kaolin deposits in Venezuela, suggesting potential demand for this kaolin to be processed for using in the pharmaceutical industry [5]. A number of researchers emphasize the need for a comprehensive study of the physicochemical properties of kaolin raw materials and their behavior under calcination conditions before the use in practice.

In the northern part of Vietnam, due to favorable geological conditions, there are diverse deposits of high quality kaolin of different origin and scale. Decades of research indicate the diversity of kaolin sources in the region, with special attention paid to hydrothermally altered and exchange types of kaolin, the formation of which is associated with complex processes of weathering, hydrothermal alteration and reprecipitation [6, 7]. Although several works have studied the quality, potential, distribution, and origin of kaolin types in North Vietnam [8, 9], studies on the differences between kaolins from different sources are very limited.

This paper presents the application of combined analytical techniques such as X-ray diffraction analysis (XRD), Fourier transform infrared spectroscopy (FT-IR), thermal analysis (thermogravimetry/differential thermogravimetry (TG/DTG)), and scanning electron microscopy with energy dispersive X-ray spectroscopy (SEM-EDS) to investigate the characteristics of kaolin raw materials of different origins from several mines in Northern Vietnam, as well as their properties/behavior under calcination conditions. The results obtained allowed to comprehensively and more completely assess the qualitative characteristics of the kaolins and contribute to their more efficient application.

Review of geological characteristics of some kaolin types at mines in Vietnam

Kaolin from weathered pegmatites

Kaolin formed in weathered pegmatites is widely distributed in the Lao Cai area in Northern Vietnam [10]. These kaolin-bearing bodies are usually cylinder-shaped and have a branched morphology. Pegmatite bodies of various sizes are distributed in metamorphic formations of Proterozoic and Lower Paleozoic age. The thickness of the kaolin body depends on the terrain. In a vertical cross-section, the pegmatite bodies are stratified: the uppermost layer consists of kaolin, followed by a layer of low-weathered pegmatites, and the lowest layer is represented by fresh pegmatites. This type kaolin mines are usually medium to small scale mining operations. This variety of kaolin is usually fine-grained, rich in aluminum and characterized by relatively high iron content, often has a yellow or dark yellow hue. The -0.21 mm undersize kaolin recovery ranges from 30 to 60%, averaging below 40%. Fig. 1 shows a geological cross-section of a kaolin body of such nature.

Kaolin from weathered felsic effusive rocks

Kaolin formed in weathering crust in effusive rocks is widely distributed throughout Northern Vietnam in different structural zones [11]. This type of kaolin deposits, usually formed in the weathering crust in rhyolite and rhyolite-porphyry rocks, is characterized by small-scale occurrences, often hopper-shaped and lens-shaped. Kaolin of this type is usually fine-grained, present in white or pinkish-white tints. The -0.21 mm undersize kaolin recovery ranges from 50 to 90%, averaging about 70%. Fig. 2 shows a cross-section of a deposit of this type of kaolin.

Kaolin of hydrothermal-metasomatic genesis

Kaolin bodies containing pyrophyllite (hereinafter referred as kaolin-pyrophyllite bodies) are the product of contact alteration processes involving hydrothermal solutions and various rocks such as rhyolites, rhyolite porphyries, felsites and tuffs [12]. These bodies are intersected by faults or, conversely, are accommodated by fault zones, identified at a mine, that determines their relatively large scale.

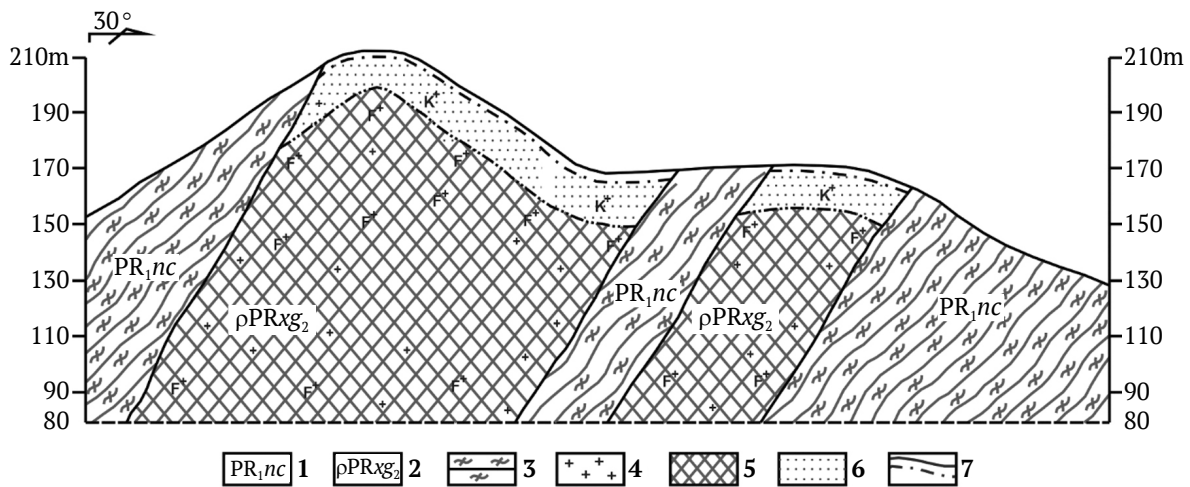


Fig. 1. Geological cross-section at Son Man kaolin mine, Lao Cai Province:

- 1 – quartz schists, mica, gneisses, interbedded quartzites; 2 – aplite and pegmatite veins; 3 – mica crystalline schists; 4 – fresh (unweathered) pegmatites; 5 – low-weathered pegmatites; 6 – kaolin; 7 – topsoil (land cover)

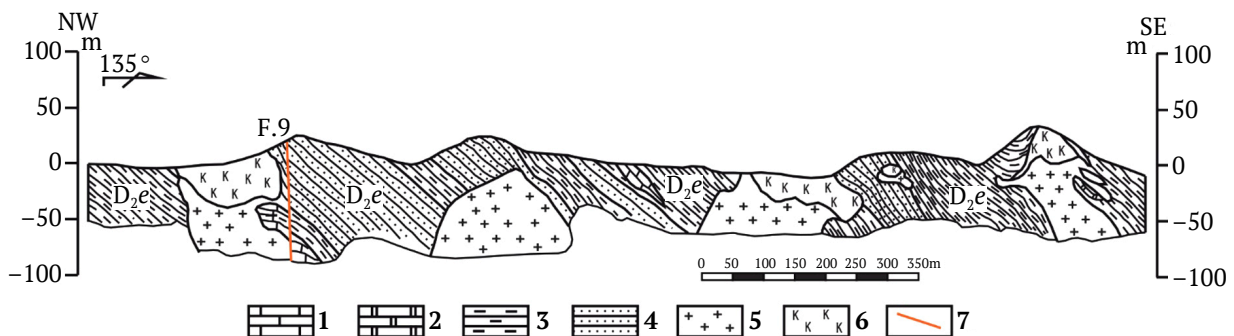


Fig. 2. Geological cross-section at Minh Tan kaolin mine, Hai Duong Province:

- 1 – quaternary sediments; 2 – limestone; 3 – silicified limestone; 4 – shale, sandstone; 5 – keratophyre; 6 – kaolin; 7 – fault

The morphology of such kaolin-pyrophyllite bodies is complex, with irregular randomly manifested bulges. Fig. 3 shows a cross-section of a kaolin-pyrophyllite body for better visualization.

Research Methodology

Sample Preparation

Bulk samples were collected from the mining zones of three kaolin mines, kaolins of which have different genesis (type): kaolin from the weathering zone of pegmatites of the Thach Khoan complex at Son Man mine, Lao Cai Province (kaolin from weathered pegmatites); kaolin from the weathering zone of rhyolites of the Binh Lieu Formation, Minh Tan mine, Hai Duong Province (kaolin from weathered effusives), and kaolin-pyrophyllite of hydrothermal-metasomatic genesis from Tan Mai mine, Quang Ninh Province (kaolin-pyrophyllite) (Figs. 1–3). These natural kaolin samples were pulverized, dissolved, mixed, and screened using a sieve with mesh size $< 63 \mu\text{m}$. The screening undersizes were placed into laboratory bags and used for subsequent analyses and tests. For the identification of clay minerals, a clay fraction with particle size $< 2 \mu\text{m}$ was obtained by decantation. The particle size fraction $< 2 \mu\text{m}$ was used to prepare cylindrical pellets for further studies. They were further subjected to various treatments including air drying, glycolation with ethylene glycol, and heating to 350°C .

The cylindrical pellets were made by uniaxial dry pressing of the samples at a pressure of 40 MPa. The cylindrical pellets were then dried at 60°C for 24 h in an oven. The dried cylindrical pellets were heated to selected temperatures of 300, 500, 700, 900 and 1100°C at a heating rate of $5^\circ\text{C}/\text{min}$ using an electric laboratory furnace. For each selected temperature,

the sample was calcined for 2 h and “quenched” to room temperature under ambient conditions to avoid crystallization of amorphous metakaolinite. The portions of the heated samples were ground using an agate mortar and pestle for subsequent analyses.

Sample characterization

The morphological properties of minerals and the mineralogical composition of the samples were investigated using a scanning electron microscope (SEM – Quanta 450) with energy dispersive X-ray spectroscopy (EDS). The mineralogical analysis of the samples was performed by X-ray diffraction (XRD) analysis. The X-ray diffraction patterns of the samples processed under different conditions were also obtained on a Siemens model D5005 powder X-ray diffractometer with $\text{Cu-K}\alpha$ radiation at 40 kV and 30 mA, scanning from 3 to 70° at an angular velocity ω (2θ in the Figures below) of $2^\circ/\text{min}$. FT-IR spectra were recorded between $4,000$ and 400 cm^{-1} with a resolution of 2 cm^{-1} using a Shimadzu IR Prestige-21 spectrometer. The thermal behavior of each sample was determined using the techniques of thermogravimetry/differential thermogravimetry (TG/DTG) in nitrogen atmosphere in the range from room temperature up to $1,100^\circ\text{C}$ at a heating rate of $10^\circ\text{C}/\text{min}$. The nitrogen adsorption and desorption isotherms of the kaolin samples heat-treated at 196°C were obtained using a Micromeritics ASAP 2020a instrument.

Findings and Discussion

Characterization of natural kaolin materials

X-ray diffraction analysis

Fig. 4 shows X-ray diffraction patterns of three natural kaolin materials (the samples: kaolin from weathered pegmatites, kaolin from weathered felsic

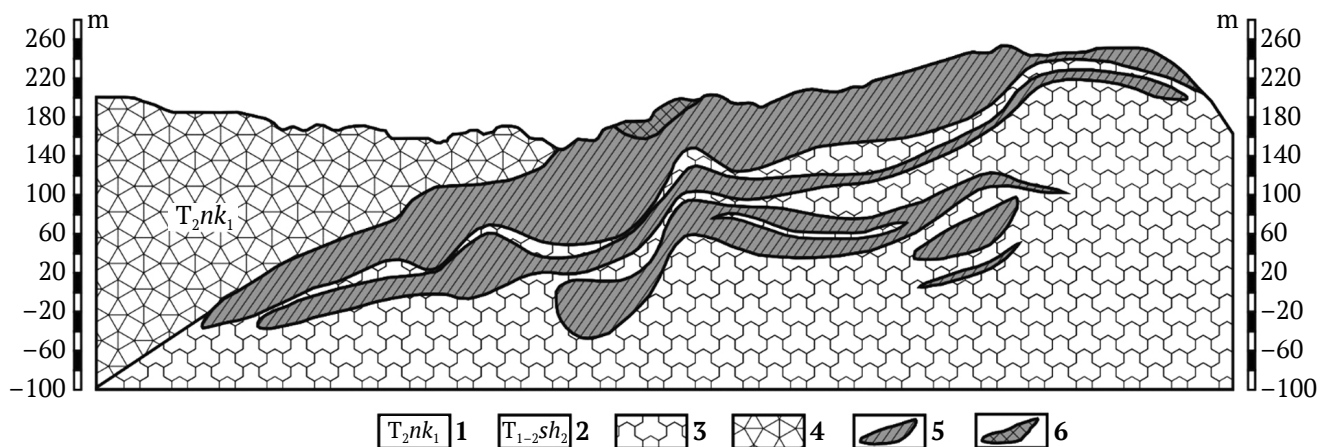


Fig. 3. Geological cross-section at a kaolin-pyrophyllite mine in Tan Mai, Quang Ninh Province:
1 – Na Khat Formation; 2 – Khon Lang Formation; 3 – rhyolite-dacite tuff;
4 – siltstone; 5 – alunite; 6 – kaolin-pyrophyllite

effusives, and kaolin-pyrophyllite) with a particle size of 2 μm subjected to different test conditions: aged at room temperature, treated with ethylene glycol, and heated at 350 °C. These XRD patterns consistently show the predominance of kaolinite in all three samples, characterized by well-defined peaks at 7.18 Å, 4.48 Å and 3.58 Å [1]. In addition, relatively weak basal reflections at 10.0 Å, 5.02 Å and 3.35 Å indicate the presence of muscovite in the kaolin samples from pegmatites and the kaolin samples from effusives [13]. It is important to note that pyrophyllite is clearly identified in the kaolin-pyrophyllite sample obtained from Tan Mai mine, as evidenced by characteristic peaks of 9.2 Å, 4.59 Å, 4.14 Å, 3.79 Å, and 3.07 Å [14]. After the treatment with ethylene glycol and heating at 350 °C, the characteristic peaks corresponding to kaolinite, muscovite, and pyrophyllite remain on the X-ray diffraction patterns. However, in the case of the kaolin from weathered effusives sample, a noticeable shift of the peak associated with montmorillonite from 15.1 Å to 16.9 Å after ethylene glycol treatment was observed. This observation shows that, in addition to the predominance of kaolinite of < 2 μm size fraction in all the samples, the kaolin from weathered pegmatites is characterized by the presence of muscovite, the kaolin from weathered effusives is accompanied by muscovite and montmorillonite, and the kaolin-pyrophyllite sample consists predominantly of pyrophyllite. These findings emphasize that different conditions during kaolin formation can lead to a variety of mineralogical compositions, which can influence the calcination processes and their outcomes.

Analysis by scanning electron microscopy and energy dispersive X-ray spectroscopy techniques

Scanning electron microscopy (SEM) images of the minerals of the kaolin samples (the kaolin from weathered pegmatites (a), the kaolin from weathered effusives (b) and the kaolin-pyrophyllite (c)), are shown in Fig. 5. These images clearly show the characteristic morphology of kaolinite with a hexagonal thin-plate structure. The mineral grains are intricately attached together, displaying their distinctive characteristics. The results of EDS (energy dispersive X-ray spectroscopy) analysis shed light on the mineral elemental compositions. Silicon oxide (SiO_2) and aluminum oxide (Al_2O_3) were found as major components, which correspond to the expected presence of silicon (Si) and aluminum (Al) in the chemical formula of kaolinite, $\text{Al}_2\text{Si}_2\text{O}_5(\text{OH})_4$. Table 1 shows the average chemical composition of the three kaolin samples (semi-quantitative determination by EDS analysis).

Fourier-transform infrared (FT-IR) spectroscopy analysis

Fourier-transform infrared (FT-IR) analysis showed the presence of various functional groups in the studied samples (Fig. 6). Notably, the absorption peaks at 3,687 and 3,619 cm^{-1} are associated with the stretching (bond) vibrations of O–H group bond. In addition, the bands at 1,114 and 684 cm^{-1} correspond to the stretching vibrations of Si–O bond, and the absorption bands at 1,034 and 998 cm^{-1} refer to the stretching vibration region of Si–O–Si bond. The band at 909 cm^{-1} corresponds to the stretching vibrations of Al–OH bond. These bands of stretching vibrations are

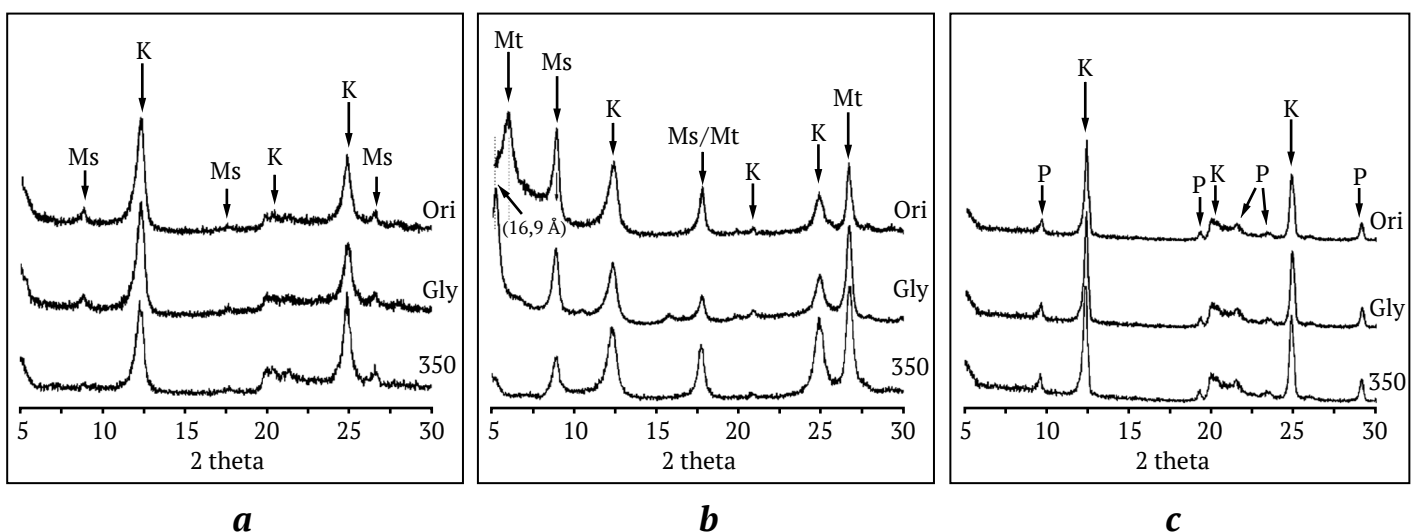


Fig. 4. X-ray diffraction pattern (XRD) of three samples (kaolin from weathered pegmatites (a), kaolin from weathered effusives (b) and kaolin-pyrophyllite (c)) with particle size < 2 μm under different test conditions: At room temperature (Ori); treatment with ethylene glycol (Gly); heating at 350 °C (350): K = kaolinite, Ms = muscovite, P = pyrophyllite and Mt = montmorillonite (in Figures hereinafter the kaolin from weathered effusives is denoted as K-Mag)

characteristic of kaolinite, indicating the significant presence of kaolinite in the samples [15–17]. Furthermore, the possible presence of quartz, in addition to kaolinite, is indicated by the bands detected in the samples at 789, 753, and 592 cm^{-1} .

Behavior of three samples under thermal action

Thermal analysis

The results of thermogravimetry/differential thermogravimetry (TG/DTG) of three samples (the kaolin from weathered pegmatites (*a*), the kaolin from weathered effusives (*b*), and the kaolin from altered rocks containing pyrophyllite (*c*)) are presented in Fig. 7. The thermal curves in Fig. 7 show the peaks of different processes (endothermic and exothermic processes) during heating. The endothermic processes occurring at low temperatures (around 79.7, 87.2, and 73.8 $^{\circ}\text{C}$) were desorption of surface H_2O and dehy-

dratation. The formation of metakaolinite phase is indicated by endothermic peaks at 494.8 $^{\circ}\text{C}$ for the kaolin from weathered pegmatite sample, 507.1 $^{\circ}\text{C}$ for the kaolin from weathered effusive sample, and 653.8 $^{\circ}\text{C}$ for the kaolin-pyrophyllite sample. The difference in the temperature of the endothermic peaks between the samples may be due to the differences in minerals morphology, composition and grain size. The kaolin-pyrophyllite sample has the highest endothermic peak temperature (653.8 $^{\circ}\text{C}$) among all the three samples, indicating the natural stability of kaolin of hydrothermal-metasomatic genesis. Analysis of the DTG data in Fig. 7 indicates a change in the weight of the tested materials during the heating process. The weight reductions were 9.77, 11.8, and 13.9% for the samples of the kaolin from weathered pegmatite, the kaolin from weathered effusives, and the kaolin-pyrophyllite, respectively.

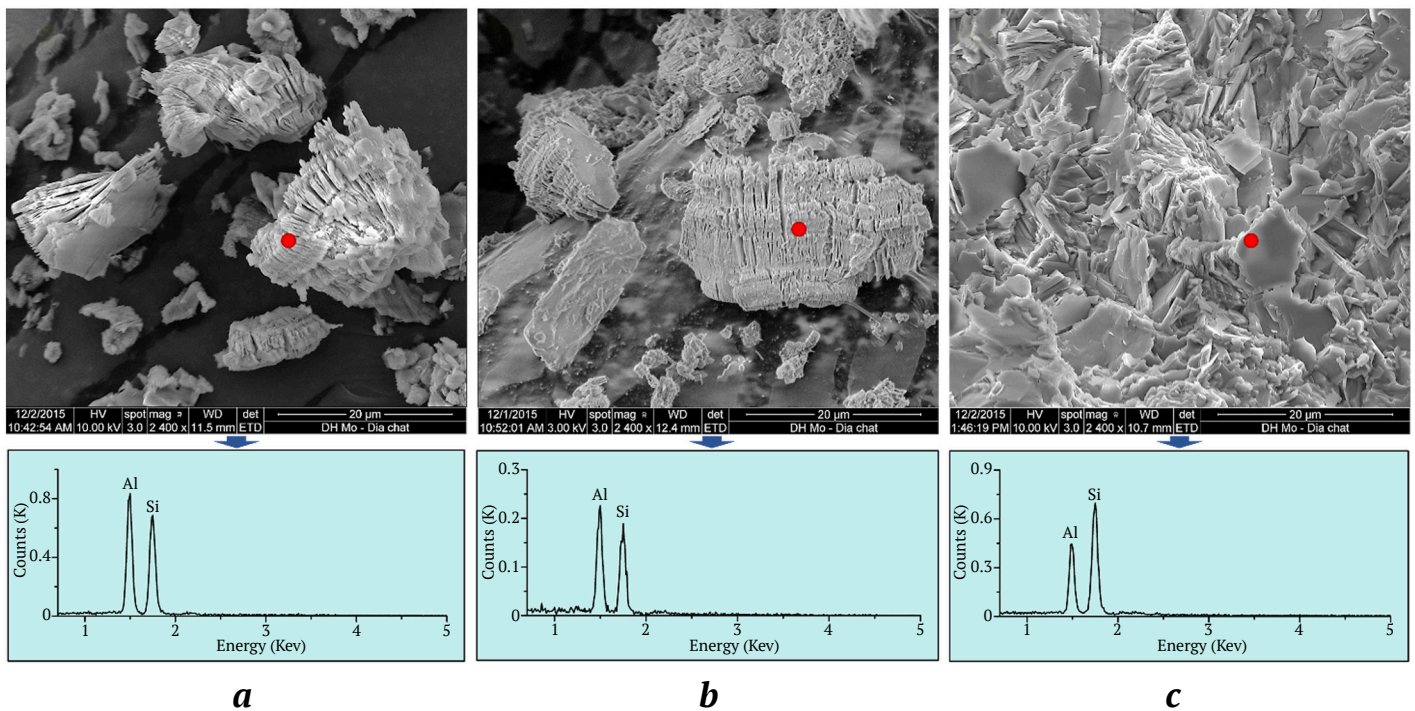


Fig. 5. SEM images and EDS results for three samples (kaolin from weathered pegmatites (*a*), kaolin from weathered effusives (*b*), and kaolin-pyrophyllite (*c*))

Chemical composition of three kaolin samples (EDS results)

Table 1

Sample	Chemical composition, % (from – to)							
	Na ₂ O	MgO	Al ₂ O ₃	SiO ₂	K ₂ O	CaO	TiO ₂	Fe ₂ O ₃
Kaolin from weathered pegmatites (<i>a</i>)	0.05–0.27	0.33–0.59	42.8–46.5	50.2–52.2	0.51–0.99	0.11–0.21	0.11–0.19	0.09–0.58
Kaolin from weathered effusives (<i>b</i>)	0.06–1.63	0.12–0.35	13.6–20.1	65.7–75.7	2.51–5.22	0.08–1.11	0.03–0.11	0.52–1.96
Kaolin–pyrophyllite (<i>c</i>)	0.21–1.30	0.05–0.56	10.5–38.6	11.5–89.3	0.16–1.20	0.05–1.42	0.05–1.35	0.03–2.51

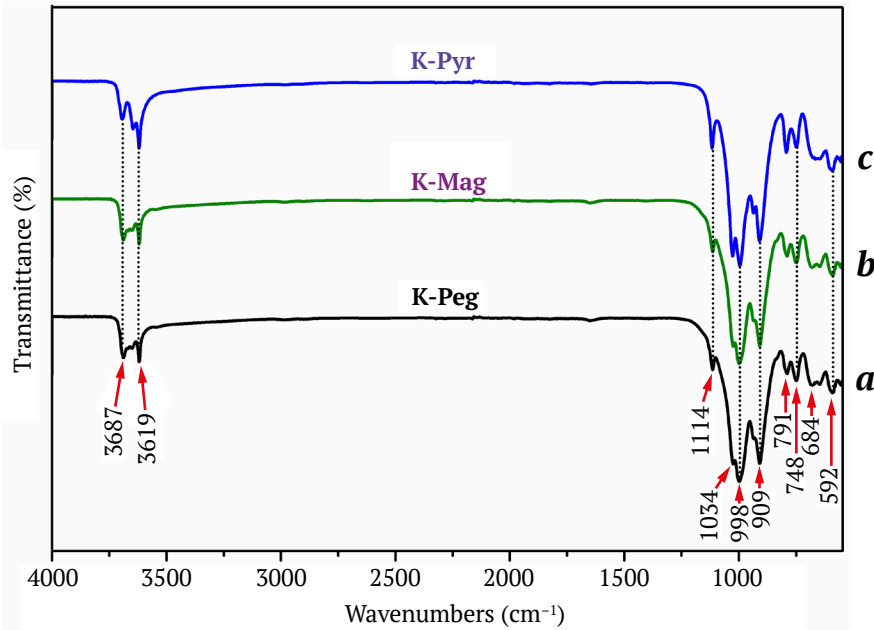


Fig. 6. FT-IR spectroscopy patterns of three samples (kaolin from weathered pegmatites (a), kaolin from weathered effusives (b) and kaolin-pyrophyllite (c))

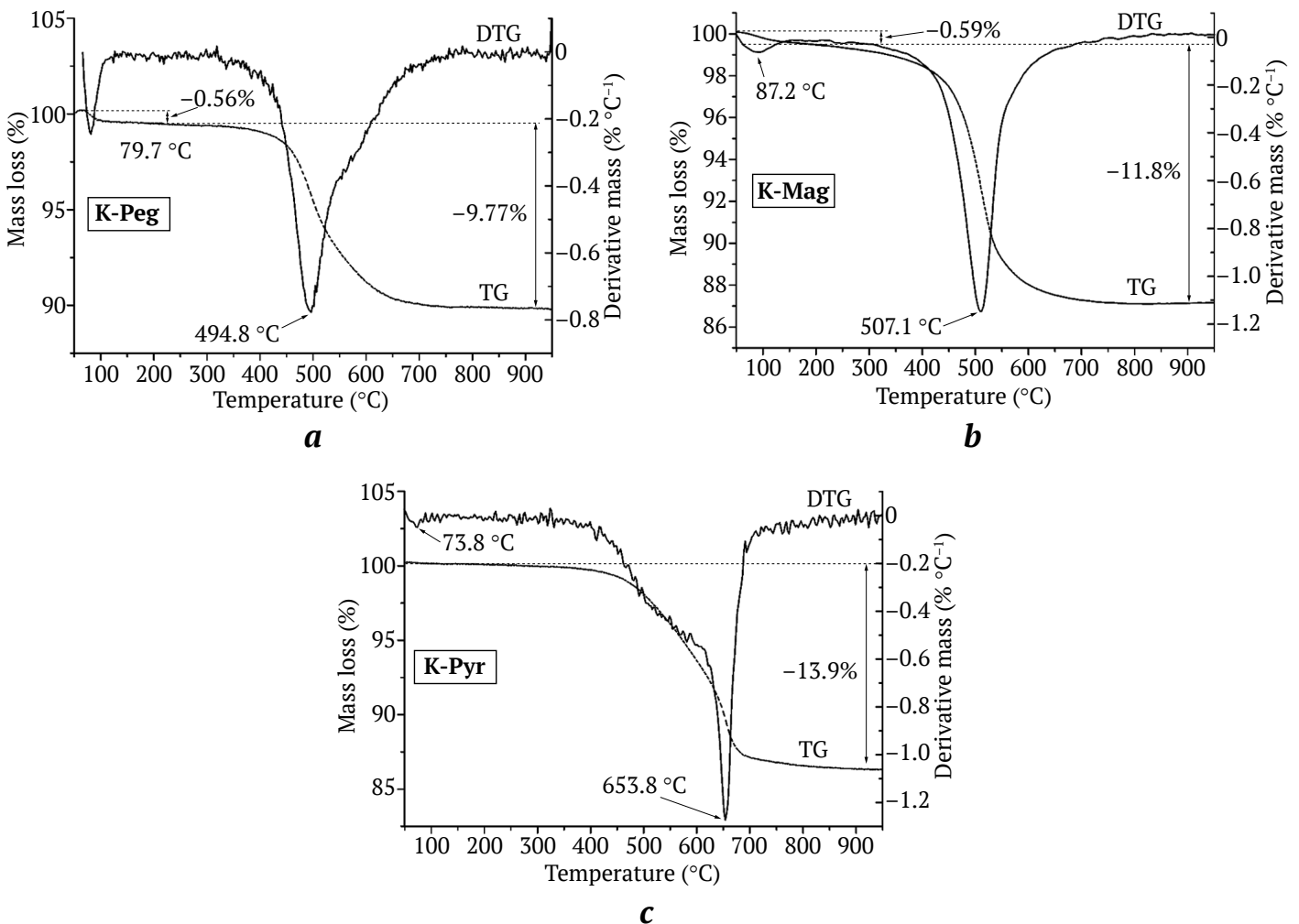


Fig. 7. Analysis of thermogravimetry/differential thermogravimetry (TG/DTG) study results for three samples (the kaolin from weathered pegmatites (a), the kaolin from weathered effusives (b), and the kaolin-pyrophyllite (the kaolin from altered rocks containing pyrophyllite) (c))

X-ray diffraction analysis

Fig. 8 shows the X-ray diffraction patterns of three samples (the kaolin from weathered pegmatites, the kaolin from weathered effusives, and the kaolin-pyrophyllite) at different temperatures (300, 500, 700, 900, and 1,100 °C). The analysis shows that the kaolin from weathered pegmatite sample consists mainly of kaolinite, but also quartz and muscovite are present. In contrast, the kaolin-pyrophyllite sample consists mainly of kaolinite and pyrophyllite, with minor quartz present. Over the entire temperature range from room temperature to 500 °C, the peaks in the X-ray diffraction (XRD) patterns corresponding to these minerals remain relatively stable, although they lose in intensity while the temperature increases. At 700 °C kaolinite peaks disappear in all the samples, while those of quartz and pyrophyllite remain. The disappearance of kaolinite peaks indicates transformation into metakaolinite characterized by amorphous structure, which is indicated by wide “bumps” on the X-ray diffraction patterns. Notably, the weak XRD peak of pyrophyllite at 700 °C emphasizes its thermal stability that is consistent with the thermal analysis findings and the hydrothermal-metasomatic genesis of pyrophyllite. The most significant changes in the X-ray diffraction patterns occur at 1,100 °C, which mean melting and destruction of the structures of the initial minerals with the formation of mullite,

a new mineral phase. This conclusion is consistent with the observations of previous studies [18, 19] emphasizing the dependence of mineralogical composition transformation during calcination on the initial mineralogical composition of samples. The presence of pyrophyllite in the kaolin-pyrophyllite sample markedly influences the phase transition, leading to the formation of new minerals.

SEM analysis

SEM images of three samples: kaolin from weathered pegmatites, kaolin from weathered effusives, and kaolin-pyrophyllite subjected to calcination at temperatures of 500 °C, 700 °C, 900 °C и 1100 °C are presented in Fig. 9. At 500 °C, a distinct minerals morphology is observed and mineral grain boundaries in all three samples remain discretely defined, indicating minimal impact on structural integrity and chemical bonds at this temperature. However, when the heating temperature is increased from 700 to 1,100 °C, noticeable transformations occur. In the interval from 700 to 900 °C, the morphology of minerals undergoes a gradual change, showing signs of melting. The differences between the initial substances in the samples begin to disappear. In particular, the SEM images at 1,100 °C clearly show melting manifestations, indicating that melting of the materials hides the initial boundaries and morphology of

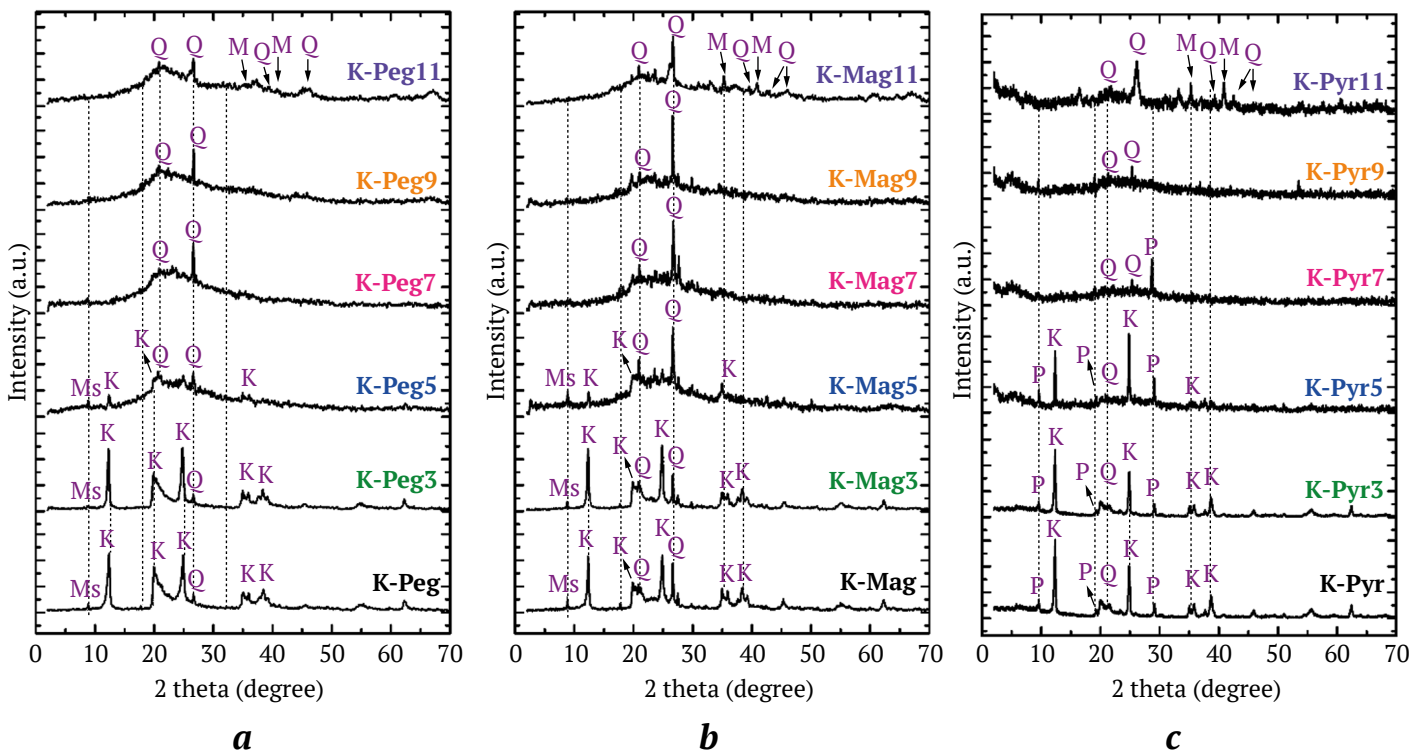


Fig. 8. X-ray diffraction patterns (XRD) of three samples (kaolin from weathered pegmatites (a), kaolin from weathered effusives (b), and kaolin-pyrophyllite (c)) at different temperatures (300 °C (3), 500 °C (5), 700 °C (7), 900 °C (9) и 1,100 °C (11)): K = kaolinite, Ms = muscovite, P = pyrophyllite, Q = quartz, M = mullite

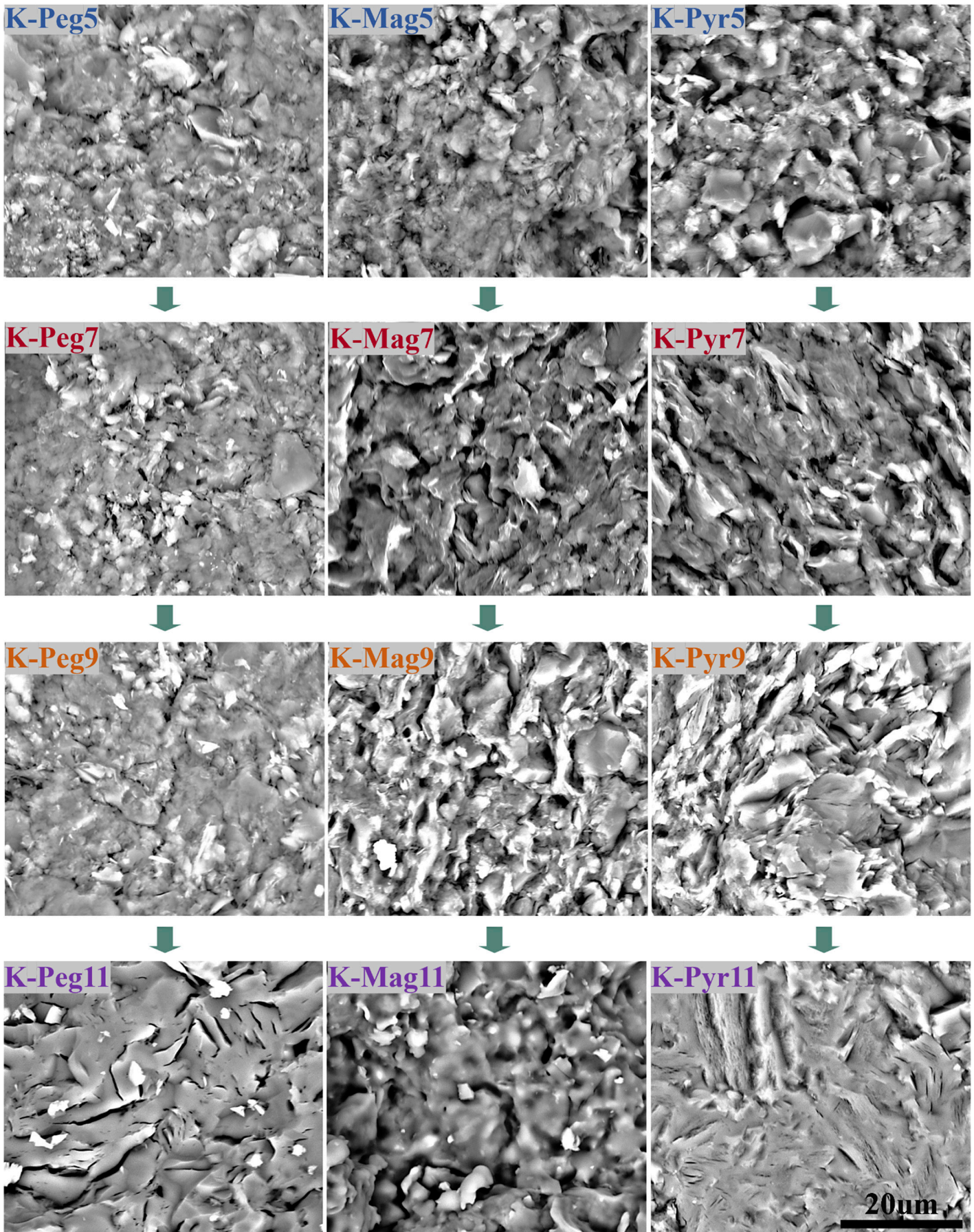


Fig. 9. SEM images of three samples (kaolin from weathered pegmatites, kaolin from weathered effusives, and kaolin-pyrophyllite) at different temperatures (500 °C (5), 700 °C (7), 900 °C (9), and 1100 °C (11))



the mineral grains. In the case of the kaolin-pyrophyllite sample, characterized by increased stability, the pyrophyllite morphology shows certain stability in the temperature range from 700 to 1,100 °C. The observed morphological changes in the samples at different calcination temperatures, as seen in the SEM images, are consistent with the other research findings, including XRD and FT-IR spectroscopy.

Conclusion

In this study, the fundamental characteristics of three types of kaolin obtained from different sources and of different genesis (from weathered pegmatites, weathered felsic effusives, and hydrothermal-metasomatic rocks), were evaluated using X-ray diffraction analysis (XRD), FT-IR spectroscopy (FT-IR), thermal analysis (thermogravimetry/differential thermogravimetry (TG/DTG)) and scanning electron microscopy with energy dispersive X-ray spectroscopy (SEM-EDS). The studies showed that kaolinite was the predominant mineral in all samples characterized by particle sizes less than 2 µm. In addition, the sample of kaolin from weathered pegmatite contains insignificant amounts of muscovite, and the sample of kaolin from weathered effusives contains montmorillonite. It is noteworthy that the

kaolin sample of hydrothermal-metasomatic genesis contains a relatively significant amount of pyrophyllite. The main chemical constituents of the kaolin samples are SiO₂ and Al₂O₃; in addition to these, K₂O + Na₂O, TiO₂ and iron are present in smaller quantities. Thermal analysis revealed phase transitions at different temperatures, with the metakaolinite phase formation around 494 and 507 °C in the kaolin samples from weathered pegmatites and weathered felsic effusives, respectively. The pyrophyllite-bearing kaolin sample (of hydrothermal-metasomatic origin) undergoes this phase transition at a higher temperature of 653.8 °C that indicates its natural stability. To evaluate the calcination behavior of the kaolins, the samples were pressed at a pressure of 40 MPa and calcined at temperatures ranging from 300 to 1,100 °C. XRD and SEM analyses showed that metakaolinitization starts around 500 °C in the kaolin samples from weathered pegmatites and weathered effusives, and around 700 °C in the pyrophyllite-bearing kaolin sample. The process of mullitization becomes evident at 1,100 °C, leading to the formation of a new mineral, mullite. The study findings presented here have key implications for the production of traditional ceramics using natural kaolin materials of different origins.

References

1. Laraba M. Enrichment of Algerian kaolin using froth flotation method. *Mining Science and Technology (Russia)*. 2023;8(3):215–222. <https://doi.org/10.17073/2500-0632-2023-04-112>
2. Muller J.P., Calas G. Genetic significance of paramagnetic centers in kaolinites. In: Murray H.H., Bundy W., Harvey C. (Eds.) *Kaolin, Genesis and Utilization. Special Publication 1*. Boulder, Colorado: The Clay Mineral Society; 1993. Pp. 261–290.
3. Fuentes I., Martínez F., Reátegui K., Bastos V. Physical, mineralogical and chemical characterization of Venezuelan kaolins for use as calcined clays in cement and concrete calcined. In: *Calcined Clays for Sustainable Concrete. Proceedings of the 1st International Conference on Calcined Clays for Sustainable Concrete*. 2015;10:565–566. https://doi.org/10.1007/978-94-017-9939-3_70
4. Milošević M., Logar M., Kaluđerović L., Jelić I. Characterization of clays from Slatina (Ub, Serbia) for potential uses in the ceramic industry. *Energy Procedia*. 2017;125:650–655. <https://doi.org/10.1016/j.egypro.2017.08.270>
5. Hernández A. C., Sánchez-Espejo R., Meléndez W., et al. Characterization of Venezuelan kaolins as health care ingredients. *Applied Clay Science*. 2019;175:30–39. <https://doi.org/10.1016/j.clay.2019.01.003>
6. Cam D.H., Phuong N. Types of formation origin and division of mine groups for exploration of kaolin mines in the Northeastern region of Vietnam. *Journal of Mining and Earth Sciences*. 2005;10:15–19. (In Vietnamese)
7. Bui H.B., Dung N.T., Khang L.Q., et al. Distribution and characteristics of nanotubular halloysites in the Thach Khoan area, Phu Tho, Vietnam. *Minerals*. 2018;8(7):290. <https://doi.org/10.3390/min8070290>
8. Cam D.H., Phuong N., Tri L.D. Potential of kaolin in the Northeast region and its use in industries. *Journal of Geology*. 2006;A/297:30–37. (In Vietnamese)
9. Tri L.Đ., Phuong N., Toan N.T. Vietnam's kaolin potential and orientation for exploration and exploitation to serve socio-economic. *Journal of Geology*. 2008;A/307:7–8. (In Vietnamese)
10. Luat T. (ed.), Boi L.V., Nhieu L.V., et al. *Report on preliminary exploration results of kaolin and feldspar in Son Man area, Hoang Lien Son*. Geological Department of Vietnam, Hanoi; 1981. (In Vietnamese)
11. Giua K.V. (ed.), et al. *Report on the results of geological exploration of Minh Tan kaolin mine, Hai Duong*. Geological Department of Vietnam, Hanoi; 1966. (In Vietnamese)



12. Duy T., Boc Đ.Đ., Thach N.V., et al. *Report on results of kaolin prospecting and exploration in northern Quang Ninh*. Geological Department of Vietnam, Hanoi. 1966. (In Vietnamese)
13. Fadil-Djenabou S., Ndjigui P.D., Mbey J.A. Mineralogical and physicochemical characterization of Ngaye alluvial clays (Northern Cameroon) and assessment of its suitability in ceramic production. *Journal of Asian Ceramic Societies*. 2015;3(1):50–58. <https://doi.org/10.1016/j.jascer.2014.10.008>
14. Ruiz Cruz M.D., Morata D., Puga E., et al. Microstructures and interlayering in pyrophyllite from the Coastal Range of central Chile: evidence of a disequilibrium assemblage. *Clay Minerals*. 2004;39(4):439–452. <https://doi.org/10.1180/0009855043940146>
15. Nallis K., Katsumata K., Isobe T., et al. Preparation and UV-shielding property of Zr_{0.7}Ce_{0.3}O₂-kaolinite nanocomposites. *Applied Clay Science*. 2013;80–81:147–153. <https://doi.org/10.1016/j.clay.2013.06.004>
16. Volzone C., Ortega J. Removal of gases by thermal-acid leached kaolinitic clays: Influence of mineralogical composition. *Applied Clay Science*. 2006;32(1–2):87–93. <https://doi.org/10.1016/j.clay.2005.11.001>
17. Caponi N., Collazzo C.C., Janh S.L., et al. Use of Brazilian kaolin as a potential low-cost adsorbent for the removal of malachite green from colored effluents. *Materials Research*. 2017;20(2):14–22. <https://doi.org/10.1590/1980-5373-MR-2016-0673>
18. Chen Y.F., Wang M.C., Hon M.H. Phase transformation and growth of mullite in kaolin ceramics. *Journal of the European Ceramic Society*. 2004;24(8):2389–2397. [https://doi.org/10.1016/S0955-2219\(03\)00631-9](https://doi.org/10.1016/S0955-2219(03)00631-9)
19. Nguyen T. T. T., Bui H. B. Characterization of some natural materials with different morphologies and their mullitization in ceramic preparation. *Journal of Ceramic Processing Research*. 2023;24(3):471–477. <https://doi.org/10.36410/jcpr.2023.24.3.471>

Information about the authors

Thi Thanh Thao Nguyen – PhD (Earth Sci.), Lecturer, Faculty of Geosciences and Geology Engineering, Hanoi University of Mining and Geology, Hanoi, Vietnam; ORCID [0000-0003-1299-2599](https://orcid.org/0000-0003-1299-2599); e-mail nguyenthithanhthao@humg.edu.vn

Hoang Bac Bui – PhD (Earth System Sci.), Associate Professor, Lecturer, Faculty of Geosciences and Geology Engineering, Hanoi University of Mining and Geology, Hanoi, Vietnam; ORCID [0000-0002-2671-3186](https://orcid.org/0000-0002-2671-3186), Scopus ID [57191982391](https://orcid.org/57191982391); e-mail buihoangbac@humg.edu.vn

Received 11.12.2023

Revised 16.01.2024

Accepted 06.02.2024



SAFETY IN MINING AND PROCESSING INDUSTRY AND ENVIRONMENTAL PROTECTION

Research paper

<https://doi.org/10.17073/2500-0632-2023-08-147>

UDC 622.4

Experimental study on forced ventilation in dead-end mine working with various setbacks of the ventilation pipeline from the working face

A. A. Kamenskikh , G. Z. Faynburg  , M. A. Semin   , A. V. Tatsiy *Mining Institute of the Ural Branch of the Russian Academy of Sciences,
Perm, Russian Federation* seminma@inbox.ru

Abstract

The study of airflow patterns at the ends of dead-end mine workings is crucial for optimizing underground mining ventilation systems. Understanding these patterns forms the basis for designing and implementing effective ventilation strategies.

Previous studies have shed light on the behavior of the main vortex and the formation of stagnant zones in such environments, but these insights remain fragmented and call for a more systematic exploration to integrate them into a comprehensive theory.

This paper presents the results of a thorough field investigation into the forced ventilation behavior in a dead-end mine working with a significant cross-sectional area (29.2 m²). We evaluated the impact of varying the setback distance of the ventilation duct's end from the working face at intervals of 10, 15, 17, 19, and 21 m. The experimental design included precise measurements of turbulent airflow velocities at 25 carefully chosen points (in a 5x5 grid) for each setback distance, covering the area from the working face to beyond the end of the ventilation duct. This included additional measurements taken 1 meter and 10 meters past the termination of the ventilation duct, moving towards the entrance of the working area.

The fieldwork was carried out in a typical dead-end stope at the Kupol gold-silver mine in the Chukotka Autonomous District, created by drilling and blasting.

The volume of fresh air delivered to the working was maintained at a consistent rate of 17.4 m³/s across all scenarios, aligning with the mine's standard air flow rate derived from the ventilation requirement for exhaust gases emitted by internal combustion engines of Load-Haul-Dump (LHD) machinery. With the duct's terminal cross-sectional area at 0.8 m², this resulted in an inflow velocity averaging 21.75 m/s.

Additionally, we included insights from three-dimensional numerical simulations performed in ANSYS Fluent, focusing on steady-state air movement and developed turbulence within the dead-end space. A comparative review of both empirical and modeled data shows that the ventilation jet, for all tested setback distances up to 21 m, successfully delivered air to the working face, where it then dispersed and initiated reverse flow patterns.

These experiments led to the formulation of a linear relationship between the maximum relative velocity (compared to the initial jet velocity) at a distance of 1 m from the working face and a key geometric factor of the ventilation setup. This factor is the ratio of the duct's setback distance to a characteristic dimension of the cross-sectional area, calculated as the square root of the cross-sectional area.

Keywords

mine ventilation, dead-end face, forced ventilation, ventilation pipeline setback, field experiment, numerical experiment, airflow structure

Funding

The research received financial support from the Ministry of Science and Higher Education of the Russian Federation (reg. number NIOKTR 124020500030).

For citation

Kamenskikh A. A., Faynburg G. Z., Semin M. A., Tatsiy A. V. Experimental study on forced ventilation in dead-end mine working with various setbacks of the ventilation pipeline from the working face. *Mining Science and Technology (Russia)*. 2024;9(1):41–52. <https://doi.org/10.17073/2500-0632-2023-08-147>



ТЕХНОЛОГИЧЕСКАЯ БЕЗОПАСНОСТЬ В МИНЕРАЛЬНО-СЫРЬЕВОМ КОМПЛЕКСЕ И ОХРАНА ОКРУЖАЮЩЕЙ СРЕДЫ

Научная статья

Экспериментальные исследования проветривания тупиковой выработки нагнетательным способом при различном отставании вентиляционного трубопровода от груди забоя

А. А. Каменских , Г. З. Файнбург  , М. А. Семин   , А. В. Таций 

Горный институт УрО РАН, г. Пермь, Российская Федерация

 seminma@inbox.ru

Аннотация

Исследование структуры вентиляционных потоков в призабойной части тупиковой выработки является важным элементом при целенаправленном управлении ее проветриванием и обеспечении безопасности ведения подземных горных работ. Ранее проведенные исследования показывают, что, несмотря на общее понимание протекающих в тупиковой выработке процессов возникновения основного вихря и застойных зон, полученные результаты носят фрагментарный характер и без дополнительных исследований практически не поддаются единому концептуальному обобщению.

В статье приведены результаты детального натурного эксперимента по исследованию процессов нагнетательного проветривания тупиковой выработки большого сечения ($29,2 \text{ м}^2$) с пятью различными вариантами отставания конца нагнетательного вентиляционного трубопровода от груди забоя: 10, 15, 17, 19 и 21 м. Для каждого варианта в соответствии с разработанной методикой эксперимента производили замеры скорости турбулентного вихревого воздушного потока в 25 различных характерных точках (сетка 5×5) в каждом сечении тупиковой горной выработки, которые выбирали через каждый метр от груди забоя до конца вентиляционного става, а также дополнительно еще через 1 м и еще через 10 м от конца вентиляционного става к устью выработки.

Исследования проводили в стандартной тупиковой очистной выработке, проходимой буровзрывным способом, на золотосеребряном руднике «Купол», расположенном в Чукотском автономном округе.

Расход подаваемого в выработку свежего воздуха во всех случаях сохраняли постоянным и равным типичному для рудника расходу $17,4 \text{ м}^3/\text{с}$, определяемому расчетным значением по фактору проветривания выхлопных газов от двигателей внутреннего сгорания погружно-доставочных машин. При площади сечения конца трубопровода $0,8 \text{ м}^2$ это дает среднюю скорость поступающей струи в $21,75 \text{ м}/\text{с}$.

Данные натурного эксперимента дополняли результатами трехмерного численного моделирования в вычислительном пакете ANSYS Fluent. Исследовали стационарное движение воздуха в тупиковой выработке в режиме развитой турбулентности. Сравнительный анализ полученных результатов натурного и численного экспериментов убедительно показал, что во всех исследуемых случаях отставания (не более 21 м) вентиляционного трубопровода от груди забоя вентиляционная струя, выходящая из вентиляционного трубопровода, достигает груди забоя, а затем разворачивается вдоль него с различной интенсивностью и формирует обратное движение воздушного потока из тупика.

Полученные результаты позволили получить линейное уравнение связи между максимальной относительной (к начальной скорости струи) скоростью на расстоянии 1 м от груди забоя и основного геометрического фактора зоны проветривания – отношения длины отставания конца трубопровода к характерному поперечному размеру – корню квадратному из площади поперечного сечения.

Ключевые слова

рудничная вентиляция, тупиковый забой, нагнетательный способ проветривания, отставание вентиляционного трубопровода, натурный эксперимент, численный эксперимент, структура воздушных потоков

Финансирование

Исследования выполнены при финансовой поддержке Министерства науки и высшего образования РФ (рег. номер НИОКТР 124020500030-7).

Для цитирования

Kamenskikh A. A., Faynburg G. Z., Semin M. A., Tatsiy A. V. Experimental study on forced ventilation in dead-end mine working with various setbacks of the ventilation pipeline from the working face. *Mining Science and Technology (Russia)*. 2024;9(1):41–52. <https://doi.org/10.17073/2500-0632-2023-08-147>



Introduction

Ensuring the reliability of effective ventilation within dead-end workings of mines represents a paramount concern in the domain of mine ventilation, governed by the regulatory frameworks of safety in underground mining operations¹. This issue garners significant attention from both domestic [1–3] and international [4–6] researchers, as evidenced by an extensive body of literature. The scholarly discourse encompasses an array of topics, including the peculiarities of ventilating dead-end workings across various mining methodologies [7, 8], as well as the issues of aerological process modeling within such environments. This entails the judicious selection of turbulence models [6] and the employment of discrete modeling approaches [9]. Research has delved into several exacerbating factors, such as the persistent dust emission during the operation of mining combines [10], gas emission within the excavated spaces [8, 11], and the analysis of oxygen transfer as a distinct component of the atmospheric milieu [5]. The literature also explores diverse criteria for assessing the ventilation efficiency of dead-end workings [4].

A critical facet of optimizing the ventilation of dead-end workings lies in the selection of ventilation methodologies and equipment parameters, including the placement of the ventilation pipeline and the regulation of airflow within [12]. Among the prevalent practices in this realm is the application of forced ventilation, characterized by the generation of an active air jet delivered via a pipeline. The terminal segment of this pipeline is intentionally positioned a specified distance from the working face, either to accommodate operational exigencies or to comply with safety regulations [6, 13].

The principal geometric determinants of the ventilation zone's volume (V) are the working's height (H) and width (B) – that is, the effective scale of the cross-sectional area (S) – as well as the distance by which the end of the ventilation conduit is set back from the working face (L). This distance shapes the overall configuration of the ventilated space [14]. Let us define the form factor of the ventilated object as the dimensionless measure of the setback distance of the pipeline's end from the working face, expressed in

units equivalent to the square root of the cross-sectional area $f = L / \sqrt{S}$.

The calculation of the ventilation zone's volume is contingent upon the specific variables and context, with V equating to either $H \cdot B \cdot L$ or $S \cdot L$. Alternatively, it may be approximated to the volume of the flue gas exhaust zone, as ascertained through the application of empirical data and analytical methods.

The efficacy of ventilation and the balance between the processes of contaminated air displacement and its mixing with fresh air are fundamentally determined by the flow rate of fresh air (Q_0) allocated for ventilation purposes. This flow rate, in conjunction with a specified pipeline diameter (d) or cross-sectional area (s) dictates the average velocity (U_0) of the ventilation jet. This jet, in turn, shapes the flow structure within the dead-end working, influenced by the degree of jet constriction, $F = s/S = (d/D)^2$, which varies between 0 and 1, alongside various other factors that govern the balance between displacement and mixing processes within the ventilated area.

The primary metric of ventilation effectiveness is the air quality at the working face under all conditions, and in the context of non-steady-state scenarios, it is the duration required for ventilation to clear contaminants, such as flue gases following drilling and blasting operations. The determination of the requisite fresh air flow rate is predicated upon achieving designated air quality benchmarks.

Given the complexity of flow dynamics and the indeterminate nature of the ratio between displacement and mixing processes, accurately gauging the actual ventilation duration is feasible solely through comprehensive, field experimentation.

In practical terms, for determining the ventilation duration, practitioners rely on the estimated air exchange time (τ) for a specific volume of contaminated air (V) expressed as

$$\tau = \frac{V}{Q}, \quad (1)$$

where Q is the rate of air supplied to the ventilated volume V .

The minimum time required to ventilate the face is realized when ideal displacement (advective transfer) processes dominate within the ventilated zone, as determined by Equation (1). Conversely, in scenarios where ideal mixing processes (thorough mixing, dilution) prevail, coupled with the presence of stagnant zones, the theoretical ventilation duration for a dead-end face is effectively infinite. The actual ventilation timeframe spans these broad extremities.

A crucial prerequisite for preventing stagnant zones at the working face and ensuring the dominance

¹ Uniform safety rules for developing ore, nonmetallic and alluvial deposits by underground mining. Appr. by Gosgortekhnadzor of the USSR on 21.10.1954, Moscow: Gosgortekhzizdat, 1959.

Federal Rules and Regulations in Industrial Safety “Safety rules in mining works and processing of solid minerals”, appr. on 08.12.2020, No. 505. Electronic text. CODEX Consortium. Electronic Fund of Legal and Regulatory Technical Documentation: official website. URL: <https://docs.cntd.ru/document/573156117> (date of access: 20.06.2023).



of displacement processes is the generation of an active jet. To this end, the jet must maintain its integrity over a distance (L_{eff}) greater than the setback from the working face (L) thereby actively “sweeping” over the working face to facilitate the efficient removal of gassed and dusty air from the vicinity of the face and the face itself. This criterion can be articulated as

$$L < L_{rated} < L_{eff} \tag{2}$$

where L_{rated} is the maximal permissible setback distance as prescribed by safety regulations.

Therefore, analyzing the flow structures in the proximity of the working face within a dead-end working is imperative for the deliberate design of its ventilation system. This analysis underscores the significance of the effective range of the jet, L_{eff} , the setback of the pipeline's end from the working face L and the flow rate of fresh air supplied Q_0 the cross-sectional dimensions of both the working and the pipeline.

Foundational Concepts of Airflow Patterns in Dead-End Workings with Forced Ventilation

Over half a century ago, significant advancements in the study of ventilation within dead-end mine workings (also known as airless ends) were made I.A. Shvyrkov [1], A.I. Ksenofontova [2], V.N. Voronin [3], P.I. Mustel [15], among others [16–18]. These researchers undertook theoretical examinations of jet ventilation in dead-end chamber-shaped workings, establishing foundational concepts on the mechanisms for removing contaminated air from the face through mixing and displacement. Additionally, they elucidated the relationship between the cross-sectional area of the working and the efficiency of jet action [18]. A key formula emerging from their work is:

$$L_{eff} = K\sqrt{S}, \tag{3}$$

where K is a dimensionless proportionality coefficient, determined either experimentally or theoretically, and typically varies widely in practice (from 2 to 8, but most commonly within 3–6) [14]. This variation underscores the dependence of K on other ventilation arrangement conditions and highlights the need for relatively large-scale studies for further elucidation.

This formula (3) can be reformulated as:

$$\frac{L_{eff}}{\sqrt{S}} = k \frac{L}{\sqrt{S}}, \tag{4}$$

where k is a new coefficient related to K by the formula $K = kf$, facilitating the delineation of the form factor f . From this, it can be inferred that $k > 1$.

Notably, for a classical ventilation pipeline setback L of 10 m, the form factor with a working cross-sectional area of 3×3 is 3.33, and for a size of

2×2 , it is 5. A setback of 15 m, permissible under current safety regulations for working cross-sections larger than 16 m^2 , yields a form factor of $f = 3.75$.

In various international studies [4, 6, 13], formula (3) is presented as

$$L_{eff} = 4\sqrt{S} \tag{5}$$

or alternatively, utilizing the ventilation pipeline diameter d , as

$$L_{eff} = 30d. \tag{6}$$

It's important to note that the concept of jet range, denoted as L_{eff} while intuitively understood, lacks a formal definition, leading to varied interpretations and the coefficient K in formula (3) fluctuating based on factors like working cross-section, pipeline location, its cross-section, jet velocity, and other ventilation conditions.

The termination of the total air flow rate towards the working face, discounting turbulent pulsations, marks the end of the jet. This distance, denoted as L_{eff} , represents the range the jet “reaches”. Defining this distance more rigorously allows for a more precise determination of the airflow rate sufficient for effective ventilation in a given cross-section near the working face. This determined airflow rate, deemed sufficient for effective ventilation at or near the working face, is labeled Q_{face} . It is calculated to ensure that the time required to ventilate the space immediately adjacent to the working face, denoted V_{face} , is less than or equal to the time needed to ventilate the entire face, expressed as:

$$t_{eff} = \frac{V_{face}}{Q_{face}} \leq t_{face} = \frac{V}{Q_0}. \tag{7}$$

The area between the working face and the cross-section positioned 1 meter away from it can be selected as the size of the near-face space. This selection is informed by the dimensions of the human breathing zone, defined as a radius of 0.5 meters from the worker's face, in accordance with SNiP 41 01 2003 standards. This distance, leading to the terminus of the pipeline's trajectory related to this area, is denoted as L_1 .

The volume of air entering this specified zone can be quantified by referencing the minimum velocity stipulated by safety regulations. The calculation employs the formula $U_{min} = 0,1 P/S$ (m/s), where S represents the cross-sectional area of the working, m^2 ; and P stands for the perimeter of the working, m. For the conditions outlined in our experiment, this results in a velocity of 0.07 meters per second. It is crucial to underscore that this velocity constitutes merely 0.32% of the initial velocity ($U_0 = 21.75 \text{ m/s}$) of the jet as it exits



the ventilation pipeline, as evidenced by the data from the comprehensive field experiment.

It's noteworthy that the air velocity detectable by humans and vane anemometers is approximately 0.15 m/s, which corresponds to 0.69% of the initial jet velocity U_0 . Furthermore, the traditional minimum velocity prescribed for stopes, fixed at 0.25 m/s, represents 1.15% of U_0 . In the context of our field experiment, this implies that the time required to ventilate the space near the face, positioned 1 meter from the working face, amounts to 8 s.

Empirical evidence indicates that the efficacy of the jet within the dead-end (constrained area) is enhanced by enlarging the cross-section of the working. This enhancement is attributed to the ability of the jet to extend over greater distances within larger cross-sectional workings without being impeded by the resistance of the return flow. The occurrence of this return flow within the dead-end is an inevitable consequence, dictated by the principles of mass conservation and the continuity equation.

Previously, the investigation into the complex, three-dimensional vortex-like structures created by forced ventilation methods was hindered by the limited scope of analytical techniques. However, advancements in computational methodologies and the expansion of computer processing capabilities have led to an increased adoption of mathematical modeling tools in a three-dimensional framework. This approach has significantly enhanced research into the ventilation processes within dead-end mine workings, as evidenced by studies [7, 8, 19].

For example, N. O. Kaledina and S. S. Kobylkin [16] leveraged numerical three-dimensional modeling techniques to explore ventilation strategies for dead-end extended workings in gas-rich mines. In such environments, the prevalent release of light, combustible gases poses a considerable risk to mining safety. E. V. Kolesov and B. P. Kazakov [18] applied these numerical three-dimensional modeling methods to investigate the effectiveness of ventilation systems in dead-end mine workings post-blasting operations.

Article [20] explores the ventilation challenges in dead-end mine workings, focusing on the effects of variations in the distance of the ventilation pipeline from the working face and different air jet velocities from the ventilation pipeline on ventilation effectiveness.

This body of research engages in a thorough examination of the selected turbulence models, the methodologies for numerical solutions, and the outcomes achieved, often tailored to a handful of specific scenarios.

The comprehensive review of these studies reveals that while there's a broad consensus on the

existence and behavior of primary vortex and stagnant zones within dead-end workings, the findings are somewhat piecemeal. The current understanding and results, though insightful, are not universally applicable or conceptually cohesive without the prospect of further, more targeted research endeavors.

Field experimental data on forced ventilation in dead-end mine workings are notably less prevalent than those obtained from computational experiments, primarily focusing on the duration of face ventilation and the overall penetration of the jet into the dead end.

Historically, a crucial standard² or forced ventilation in these settings was to maintain the distance from the end of the ventilation duct to the working face at no more than 10 meters. This standard was suitable for the use of 400–600-mm pipes and low-power fans, which matched the typical dead-end working dimensions of the era, approximately 2×2 m in cross-section (with a form factor of $f = 5$). However, contemporary updates to the regulatory framework, as exemplified by the revised FNiP PB³, now acknowledge the feasibility of extending this setback up to 15 m from the working face, provided that the face cross-section exceeds 16 m^2 (indicating a form factor of $f < 3.75$).

Despite this regulatory shift, practical implementation often faces challenges, as indicated by safety justifications reviews such as in [18]. These challenges highlight the need for a deeper, scientifically grounded comprehension of the ventilation dynamics within dead-end workings. This is the core focus of the current study.

Below are the findings from comprehensive field research on forced ventilation in dead-end stopes at the Kupol gold-silver mine, specific to its conditions. These are accompanied by selected results from numerical modeling that enhance the insights gained from the field experiment.

Subject of the Field Study

The Kupol mine, situated in the Far North-East of the Russian Federation within the permafrost zone, adopts specific measures to counteract rock thawing and enhance stability. Here, underground workings are ventilated using a forced method, with air entering the mine at temperatures of -20°C or lower, without

² Uniform safety rules for developing ore, nonmetallic and alluvial deposits by underground mining. Appr. by Gosgortekhnadzor of the USSR on 21.10.1954, Moscow: Gosgortekhnizdat, 1959.

³ Federal Rules and Regulations in Industrial Safety "Safety rules in mining works and processing of solid minerals, appr. on 08.12.2020, No. 505. Electronic text. CODEX Consortium. Electronic Fund of Legal and Regulatory Technical Documentation: official website. URL: <https://docs.cntd.ru/document/573156117> (date of access: 20.06.2023).



the need for heating. This location is not considered hazardous in terms of gas or dust presence.

Mining operations, including development, preparatory work, and stoping at the Kupol mine, are executed via the drilling and blasting method. This approach is necessitated by the high strength characteristics of the ores and rocks encountered. Drilling and blasting activities are organized into two shifts per day, incorporating two-hour breaks between shifts and two lunch breaks. During these working shifts, drilling and the transportation of blasted ore take place, while blasting operations are scheduled between shifts and during lunch breaks.

The mining cycle encompasses not just drilling, charging, and blasting of blast-holes, along with the loading and transportation of blasted ore from the face, but also ventilation of the face and ensuring its safety post-operation. High-performance self-propelled equipment is employed for the principal tasks of the drivage cycle.

Dead-end faces at the Kupol mine vary in length from 15 to 150 m, boasting an average cross-section of 29.2 m² in the light, and an average advance of 4.2 m per blast. The majority of the blasted ore is displaced by blasting to a range of 10–15 m from the working face, though some fragments can reach up to 40 m, posing a risk to the ventilation pipeline. Consequently, considering the length of the LHD machines with internal combustion engines is about 12 m, it's advisable to maintain a setback of approximately 20 m for the ventilation duct from the working face.

The pressure pipeline, typically mounted on the right side under the roof of the working area and having a diameter of 1.2 m (with a cross-sectional area of 1.13 m²), employs a technique to mitigate end oscillations (termed “squelch”) and associated flow pulsations. This is achieved by narrowing the ventilation pipeline at the outlet to form a “contraction cone”, a practice standard across all forced ventilation pipelines at the Kupol mine. The cross-sectional area at the “nozzle” of this “contraction cone” is between 0.75 and 0.8 m², resulting in a contraction degree of 1.4, which improves the stability of the jet flow and extends its effective range.

Experimental Approach and Methodology

Experimental studies were conducted in a dead-end mine working (crossdrift NE 931-250) at the Kupol mine. An industrial mine fan, the Alphair 4200-VAX-2700 VMP, with a rated capacity of 17.9 m³/s and head of 233.5 daPa, was in operation, supplying ventilation to the pressure pipeline.

Air velocity measurements were taken in a steady-state flow mode, achieved by directing a fresh air jet at

a flow rate of 17.4 m³/s (initial jet velocity of 21.75 m/s) towards the face.

The study evaluated five variations in the distance between the ventilation pipeline's end and the working face. The initial setup included a conventional 10-m setback, followed by a 15-m setback as permitted by safety regulations for workings with a cross-section larger than 16 m². Experimental setups included setbacks of 17, 19, and 21 m, with the latter being of particular interest for its practical applicability and acceptance by the Kupol mine management.

To thoroughly examine the flow's spatial structure, the air space at the dead-end face was mapped with a grid of velocity measurement points across various cross-sections. In each selected cross-section, velocities were measured at 25 points (forming a 5 × 5 grid with 0.75 m between points, approximating 1 m near the walls).

Cross-sections for measurement were arranged sequentially from the working face (1, 2, 3, 4... m), including one 1 m from the flight's end towards the working face. Measurements were also conducted at two additional cross-sections, one 1 m from and another 10 m from the flight's end towards the mine's entrance, with the latter cross-section assessing the outflow from the working. Incoming and outgoing airflow rates were compared to verify the data. This comprehensive mapping allowed for a detailed analysis of the flow's spatial dynamics.

Airflow velocities were measured using two APR-2 anemometers, with an error margin of $\pm(0.2 + 0.05U)$ m/s, where U denotes the airflow velocity. Distances within the dead-end working were measured using a Leica DISTO D3 laser distance gauge, accurate to ± 1.5 mm.

Additional insights and the flow's spatial dynamics were further delineated through three-dimensional mathematical modeling in the ANSYS Fluent software.

Both empirical and numerical simulations identified consistent flow patterns within the dead-end working under forced ventilation and varying pipeline setbacks of 15–21 m (with form factor of $f = L/\sqrt{S} = 2.78, 3.14, 3.52, 3.89$).

A 10-m setback was also examined for comparison, given its lower form factor ($f = 1.85$), which is not typically practiced.

Results of field and numerical experiments

When the ventilation duct's end is positioned 15–21 m from the working face, which has a cross-sectional area of 29.2 m², injected air jet broadens and generates a substantial primary vortex that encompasses the whole area being ventilated. This obser-

vation aligns with well-established concepts derived from previously published research.

The creation of this vortex is a consequence of the mass conservation principle (continuity equation) and is consistent across various implementations of forced ventilation. This has been validated through comprehensive field and computational experiments, which have also uncovered new insights.

Let us outline the key patterns of the vortex flow that emerges when a constricted jet enters a dead-end face.

The core dynamics of the vortex flow initiated by the inflow of a constricted jet to a dead-end face can be summarized as follows: The flow rate of fresh air in the incoming jet (Q_0) equals the flow rate of air exiting the dead-end face (Q_-). Therefore, by the law of conservation of mass, the average cross-sectional velocities of the incoming jet (U_0) and the exiting air (U_-) near the working's entrance are proportional to the cross-sectional area of the working (S) relative to the cross-sectional area of the pipeline (s).

It can be deduced that the ratio of the kinetic energy of the incoming flow E_0 , as determined by U_0 , to the kinetic energy of the outgoing flow E_- , as determined by U_- , is equivalent to the ratio of the jet velocity at the initial cross-section to the air velocity exiting the dead-end working.

In algebraic terms, the foundational equations of forced ventilation, assuming constant density, are as follows:

$$\frac{U_0}{U_-} = \frac{S}{s}, \quad \frac{E_0}{E_-} = \frac{U_0^2 s}{U_-^2 S} = \frac{U_0}{U_-} = \frac{S}{s}. \quad (8)$$

From these equations, it's clear that a larger S/s ratio indicates a more powerful jet, capable of expending more energy on vortex formation (including turbulent pulsations) and penetrating the working face. In our case, this ratio is 36.25. For comparison, a traditional working of 4 m² (2 m × 2 m) with a 400-mm pipeline has a smaller ratio of 31.85, similar to a 16 m² working with an 800-mm pipeline.

Figure 1, produced from numerical modeling for the maximum permissible setback in workings larger than 16 m² with a 15 m distance from the working face, vividly shows how the jet impinges on the working face and scatters. This effectively aerates the area adjacent to the working face and triggers the return flow. The modeling was performed in ANSYS Fluent software, set to a steady-state with the Realizable k-epsilon turbulence model [21–23].

Since the axis of the ventilation pipeline is conveniently located at the top right (from the perspective of facing the working face), the cross-section of the working, aerodynamically speaking, is divided into two zones. The “concurrent” zone is adjacent to the axis of the ventilation jet in the upper right corner of the working cross-section, conceptually separated by a diagonal from the upper left to the lower right. In this zone, the air drawn by the active jet moves toward the working face. The opposite side is the “return” zone, where air flows away from the working face.

This fundamental large-scale flow pattern is evident in both the field experiment (in Fig. 2, a, b) and the computational modeling (Fig. 3), outlining the overall structure of air movement at the face.

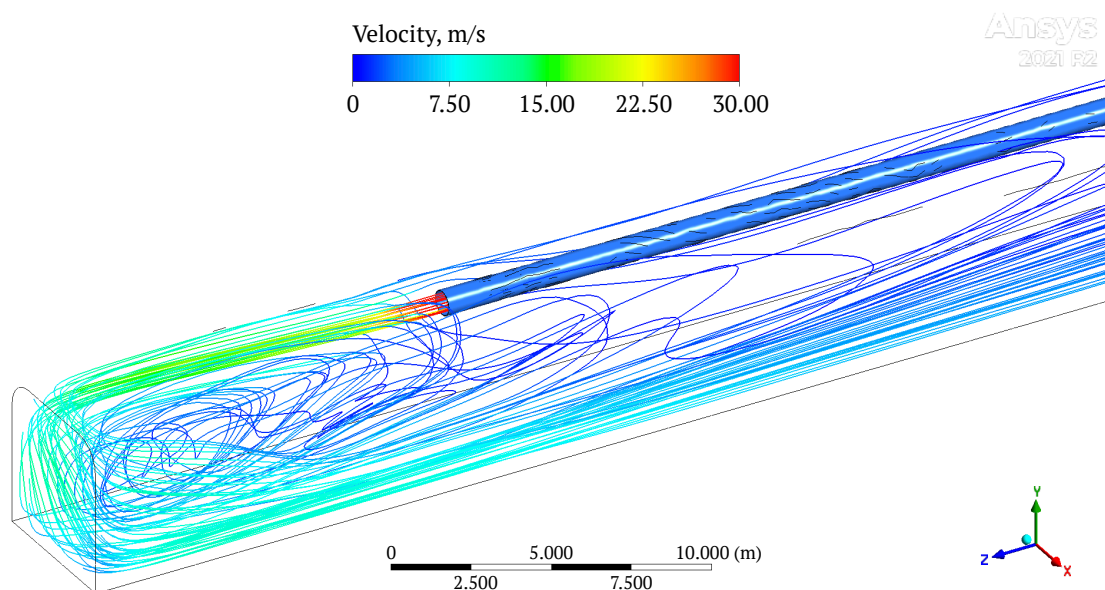


Fig. 1. Illustration of the spatial structure of streamlines with color coding corresponding to the magnitude of the velocity vector during forced ventilation in a dead-end working, showcasing the ventilation duct end setback 15 m from the working face where the jet impacts the working face

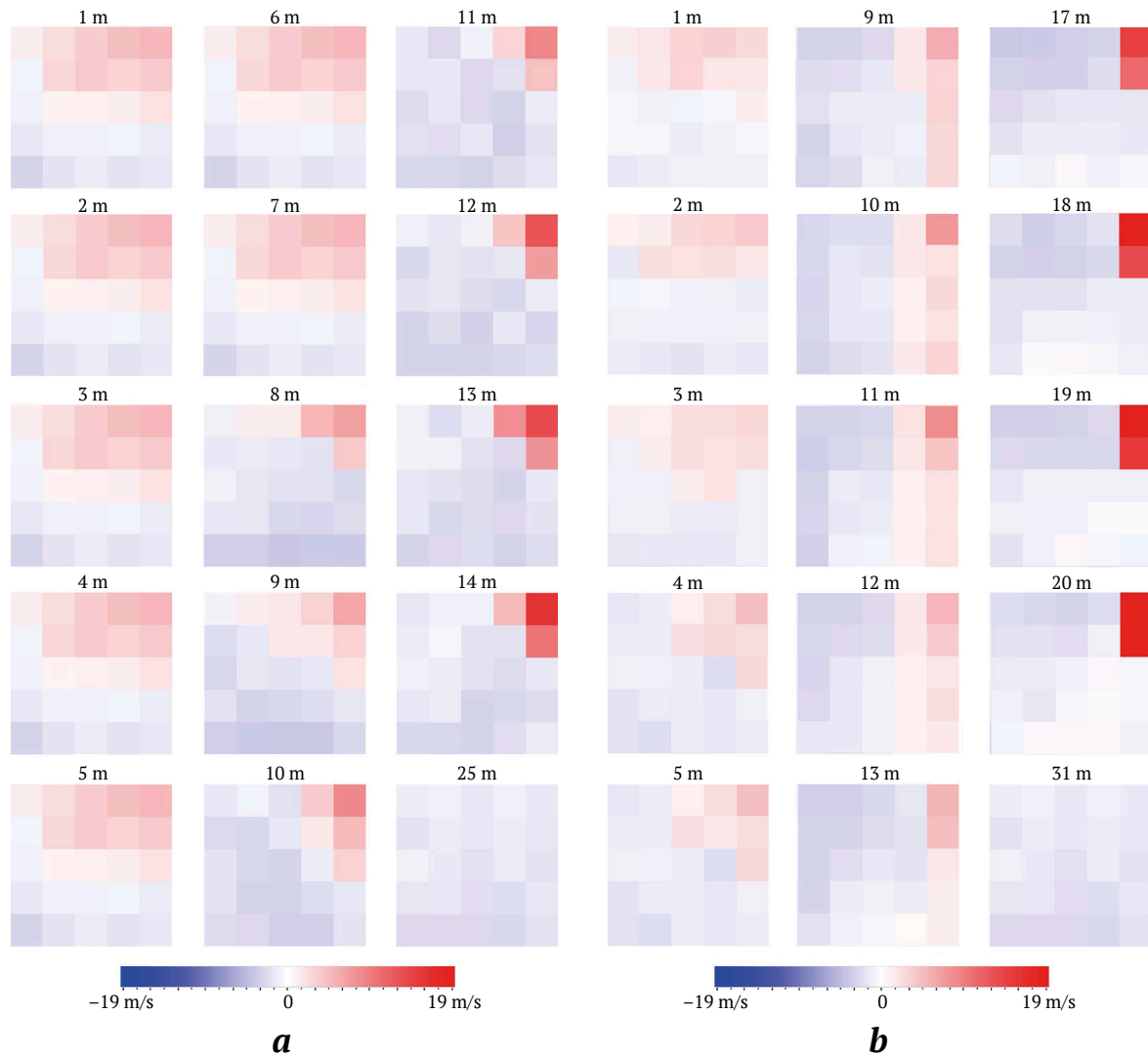


Fig. 2. Airflow velocity measurements at various cross-sections and points with the ventilation duct setback from the working face: *a*) at 15 m (note: 25 m marks the distance of 10 m from the pipeline's end to the working's entrance); *b*) at 21 m (note: 31 m indicates the distance of 10 m from the pipeline's end to the working's entrance)

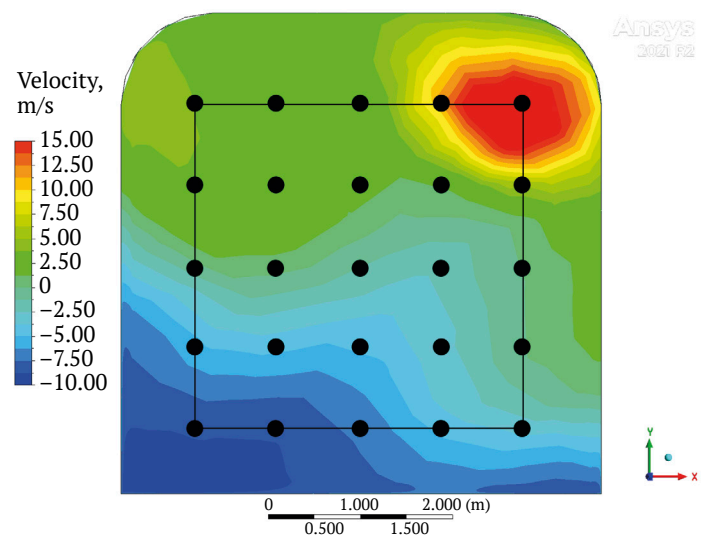


Fig. 3. Calculated air velocity distribution across the working's cross-section (facing the working face) 5 m from the working face with a 10-m setback of the flight's end and the standard "grid" of air velocity measurement points used in the field experiment

In the studied scenario, mass balance is maintained across any cross-section of the dead-end working—the flow rate moving from the working face (either concurrent with or outgoing from the jet flow) is equal to the flow rate moving toward the working face (either concurrent with or fresh flow entering through the pipeline).

Consequently, the flow rate directed to the working face varies from section to section. This variation allows the division of the dead-end working space under normal ventilation by an active jet into five conditionally demarcated zones (starting from the working face):

1. The zone of main flow reversal and “washing” near the working face surface.

2. The zone encompassing the “head” and “body” of the main vortex of the flow structure, extending from the end of the ventilation flight to the point of reversal and initiation of the main return flow from the working face.

3. The zone of the “tail” of the main vortex, which is shaped by the ejection (suction) of air not only from the side of the jet but also due to the constriction from behind the jet around the end of the ventilation pipeline.

4. The zone of flow “return” within the “tail” of the main vortex, resulting in an asymmetric distribution of flow velocities.

5. The classical flow zone, where the entire cross-section of the working is filled with the outgoing flow, and the velocity is purely axial (along the working’s length axis), excluding turbulent pulsations.

A schematic of this 5-zone structure is illustrated in Fig. 4.

In the first zone, the “longitudinal (axial) air flow rate” is nearly zero; it substantially exceeds the supplied ventilation air flow rate in the second and third zones and matches the supplied ventilation air flow rate in the fourth and fifth zones.

We highlight that this 5-zone structure along the length of the working effectively describes the jet’s

active influence on ventilation when it extends to the working face. Should the jet lack sufficient energy and momentum to reach the working face, a sixth zone emerges. This is not a single vortex but a cascade of progressively weaker vortices, often leading to the development of a “stagnant” zone.

In our comprehensive field and computational studies with a maximum setback of 21 m (corresponding to a form factor of 3.75), a stagnant zone did not form. Under the conditions described (working cross-section and fresh air flow rate), a 21-m setback ensured a vigorous jet “flow” towards the working face.

Figure 5 illustrates the distributions of the concurrent (from the working face) air flow rate Q along the entire length of the working, normalized to air flow rate Q_0 at the ventilation pipeline outlet. The concurrent air flow was determined by integrating the axial component of the air velocity in the working across the portion of the cross-section where the airflow is directed from the face towards the mine’s opening.

In all three modeled scenarios, a single vortex with a complex three-dimensional structure was present in the portion of the working closest to the face. Due to this asymmetry, a local maximum in the concurrent airflow was detected near the face (within a 3–4 m range) as depicted in Fig. 5.

Near the working face in zone 1, there are generally three possible airflow behaviors: the jet can “bump” against the working face, the incoming air can “wash” over the face, or a separate low-intensity vortex can form, creating a stagnant zone and effectively “isolating” the working face from the active jet. It is important to note that this last scenario was not observed in our field and computational experiments for setback distances up to 21 m.

The longitudinal airflow velocities directed towards the working face, measured 1 m from it, are typically found to be within 10–20% of the initial velocity of the jet entering the working. This is adequate for efficient ventilation of the space near the face and prevents the formation of stagnant zones.

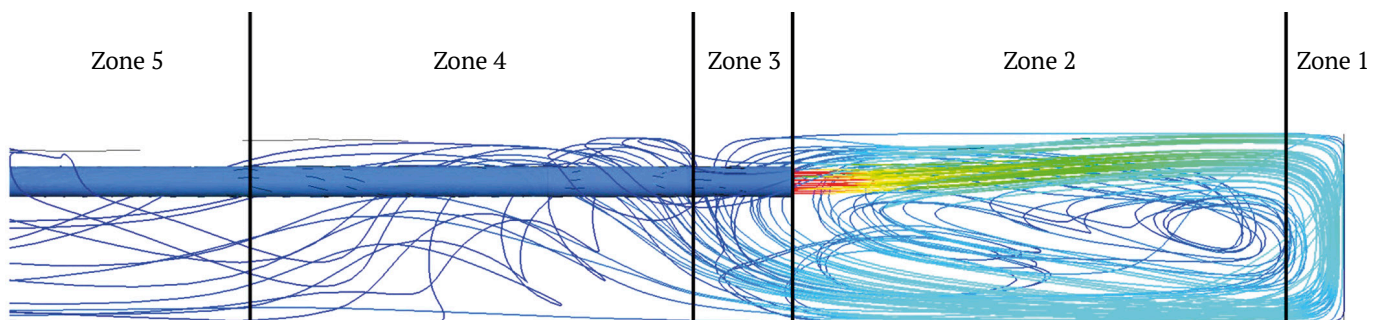


Fig. 4. Schematic illustration of the 5-zone structure of ventilation at the dead-end face

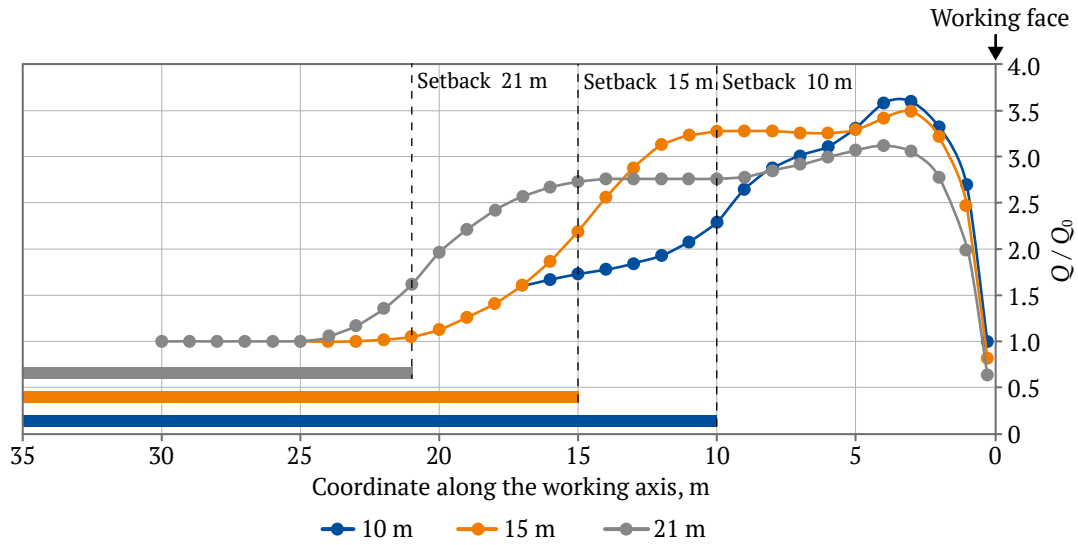


Fig. 5. Relationships of concurrent airflow along the working axis for various setback distances of the ventilation duct's end (vertical dashed lines indicate the positions of the ventilation duct's end for enhanced clarity)

Moreover, these velocity values tend to decrease as the setback distance of the pipeline from the working face increases, or, given the constant cross-sectional conditions of the described experiment, as the form factor increases (Fig. 6).

For the conditions of the mentioned experiment, the jet has not yet reached its limit of forward movement with a 21 m setback from a 29.2 m² working (form factor of 3.75) and a fresh air supply rate of 17.4 m/s. However, with further increases in the setback (and a form factor of about 6), the jet's range reaches its limit.

The trend line in Figure 6, determined by the least squares method, corresponds to the following formula:

$$\frac{U_{\max}(L-1)}{U_0} = 0.388 - 0.065 \frac{L}{\sqrt{S}}. \quad (9)$$

The numerical experiment's results demonstrate a comparable pattern. For the maximum longitudinal velocity at a distance of 1 m from the working face, the equation is:

$$\frac{U_{\max}(L-1)}{U_0} = 0.554 - 0.083 \frac{L}{\sqrt{S}}. \quad (10)$$

The numerically calculated relationship for the concurrent air flow rate relative to parameter L/\sqrt{S} one meter from the face is:

$$\frac{Q(L-1)}{Q_0} = 0.195 - 0.02 \frac{L}{\sqrt{S}}. \quad (11)$$

The values from equations (9) and (10) are approximately proportional, but the numerically calculated

maximum air velocities at a cross-section 1 m from the face are about 1.7–1.8 times greater. This discrepancy may be due to at least two factors:

1. The model's failure to account for potential non-stationary, random factors such as oscillations at the end of the ventilation pipeline.
2. The imprecision in capturing measurement points within the local zone of the working cross-section where maximum flow velocity occurs.

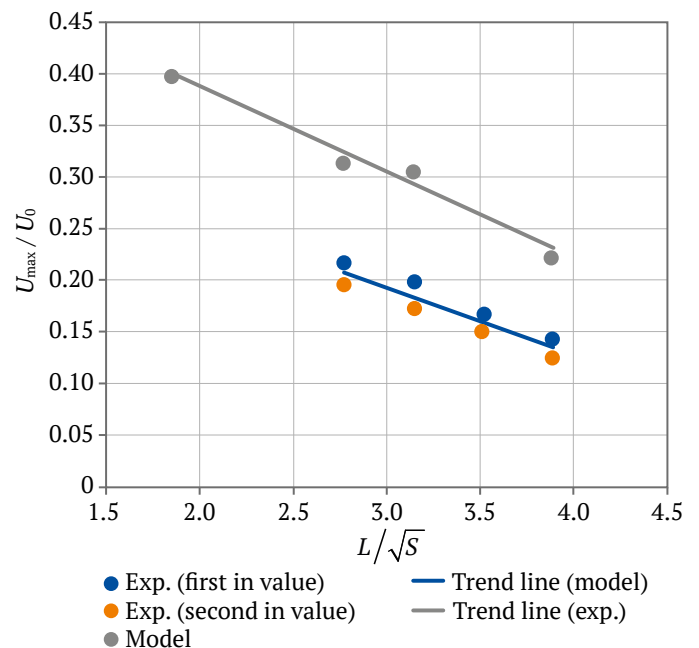


Fig. 6. Relationship between the maximum longitudinal velocity (relative to the jet's initial velocity) at the working face and the form factor; comparative analysis of modeling and experimental data: highlighting the two highest velocities at measurement points 1 m from the working face



It is crucial, however, that the velocity field in numerical modeling is not lower than that in the experiment, which allows us to use the experimental data as a conservative estimate for evaluating the efficiency of working ventilation.

Formulas (9)–(11) indicate that, within $L < 6\sqrt{S}$, the jet's range is ample for effective face ventilation ($100\%U_{\max}/U > 1.15\%$). This reinforces the accuracy of formulas (1)–(3).

Consequently, the field experiment's findings indicate that as the distance from the pipeline's end increases, there's a corresponding decrease in air exchange intensity. This pattern suggests the feasibility of significantly extending the setback of the ventilation duct's end from the working face, provided the form factor remains below 6.

Conclusion

The comprehensive field experiment aimed at analyzing the flow structure (specifically, air velocity) within a dead-end working utilizing forced ventilation was conducted across five different ventilation pipeline setback distances. These distances ranged from 10, 15, 17, 19, to 21 m for a pipeline with a diameter of 1200 mm. The cross-section of the working averaged 29.2 m^2 , with a fresh air supply rate of $17.4 \text{ m}^3/\text{s}$, and the initial cross-sectional area of the jet ranged from 0.75 to 0.8 m^2 . This setup ensured an initial jet velocity of 21.75 to 23.8 m/s , conducive to effective, long-range ventilation.

In all scenarios where the ventilation pipeline setback behind the working face (10 to 21 m), the

ventilation jet effectively reached the working face of the dead-end working, washed over it, turned around, and proceeded towards the entrance of the dead-end working. This process generated multiple turbulent vortices of varying sizes within the near-face ventilated zone, actively mixing the air flow.

The result was an air mixture near the face that was nearly homogeneous, displaced by the incoming fresh jet, and evacuated from the working space by the outgoing flow. Importantly, no stagnant zones were formed, which could potentially retain air contaminated with flue gases and dust. Such stagnant zones were not detected in the field experiment.

The data from computer simulations of the three-dimensional turbulent flow in the ANSYS software provided corroboration for the patterns observed in the field experiment. In all cases examined, the outgoing air flow within the working stabilized at a distance of 10 m from the end of the ventilation pipeline and remained constant up to the working face.

The findings of this study support the practicality of increasing the setback of the ventilation pipeline to up to 20 m from the working face in dead-end mine workings with a cross-section larger than 20 m^2 , particularly when the air velocity at the outlet of the ventilation pipeline is around 20 m/sec .

The findings from this investigation underpin the safety rationale for a hazardous production facility that has been developed and successfully applied in practice. This implementation has ensured high productivity and a consistent level of safety for underground mining operations at the Kupol gold-silver mine.

References

1. Shvyrkov I.A. Ventilation of blind faces after burning. *Occupational Safety in Industry*. 1934;(5):5–12; 1934(6):4–15. (In Russ.)
2. Ksenofontova A.I., Voropaev A.F. *Ventilation of blind workings*. Moscow: Ugletekhizdat; 1944. 112 p. (In Russ.)
3. Voronin V.N. *Fundamentals of mine aero-gasdynamics*. Moscow-Leningrad: Ugletekhizdat; 1951. 492 p. (In Russ.)
4. Adjiski V., Mirakovski D., Despodov Z., Mijalkovski S. Determining optimal distance from outlet of auxiliary forcing ventilation system to development of heading in underground mines. *Journal of Mining and Environment*. 2019;10(4):821–832. <https://doi.org/10.22044/jme.2019.8140.1683>
5. Li Z., Li R., Xu Y., Xu Y. Study on the optimization and oxygen-enrichment effect of ventilation scheme in a blind heading of plateau mine. *International Journal of Environmental Research and Public Health*. 2022;19(14):8717. <https://doi.org/10.3390/ijerph19148717>
6. Branny M., Jaszczur M., Wodziak W., Szmyd J. Experimental and numerical analysis of air flow in a dead-end channel. *Journal of Physics: Conference Series*. 2016;745:032045. <https://doi.org/10.1088/1742-6596/745/3/032045>
7. Kozyrev S.A., Amosov P.V. Mathematical modeling of blind working ventilation during blasting works with CFD-models used. In: *Aerology and Safety of Mining Enterprises. Collection of Research Papers*. 2013;(1):23–29. (In Russ.)
8. Kulik A.I., Timchenko A.N., Kosterenko V.N., Kobylkin S.S. Features of modelling aerogasodynamics of coal mine face. *Ugol'*. 2023;(3):75–78. (In Russ.) <https://doi.org/10.18796/0041-5790-2023-3-75-78>



9. Juganda A., Strebinger C., Brune J. F. Discrete modelling of a longwall coalmine gob for CFD simulation. *International Journal of Mining Science and Technology*. 2020;(30):463–469.
10. Isaevich A., Semin M., Levin L. et al. Study on the dust content in dead-end drifts in the potash mines for various ventilation modes. *Sustainability*. 2022;14(5):3030. <https://doi.org/10.3390/su14053030>
11. Liu A., Liu S., Wang G., Elsworth D. Predicting fugitive gas emissions from gob-to-face in longwall coal mines: coupled analytical and numerical modeling. *International Journal of Heat and Mass Transfer*. 2020;150:119392. <https://doi.org/10.1016/j.ijheatmasstransfer.2020.119392>
12. Xin S., Wang W., Zhang N. et al. Comparative studies on control of thermal environment in development headings using force/exhaust overlap ventilation systems. *Journal of Building Engineering*. 2021;38:102227. <https://doi.org/10.1016/j.jobe.2021.102227>
13. García-Díaz M., Sierra C., Miguel-González C., Pereiras B. A discussion on the effective ventilation distance in dead-end tunnels. *Energies*. 2019;12(17):3352. <https://doi.org/10.3390/en12173352>
14. Fainburg G.Z. *Digitalization of the processes of ventilation of potash mines*. Monograph. Perm-Ekaterinburg; 2020. 422 p. (In Russ.)
15. Mustel P. I. *Mine aerology*. M.: Nedra Publ.; 1970. 215 p. (In Russ.)
16. Kaledina N.O., Kobylkin S.S. On the choice of a method for ventilating dead-end mine workings in gas-rich coal mines. *Gornyi Zhurnal*. 2014;(12):99–104. (In Russ.)
17. Kolesov E. V., Kazakov B.P. Efficiency of ventilation of dead-end development headings after blasting operations. *Bulletin of the Tomsk Polytechnic University. Geo Assets Engineering*. 2020;(7):15–23. (In Russ.) <https://doi.org/10.18799/24131830/2020/7/2715>
18. Kazakov B.P., Shalimov A.V., Grishin E.L. Ejecting the return air flow on increasing the range of the air jet directed into the face of the dead-end drift. *Bulletin of the Tomsk Polytechnic University. Geo Assets Engineering*. 2022;333(9):27–36. (In Russ.) <https://doi.org/10.18799/24131830/2022/9/3624>
19. Kazakov B.P., Kolesov E.V., Nakariakov E.V., Isaevich A.G. Models and methods of aerodynamic calculations for ventilation networks in underground mines: Review. *Mining Informational and Analytical Bulletin*. 2021;(6):5–33. (In Russ.) https://doi.org/10.25018/0236_1493_2021_6_0_5
20. Mostepanov Yu.B. Study of the range of a constrained jet acting in the face of a dead-end mine. *Izvestiya Vysshikh Uchebnykh Zavedenii. Gornyi Zhurnal*. 1978;(11):47–50. (In Russ.)
21. Parra M.T., Villafruela J.M., Castro F., Mendez C. Numerical and experimental analysis of different ventilation systems in deep mines. *Building and Environment*. 2006;41(2):87–93. <https://doi.org/10.1016/j.buildenv.2005.01.002>
22. Hasheminasab F., Bagherpour R., Aminossadati S.M. Numerical simulation of methane distribution in development zones of underground coal mines equipped with auxiliary ventilation. *Tunnelling and Underground Space Technology*. 2019;89:68–77. <https://doi.org/10.1016/j.tust.2019.03.022>
23. Maltsev S.V., Kazakov B.P., Isaevich A.G., Semin M.A. Air exchange dynamics in the system of large cross-section blind roadways. *Mining Informational and Analytical Bulletin*. 2020;(2):46–57. (In Russ.) <https://doi.org/10.25018/0236-1493-2020-2-0-46-57>

Information about the authors

Anton A. Kamenskikh – Cand. Sci. (Eng.), Researcher at the Department of Aerology and Thermophysics, Chief Researcher of the Department of Aerology and Thermophysics, Mining Institute of the Ural Branch of the Russian Academy of Sciences, Perm, Russian Federation; ORCID [0000-0002-6456-5487](https://orcid.org/0000-0002-6456-5487); e-mail timir2418@gmail.com

Grigoriy Z. Faynburg – Dr. Sci. (Eng.), Professor, Chief Researcher of the Department of Aerology and Thermophysics, Mining Institute of the Ural Branch of the Russian Academy of Sciences, Perm, Russian Federation; ORCID [0000-0002-9599-7581](https://orcid.org/0000-0002-9599-7581), Scopus ID [57217891724](https://scopus.org/57217891724); e-mail faynburg@mail.ru

Mikhail A. Semin – Dr. Sci. (Eng.), Scientific Secretary, Mining Institute of the Ural Branch of the Russian Academy of Sciences, Perm, Russian Federation; ORCID [0000-0001-5200-7931](https://orcid.org/0000-0001-5200-7931), Scopus ID [56462570900](https://scopus.org/56462570900), ResearcherID [S-8980-2016](https://orcid.org/S-8980-2016); e-mail seminma@inbox.ru

Aleksey V. Tatsiy – Engineer, Mining Institute of the Ural Branch of the Russian Academy of Sciences, Perm, Russian Federation; ORCID [0009-0001-2514-6204](https://orcid.org/0009-0001-2514-6204); e-mail alexeytaciya@gmail.com

Received 28.08.2023

Revised 31.01.2024

Accepted 02.02.2024



SAFETY IN MINING AND PROCESSING INDUSTRY AND ENVIRONMENTAL PROTECTION

Research paper

<https://doi.org/10.17073/2500-0632-2024-01-203>

UDC 622.4

Determining airflow requirements in mine workings based on field measurements of actual emissions from internal combustion engine equipment

V. A. Senatorov

South and Center Region Paramilitary Mine Rescue Team, Paramilitary Mine Rescue Unit, Gubkin, Russian Federation

senatorov.vladimir.1970@mail.ru**Abstract**

The increasing complex geological and hydrogeological conditions ore deposit mining, deeper excavation sites, and ambitious business expansion strategies, necessitate the use of high-performance, heavy-duty self-propelled machinery and winning equipment. Such activities significantly strain mine ventilation systems and demand innovative safety measures during mining.

This study assesses the influence of interconnected production variables on the aerological safety of mining operations. It provides real-world data on emissions from diverse sources within mines. The analysis includes an examination of current methodologies for estimating the air volume needed to dilute exhaust gases from diesel-powered machinery. Through numerical simulation that accounts for changes over time, the study was able to predict how exhaust gas concentrations would disperse within mines. These theoretical findings were then confirmed through empirical observations made in actual mining setting. The field studies conducted, alongside their thorough analysis, underscored the necessity for adopting new, more sophisticated approaches to calculate airflow requirements in mines operating ICE machinery. A particular methodology developed by the MMI of the NUST MISIS (hereinafter referred to as the Methodology) was put forward as the primary tool for this purpose. The Methodology's precision and benefits were closely scrutinized, revealing its effectiveness in ensuring aerological safety in mines.

Keywords

mine, ventilation, exhaust gases, required airflow, internal combustion engine, rated exhaust, gas dynamics, numerical simulation, field tests

For citation

Senatorov V.A. Determining airflow requirements in mine workings based on field measurements of actual emissions from internal combustion engine equipment. *Mining Science and Technology (Russia)*. 2024;9(1):53–59. <https://doi.org/10.17073/2500-0632-2024-01-203>

ТЕХНОЛОГИЧЕСКАЯ БЕЗОПАСНОСТЬ В МИНЕРАЛЬНО-СЫРЬЕВОМ КОМПЛЕКСЕ И ОХРАНА ОКРУЖАЮЩЕЙ СРЕДЫ

Научная статья

Определение расхода воздуха в горных выработках на основе натуральных измерений фактической газовойности оборудования с двигателями внутреннего сгорания

В. А. Сенаторов

Филиал «Военизированный горноспасательный отряд Юга и Центра»
ФГУП «Военизированная горноспасательная часть», г. Губкин, Российская Федерация senatorov.vladimir.1970@mail.ru**Аннотация**

Все более сложные геологические и гидрогеологические условия отработки рудных месторождений, ведение работ на более глубоких горизонтах, а также амбициозные планы экономического развития предприятий поставили задачи использования высокопроизводительного, мощного дизельного самоходного и добычного оборудования. Это сказалось на увеличении нагрузки на вентиляционную сеть и потребовало использования новых методов обеспечения безопасности при ведении горных работ.



Приведена оценка влияния взаимосвязанных производственных факторов на аэрологическую безопасность рудника. Представлены фактические данные по газам, поступающим от различных источников. Проведен анализ метода расчета необходимого количества воздуха по фактору выхлопные газы дизельного оборудования. Проведено численное моделирование динамических процессов (с изменяющимися во времени параметрами), позволившее установить распределение концентраций выхлопных газов по горным выработкам. Последующие натурные измерения позволили верифицировать полученные результаты математического моделирования в условиях горных предприятий. Проведенные натурные эксперименты и их анализ позволили обосновать необходимость внедрения новых, более совершенных методов расчета расхода воздуха для рудника, использующего оборудование с ДВС. В качестве основного метода расчета требуемого количества воздуха использовалась методика, разработанная в МГИ НИТУ «МИСИС» (далее – Методика), были оценены ее точность и преимущества.

Ключевые слова

рудник, вентиляция, выхлопные газы, требуемый расход воздуха, двигатель внутреннего сгорания, норма выбросов, газодинамические процессы, численное моделирование, шахтные измерения

Для цитирования

Senatorov V.A. Determining airflow requirements in mine workings based on field measurements of actual emissions from internal combustion engine equipment. *Mining Science and Technology (Russia)*. 2024;9(1):53–59. <https://doi.org/10.17073/2500-0632-2024-01-203>

Introduction

Advancements in mining technologies necessitate refined methodologies for estimating ventilation airflow per unit of diesel power, which emerges as a principal variable

Previous techniques (e.g.,¹) failed to consider numerous determinants influencing the infiltration of pollutants from diesel vehicles into mine air. It is noteworthy that self-propelled diesel machinery constitute the primary source of air pollution in many mines. The prevailing analytical methods exhibited poor correlation with actual gas concentrations, often resulting in a substantial overestimation of the necessary fresh air flow.

The accuracy of airflow estimation stands at approximately 50%, a level of precision that detrimentally impacts mining operations.

To address this issue, evaluations were carried out at a facility managed by Yakovlev Mining and Processing Plant in 2021² aiming to assess the methodologies for analyzing the relationship between airflow and diesel engine exhaust emissions.

The approach developed by the Moscow Mining Institute³ was enhanced through novel measurement techniques, designed to evaluate exhaust gas dynamics across varying vehicle loads.

The deployment of specialized instruments enabled the precise quantification of actual exhaust volumes and other relevant gas metrics over time. For this purpose, an array of specialized mine air analyzers was utilized, including APR-2, MBGO-2, TGO-2MP, APA-1, MRU Delta 2000 CD, Testo 350, Microsense M3), with all supplementary measurements adhering to established procedural standards.

The current practice of estimating required airflow does not differentiate between ore and coal mines⁴, despite the distinctive patterns of exhaust gas emissions inherent to each type. Specifically, ore mines are characterized by significantly more extensive blasting operations [1, 2].

Self-propelled diesel machines and equipment are the main sources of exhaust and thermal emissions in mines, as well as technologies that use consolidating backfill [3–5]. The estimation of the requisite air volume in standard ore mines takes into account several critical factors: [1, 6, 7]:

- toxic fumes from blasting operations;
- toxic diesel exhausts;

¹ Federal Industrial Safety Code. Mining and Solid Minerals Processing Safety. Directive No. 505, Dec. 8, 2020.

Coal Mines Ventilation Design Guidelines. Moscow, Nedra Publishing, 1975.

Safety of Coal Mine Vehicles: Collected papers. Series 05 Issue 12. Moscow: Industrial Safety Research Center, Russian National Mining Safety Agency, 2004.

² Mine Air Flow Estimation Method and Ventilation Options. Research Report. Supervisor: S. Kobylkin, Doctor of Science (Engineering), MISIS Univ., 2021.

³ Efficient Ventilation for Deep Mines with Diesel-Powered Equipment. Research Report. Supervisor: Prof. L. Puchkov, Doctor of Science (Engineering), 1976.

⁴ Federal Industrial Safety Code. Mining and Solid Minerals Processing Safety. Directive No. 505, Dec. 8, 2020.

Coal Mines Ventilation Design Guidelines. Moscow, Nedra Publishing, 1975.



- toxic gases emanating from exposed rock and broken ore;
- dust content;
- heat emission;
- airflow needed for respiration, correlating with the number of individuals in the mine.

Among these, methods accounting for dust content and blast fumes are notably advanced, presenting minimal error in calculating needed air volumes [2, 8, 9]. Conversely, gases from ore and air for breathing, based on personnel count, are less impactful.

Operational experience in mines employing high-performance diesel equipment demonstrates that diesel exhaust gases are the critical factor in calculating the necessary air volume [5, 10].

Despite the long-standing use of diesel machinery in mining, a universally accepted standard for air quantity estimation to mitigate diesel exhaust effects remains elusive. The historical benchmark of a minimum 5 m³/min per horsepower is still in use⁵ [11].

Hence, the primary considerations for determining the air supply in mines are the toxic fumes from blasting and emissions from diesel machinery. Enhancing the precision and optimization of airflow estimation methods is vital for significantly reducing ventilation costs in mining operations.

The typical rate of fresh air supply to mines is in the order of hundreds of cubic meters per second. Inaccuracies in estimating the necessary airflow result in substantial losses. For instance, while an acceptable margin of error ranges from 15 to 20%, the actual volume of air delivered frequently surpasses the required amount by as much as 50%. Managing such a vast influx of air, and ensuring its distribution meets the specific requirements of each ventilated area, poses significant engineering challenges.

These issues underscore the need for innovative, modern analysis techniques. A particularly promising approach is one that adopts a more nuanced consideration of dust and exhaust sources within mines, especially focusing on the primary emission contributors: blasting operations and diesel-powered equipment [4, 6, 12].

The proposed method for air volume estimation, aimed at mitigating diesel exhaust impacts, significantly lowers ventilation costs by incorporating a comprehensive range of factors.

Materials and Methods

The Yakovlev Mining and Processing Plant operates a mine with complex ventilation ductwork, featuring numerous parallel and diagonal connections and requiring extensive air gate control. The mine's challenging geology and its location in a densely populated area add layers of complexity, complicating efforts to maintain optimal mine air conditions such as temperature, humidity, and safety, especially considering the diminished oxygen levels and the presence of toxic fumes from blasting and internal combustion engines [12, 11].

These factors impact the air's humidity, temperature, and absolute pressure.

Experimental air quality assessments in the mining work areas identified the primary sources of hazardous gases and dust in underground mines as follows:

- blasting;
- diesel equipment;
- oxidation;
- mineral extraction production processes.

These activities release toxic substances like carbon monoxide, nitrogen oxides, acrolein, and formaldehyde, posing risks to human health, including respiratory issues [12].

To evaluate the mine's ventilation efficiency, we compared actual and required airflow rates and analyzed the composition and volume of internal combustion engine (ICE) exhaust emissions under various conditions.

Our numerical estimates were cross-verified with direct field measurements of air properties within the mine and the mine ventilation system's (MVS) performance, including regular monitoring of hazardous pollutants in the mine air. The South and Center Region Paramilitary Mine Rescue Team's Test Lab analyzed the exhaust gas's composition, volume, temperature, and air quality near the self-propelled diesel equipment.

In addition to increased levels of harmful gases and dust in the work area's air, mines also face harmful physical factors such as heat emissions, originating from equipment and stowing operation⁶ [9].

The assessment of thermal impacts included applying thermal imaging principles in mines to analyze heat emissions from the operation of machinery and equipment.

⁵ Coal Mines Ventilation Design Guidelines. Moscow, Nedra Publishing, 1975.

Safety of Coal Mine Vehicles: Collected papers. Series 05 Issue 12. Moscow: Industrial Safety Research Center, Russian National Mining Safety Agency, 2004.

⁶ Mine Air Flow Estimation Method and Ventilation Options. Research Report. Supervisor: S. Kobylkin, Doctor of Science (Engineering), MISIS Univ., 2021.



The investigation into the underground mine’s microclimate revealed that fresh air, differing in temperature from the surrounding rocks and in gas composition from the outgoing air, flows into the mine.

Furthermore, exhaust gases, with temperatures between 40 to 370 °C, additionally heat the mine’s atmosphere.

The concentration of toxic gases in the ICE exhaust was measured by analyzing both the standard samples taken regularly and express analyses used to determine the composition of undiluted exhaust under various loads of the ICE-driven equipment. Both steady-state and transient engine operations were studied.

The required amount of air to offset the above factors was estimated using the actual exhaust emissions of the existing equipment. The actual exhaust volume was determined as a function of the maximum fuel consumption and concentrations of all toxic gases. This volume was then used to calculate the amount of air required to dilute the toxic gases to the maximum allowable concentration (MAC) for each type of equipment.

The engine was started, and its rpm in steady and transient operations under various loads as the equipment performed its typical duty was recorded. The measurement results, gas emission rate

vs. time, and exhaust gas temperatures are shown in Fig. 1.

Based on the actual exhaust measurements, a method for estimating air consumption in mines with ICE equipment was developed⁷.

Estimation of the Amount of Air Required to Dilute Toxic ICE Exhaust Gases

The volume of fresh air supplied to areas of the mine where ICE equipment operates, either continuously or intermittently, must be adequate to dilute the primary toxic components of the exhaust gas (specifically carbon monoxide and nitrogen dioxide, assessed in NO₂ equivalent) to maximum allowable concentrations or to maintain the prescribed oxygen levels. This volume is calculated as follows:

$$Q_{ICE} = k_{para} \sum k_{duty} Q_{eq}, \text{ m}^3/\text{s}, \quad (1)$$

where k_{para} is the factor for parallel operation of multiple ICEs at the same location, with $k_{para} = 1.0, 0.9, 0.85$ for the simultaneous operation of 1, 2, 3, or more engines within the same ventilation system segment; k_{duty} is the ICE duty cycle factor, reflecting the proportion of time the vehicle spends at the location relative

⁷ Mine Air Flow Estimation Method and Ventilation Options. Research Report. Supervisor: S. Kobylkin, Doctor of Science (Engineering), MISIS Univ., 2021.

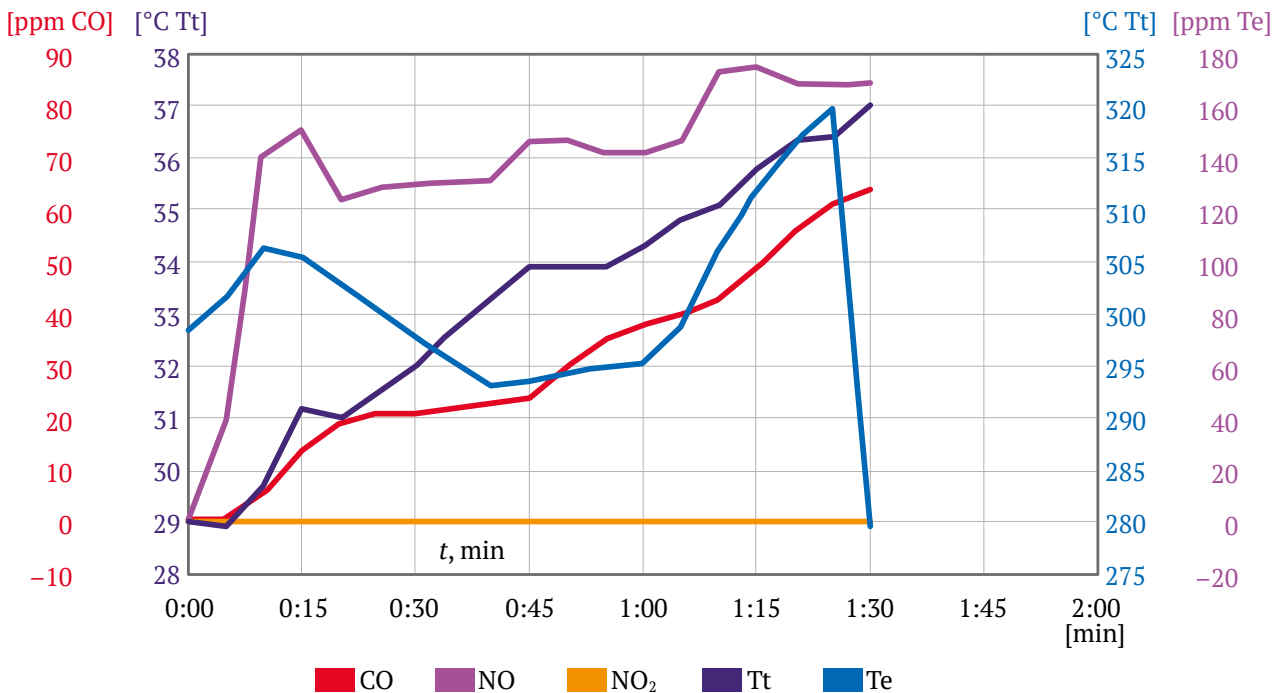


Fig. 1. Composition and Temperature of Exhaust Gases at Engine Idle: time-dependent concentrations of carbon monoxide (CO), nitrogen oxide (NO), and nitrogen dioxide (NO₂), ppm; ambient temperature (Tt) and exhaust gas temperature (Te) over time, °C; t is time, min



to the entire cycle time, ranging from 0.1 to 1; Q_{eq} is the volume of air needed to ventilate each ICE, m^3/s .

The duty cycle factor is defined as

$$k_{duty} = \frac{t}{t_c}, \quad (2)$$

where t is the duration of ICE operation at the specified location, min; t_c is the equipment cycle time, min.

Air consumption required to neutralize each exhaust gas component is calculated as

$$Q_m = \frac{c_{out}}{c_{MAC}} g_{out}, \quad m^3/s \quad (3)$$

where c_{out} is the concentration of toxic exhaust components (maximum concentration of nitrogen oxides in NO_2 equivalent in undiluted engine exhaust), % vol.; c_{MAC} is the MAC of the component, % vol.; g_{out} is the flow rate of purified exhaust gas, m^3/s .

The quantity of exhaust gases is assessed based on direct measurements. For self-propelled diesel machinery used within the mine, the amount of exhaust emissions is established from the actual figures presented in Table 1.

When calculating the required ventilation flow, emissions from diesel-driven drilling equipment used in conjunction with other self-propelled diesel vehicles, as well as machinery used for secondary operations that do not operate continuously for more than

10 min within an hour or 40 min per shift, are not considered.

The findings highlighted consistent trends in how exhaust gases spread throughout the mine's spaces, irrespective of the mining technology applied. The positioning of the exhaust pipe plays a crucial role in influencing gas movement, with the highest concentrations of exhaust gases found in areas close to the pipe. Dynamic simulations facilitated the analysis of time-related changes in gas distribution, the visualization of airflow dynamics, and the assessment of gas dispersion metrics within the mine.

Research and analysis provided an average overview of the time allocated to production tasks and the rate at which gases are emitted from the main toxic elements found in exhaust gases.

The highest emission rates are confined to specific periods within the shift, not spanning the entire duration. This fact is vital for accurately calculating the volume of air needed for adequate ventilation.

Such precision enables the determination of the essential volume of fresh air for the mine when using ICE equipment, factoring in the actual volume of harmful emissions as the primary source of pollution. By analyzing the levels of toxic contaminants, it is feasible to set a ventilation standard for the use of ICE machinery, considering the machinery's power, operational conditions, and type, specific to each mine.

Table 1

Actual toxic gas concentrations, exhaust gas volumes from load haul dumpers (LHD), and estimated air quantity for maximum gas emission

LHD name	Engine power, N		Purified exhaust gas volume g_{out}	Toxic exhaust component concentration c_{out} CO	Maximum allowable concentration c_{MAC} CO	Maximum allowable concentration c_{out} NO_x	Toxic exhaust component concentration nox (total nitrogen oxides) c_{MAC} NO_x	Air consumption to offset Q_m CO	Air consumption to offset Q_m NO_x	Rated specific air consumption per LHD
	kW	h.p.								
Caterpillar CAT R1300G	123	165	0.077	79.68	20	476	5	0.3	7.3	2.7
SANDVIK LH307	160	215	0.060	925	20	837	5	2.8	10.0	2.8
Sandvik LH410	235	315	0.175	73.81	20	315	5	0.6	11.0	2.1
EPIROC ST1030	186	249	0.059	48.4	20	412	5	0.1	4.9	1.2
Caterpillar CAT R1300G	123	165	0.077	79.68	20	476	5	0.3	7.3	2.7
SANDVIK LH307	160	215	0.060	925	20	837	5	2.8	10.0	2.8
Sandvik LH410	235	315	0.175	73.81	20	315	5	0.6	11.0	2.1
EPIROC ST1030	186	249	0.059	48.4	20	412	5	0.1	4.9	1.2

Note: the NO_x concentration is in the NO_2 equivalent = $1.53 NO + NO_2$.



This standard is not a one-size-fits-all for the mining sector, as evidenced by international practices [9].

Numerical simulations of how exhaust gases disperse under different ventilation conditions revealed that an increase in airflow velocity (or flow rate) significantly shortens the exhaust gas dilution period. This enhancement also hastens the evacuation of gases from the mine.

When ventilating at the maximum allowable velocity, the concentration of gases is reduced by 3.5 times compared to the concentration observed when ventilating at the lowest airflow velocities.

Conclusions

Real-world emission data from self-propelled machinery show that different types of equipment emit varying levels of gases, and even within the same type of machinery, the concentration of harmful gases can differ. Interestingly, more powerful machines do not necessarily produce more harmful emissions. Additionally, it has been found through experiments that an increase in engine revolutions per minute (rpm) does not invariably lead to higher concentrations of exhaust gases.

These findings have informed the setup of initial and boundary conditions for computational modeling. Dynamic numerical modeling, which accounts for changes over time, indicates that the concentration of exhaust gases from ICE machinery tends to even out throughout the mine over time. The leveling of gas concentrations occurs approximately 100 meters from the emission source (exhaust pipe). Furthermore, an increase in the velocity of airflow markedly reduces the time required for the dilution of exhaust gases, thereby speeding up their removal from the mine. At the highest allowable airflow velocity, gas concentrations are diminished by 3.5 times compared to levels observed when air is circulated at the minimum allowable speed.

When multiple ICE machines are operated simultaneously in separate entries of a single mining block, the combined exhaust gases merge into the main ventilation passageway of the mine. In scenarios where ventilation is conducted sequentially, there's a possibility that some exhaust gases might flow into other active mining areas. This factor needs to be carefully considered in the design of ventilation schemes.

References

1. BVoronin V.I., Voronina L.D., Vagrinovskiy A.D. *Guidelines for the design and practical implementation of anti-dust ventilation regimes in metal mines*. Moscow: State scientific and technical publishing house of literature on mining; 1960. (In Russ.)
2. Olkhovskiy D.V., Parshakov O.S., Bublik S.A. Study of gas hazard pattern in underground workings after blasting. *Mining Science and Technology (Russia)*. 2023;8(1):47–58. <https://doi.org/10.17073/2500-0632-2022-08-86>
3. Smailis V.I., Iktrov V.A., Sokolov V.S. Study of the toxicity of exhaust gases of diesel engines D-108 and D-130. *Proceedings of the Central Research Diesel Institute*. 1963;47.
4. Levin L.Yu., Zaitsev A.V., Grishin E.L., Semin M.A. Calculation of the amount of air based on oxygen content for ventilating work areas when using machines with internal combustion engines. *Occupational Safety in Industry*. 2015;(8):43–46. (In Russ.)
5. Kuzminykh E.G., Kormshchikov D.S. Analysis of methods for calculating the required amount of air to dilute exhaust gases. *Gornoye Ekho*. 2020;(3):107–115. (In Russ.) <https://doi.org/10.7242/echo.2020.3.21>
6. Semin M., Levin L. Mathematical modeling of air distribution in mines considering different ventilation modes. *Mathematics*. 2023;11(4):989.
7. Puchkov L.A., Kaledina N.O., Kobylkin S.S. Methodology of system design mine ventilation. *Mining Informational and Analytical Bulletin*. 2014;(S1):128–136. (In Russ.)
8. Kobylkin A.S. Comparison of the results of mine research with the results of modeling the processes of dust transfer and dust deposition. In: *Problems and Prospects for the Integrated Development and Conservation of the Earth's Interior*. 2018. Pp. 269–273. (In Russ.)
9. Barrett Ch., Gaillard S., Sarver E. Demonstration of continuous monitors for tracking DPM trends over prolonged periods in an underground mine. In: *Diesel Particulate Control. Proceedings of the 16th North American Mine Ventilation Symposium*. Colorado School of Mines, Colorado, USA, June 17–22, 2017. Pp. 5-29–5-36.
10. Kobylkin S.S., Kaledina N.O. Diesel exhaust gas dynamics in underground mines. *Gornyi Zhurnal*. 2023;(12):94–102. (In Russ.) <https://doi.org/10.17580/gzh.2023.12.15>



11. Kuzminykh E. G., Levin L. Yu., Maltsev S. V. Distribution of exhaust gas products from equipment with internal combustion engines in the mine ventilation network. *Gornoye Ekho*. 2023;(2):96–103. (In Russ.) <https://doi.org/10.7242/echo.2023.2.17>
12. Surikov A., Leshenyuk N. Modeling of visibility in a room under fire conditions with application of the FDS software complex. *Journal of Civil Protection*. 2018;2(2):147–160. (In Russ.) <https://doi.org/10.33408/2519-237X.2018.2-2.147>

Information about the author

Vladimir A. Senatorov – Assistant Detachment Commander, Branch of the “Military Mine Rescue Squad of the South and Center” of the Federal State Unitary Enterprise “Military Mine Rescue Unit”, Gubkin, Russian Federation; ORCID [0009-0003-0486-4623](https://orcid.org/0009-0003-0486-4623); e-mail: senatorov.vladimir.1970@mail.ru

Received 12.01.2024

Revised 07.02.2024

Accepted 17.02.2024



POWER ENGINEERING, AUTOMATION, AND ENERGY PERFORMANCE

Research paper

<https://doi.org/10.17073/2500-0632-2024-01-198>

UDC 621.316:622.272

**Assessing the efficiency of measures to enhance electric power quality in variable-frequency drive for scraper conveyors**V.L. Petrov  , A.V. Pichuev   *University of Science and Technology MISIS, Moscow, Russian Federation* allexstone@mail.ru**Abstract**

The intensive implementation of variable-frequency drive machines and installations in underground mining processes necessitates addressing several issues, with a primary focus on ensuring the quality of electric power. Elevating the energy resource of mining machines and enhancing the energy efficiency of mining operations requires maintaining the rated indicators of electric power quality in mine power distribution systems. Achieving this involves assessing the level and composition of higher harmonic components in voltage and current within power circuits equipped with variable-frequency drives (VFD). Key objectives encompass the development of a simulation model based on the equivalent diagram of the power distribution system substitution with a scraper conveyor VFD to scrutinize the spectral composition of higher harmonic components in the power circuits of the mine power distribution system (MPDS). Additionally, the study involves analyzing the impact of harmonic filters (HFs), reactors, and sine filters on the quality of electric power in the VFD system of a scraper conveyor. Further analysis extends to the spectral composition of higher harmonic components in circuits related to insulation leakage and metering circuits of the residual-current device. Practical recommendations for improving electric power quality in the VFD system of a scraper conveyor are then developed based on the research findings. The established model of a variable-frequency drive system for scraper conveyors facilitates the assessment of the effectiveness of electric power quality improvement measures. The harmonic composition of voltage and current in the mine power distribution system is determined under maximum distortion conditions and in the presence of HFs, reactors, and sine filters. Research methods are chosen to unveil the spectral composition of voltage and current in symmetrical and single-phase modes of insulation leakage, as well as in metering circuits of residual-current devices (RCDs). It is noted that the harmonic composition of leakage voltage and current is primarily influenced by the parameters of the output voltage modulated by the autonomous frequency converter inverter. Considering the high level of harmonic components in voltage and current, adjustments to RCD settings, capacitive current compensator, and the protective shunting unit are recommended for electrical safety. The study emphasizes the importance of scientifically substantiating the rated indicators of higher harmonic components for leakage circuits and further exploring the physiological effects of higher current harmonics on the human body. The feasibility of installing a harmonic filter (HF) directly on the low-voltage supply section of a scraper conveyor should be technically justified. Interestingly, the presence of HFs, reactors, and sine filters does not significantly impact the harmonic composition or the magnitudes of coefficients of the harmonic components in the phase voltage of the system concerning ground and leakage currents through insulation. However, higher harmonic components induced in leakage current circuits may pose a potential hazard, leading to a violation of magnetic compatibility and posing risks in case of contact with live parts of electrical equipment.

Keywords

underground mining operations, mine power distribution system, electric power quality, electrical safety, scraper conveyor electric drive, filter-compensating device, sine filter, residual-current device, power distribution system insulation

For citation

Petrov V.L., Pichuev A.V. Assessing the efficiency of measures to enhance electric power quality in variable-frequency drive for scraper conveyors. *Mining Science and Technology (Russia)*. 2024;9(1):60–69. <https://doi.org/10.17073/2500-0632-2024-01-198>



ЭНЕРГЕТИКА, АВТОМАТИЗАЦИЯ И ЭНЕРГОЭФФЕКТИВНОСТЬ

Научная статья

Оценка эффективности средств повышения качества электроэнергии в системе частотно-регулируемого электропривода скребковых конвейеров

В. Л. Петров  , А. В. Пичуев   

Университет науки и технологий МИСИС, г. Москва, Российская Федерация

 allexstone@mail.ru

Аннотация

Интенсивное внедрение частотно-регулируемых электроприводов машин и установок в технологических процессах при подземной добыче полезных ископаемых предусматривает необходимость решения ряда проблем, одной из которых является обеспечение качества электроэнергии. Именно поэтому повышение энергоресурса горных машин и энергоэффективности ведения горных работ требует обеспечения нормативных показателей качества электроэнергии в подземных комбинированных электрических сетях (ПКЭС). Это возможно на основе оценки уровня и состава высших гармонических составляющих напряжения и тока в силовых цепях с частотно-регулируемым электроприводом (ЧРЭП). Основными задачами являются: разработка на основе эквивалентной схемы замещения электрической сети с ЧРЭП скребкового конвейера имитационной модели для исследования спектрального состава высших гармонических составляющих напряжения и тока в силовых цепях ПКЭС; исследование и анализ влияния фильтро-компенсирующих устройств (ФКУ), реакторов и синус-фильтров на качество электроэнергии в системе с ЧРЭП скребкового конвейера; анализ спектрального состава высших гармонических составляющих напряжения и тока в цепях утечки через изоляцию и цепи измерителя устройства защитного отключения; разработка практических рекомендаций в области повышения качества электроэнергии в системе с ЧРЭП скребкового конвейера. Разработанная модель системы частотно-регулируемого электропривода скребковых конвейеров позволила провести исследования эффективности средств повышения качества электроэнергии. Определен гармонический состав напряжения и тока в подземной комбинированной электрической сети в режиме максимального искажения и при наличии ФКУ, реакторов и синус-фильтров. Выбранные методы исследований позволили выявить спектральный состав напряжения и тока в симметричном и однофазном режиме утечки через изоляцию, а также в измерительных цепях устройств защитного отключения (УЗО). Установлено, что гармонический состав напряжения и тока утечки в основном определяется параметрами выходного напряжения, модулируемого автономным инвертором преобразователя частоты. Высокий уровень гармонических составляющих напряжения и тока необходимо учитывать при определении уставок УЗО, настройке компенсатора емкостного тока и блока защитного шунтирования. Для обеспечения электробезопасности необходимо научное обоснование нормативных показателей высших гармонических составляющих напряжения для цепей утечки и дальнейшее исследование физиологического воздействия высших гармоник тока на организм человека. Целесообразность установки ФКУ непосредственно на низковольтном участке питания скребкового конвейера должна быть технически обоснована. Наличие ФКУ, реакторов и синус-фильтров практически не оказывает влияния как на гармонический состав, так и на величину коэффициентов гармонических составляющих фазного напряжения сети относительно земли и токов утечки через изоляцию. Наличие наводимых в цепях утечки тока высших гармонических составляющих в симметричном режиме и режиме однофазной утечки тока может привести к нарушению магнитной совместимости при работе электронной измерительной схемы, блока питания и компенсатора емкостного тока утечки УЗО и представлять потенциальную опасность в случае прикосновения к токоведущим частям электрооборудования.

Ключевые слова

подземные горные работы, подземная электрическая сеть, качество электроэнергии, электробезопасность, электропривод скребкового конвейера, фильтро-компенсирующее устройство, синус-фильтр, устройство защитного отключения, изоляция электрической сети

Для цитирования

Petrov V. L., Pichuev A. V. Assessing the efficiency of measures to enhance electric power quality in variable-frequency drive for scraper conveyors. *Mining Science and Technology (Russia)*. 2024;9(1):60–69. <https://doi.org/10.17073/2500-0632-2024-01-198>



Introduction

Currently, modern mines are actively adopting an advanced system of asynchronous variable-frequency drive (VFD) for heavy-duty stoping machines. This system enables the control of electric motor speed both during start-up and directly during mining operations. As a result, the structure of the mine power distribution system has been upgraded, giving rise to sections with direct current and variable-frequency current, collectively referred to as mine power distribution systems (MPDS).

These systems incorporate the use of asynchronous VFD for scraper conveyors based on frequency converters with an autonomous voltage inverter (FC with AVI) and pulse-length modulation (PLM).

Implementing a scraper conveyor VFD with frequency converters offers benefits such as smooth start-up, load limitation in a tow chain during jamming, equalization of loads between head and tail drives, and the ability to maintain a constant linear load of a scraper conveyor by regulating the speed of the scraper chain with varying coal inflow from a combine during its cyclic operation [1–3]. In MPDS, a frequency converter with a straight rectifier and autonomous voltage inverter is primarily employed to control the electric drive.

To enhance the energy efficiency of mining operations and the energy resource of mining machines, it is crucial to ensure the rated indicators of electric power quality in MPDS. This involves evaluating the level and composition of higher harmonic components (HHC) of voltage and current in power circuits with [4].

Scientific studies indicate that the level and composition of HHC depend significantly on factors such as the length of the supply line, the power of frequency converters (FC), the load of induction motors, and the presence of FCs at adjacent sections [5–8].

In the section-related power distribution system with a voltage of up to 1140 V, which powers the electric drive of a scraper conveyor, the total coefficients of harmonic components of voltage ($K_{U\%}$) increase from 8.2% to 15.8% when the length of the 6 kV cable line supplying the section is increased from 3 to 6 km, and the total installed power of induction motors is increased from 1200 to 2000 kW, in the absence of harmonic filters (HF). This exceeds the rated values not only directly at the load node ($K_{U\text{rat}} = 8\%$) but also at adjacent sections ($K_{U\text{rat}} = 5\%$). The application of HFs in the first compensation stage helps reduce the level of voltage HHC to 5.14–7.6% [9].

A method to enhance electric power quality involves installing sine filters (SF) downstream from the frequency converter, enabling the filtration of volt-

age modulated by the frequency converter at the motor terminals¹ [10]. However, the current limitations in terms of design complexity and the challenges of parameter selection and adjustment for SF make it challenging to assess its efficiency in mine power distribution systems, rendering the analysis primarily theoretical.

An essential aspect is the examination of the harmonic composition of voltage and current leakage through insulation circuits in the power distribution system, as well as in metering circuits of residual-current devices (RCD). The prevailing trend in the advancement of leakage current protection involves the incorporation of microprocessor-based devices in electronic power supply units. This includes insulation control, automatic compensation control, and protective shunting to ensure self-check, fault diagnostics, and telemetry of data regarding the state of protection complexes. When operating in MPDS conditions, the issue of magnetic compatibility needs to be addressed [11]. Scientific studies in this domain reveal that HHC can significantly impact the efficiency of RCDs and the safety level of the power distribution system² [12, 13].

Hence, researching the impact of electric power quality on the effectiveness of variable-frequency drives for stoping machines in the mine power distribution systems of mining enterprises is a pertinent scientific problem.

The primary methodology employed in this study is mathematical simulation, providing a means to discern new scientific insights and the practical significance of these findings.

Purpose and objectives

The primary aim of this study is to assess the effectiveness of measures aimed at enhancing electric power quality in the control system of VFD for scraper conveyors within the MPDS of mining enterprises.

The primary objectives are as following.

1. Develop a simulation model based on the equivalent substitution diagram of the power distribution system, incorporating a VFD for a scraper conveyor.

¹ EPCOS. Power Factor Correction. Power Quality Solutions. Product Profile 2009. URL: http://biakom.com/hfuhf/production/passive/EPCOS/PFC_Katalog2009.pdf

Danfoss. Output Filters Design Guide. URL: www.danfoss.com/NR/rdonlyres/27F81E1-3779-4406-8EA0-849044873F59/0/Output_Filters_Design_Guide.pdf

LC Sine Wave Filter for Motor Drives. Output Filters FN5040/FN5045. Schaffner. URL: <http://www.schaffner.com/en/products/datasheet-low-res/product/fn-5040-fn-5045-lc-sine-wavefilter-for-motor-drives.html>

² O'shea P. Counteracting high leakage currents. URL: <https://www.powerelectronicsnews.com/counteracting-high-leakage-currents/>

This model aims to investigate the spectral composition of the higher harmonic components of voltage and current in the power circuits of the mine power distribution systems (MPDS).

2. Conduct research and analysis on the impact of HFs, reactors, and sine filters on the electric power quality within the VFD system of a scraper conveyor.

3. Analyze the spectral composition of the voltage and current higher harmonic components in the insulation leakage current circuits and circuits of the residual-current device metering unit.

4. Formulate recommendations for improving electric power quality in the VFD system of a scraper conveyor.

Simulation model structure

The structure of the mine power distribution system for the electric motors of a scraper conveyor comprises various components. These include a site-specific substation’s power transformer (TSVP) equipped with a built-in circuit breaker (AVDO) and a leakage current protection device (RCD) of the AZUR type. Additionally, there is a group of magnetic starters belonging to the PVIT series, and explosion-proof frequency converters situated in the power train. These converters are strategically placed at maximum proximity to the longwall face, main-

taining a distance of not less than 50 meters from the face junction with an air drift. The length of the supply cable (CL) extending from the frequency converter to the conveyor’s remote motors is determined by the longwall face length, which typically ranges from 400 to 600 meters.

Fig. 1 depicts the equivalent substitution diagram of the MPDS designed to power a scraper conveyor.

In the section with the industrial-frequency voltage, the active resistance of the system insulation relative to the ground is assumed to be $R_I \geq 300 \text{ k}\Omega/\text{phase}$, and the capacitance is $C_I \approx 0$. Considering the substantial length of the MPDS section with variable frequency, the active insulation resistance R_{IA}, R_{IB}, R_{IC} is accepted within the range from 31.5 to 300 $\text{k}\Omega/\text{phase}$, and the capacitance C_{IA}, C_{IB}, C_{IC} is taken from 0.01 to 1 $\mu\text{F}/\text{phase}$. A single-phase leakage circuit was simulated with an active resistance $R_y = 1 \text{ k}\Omega$, equivalent to the resistance of a human body. The parameters of the RCD, including the connection to the power distribution system filter (R_{FI}, L_{FI}), the metering circuit (R_0, R_{PN}, L_{PN}) with the operational rectified current source e_{\rightarrow} , and the parameters of the capacitive leakage current compensator (connection filter R_0 , compensator R_g, L_g , shunting capacitance C_{sh}), were determined based on AZUR characteristics [14].

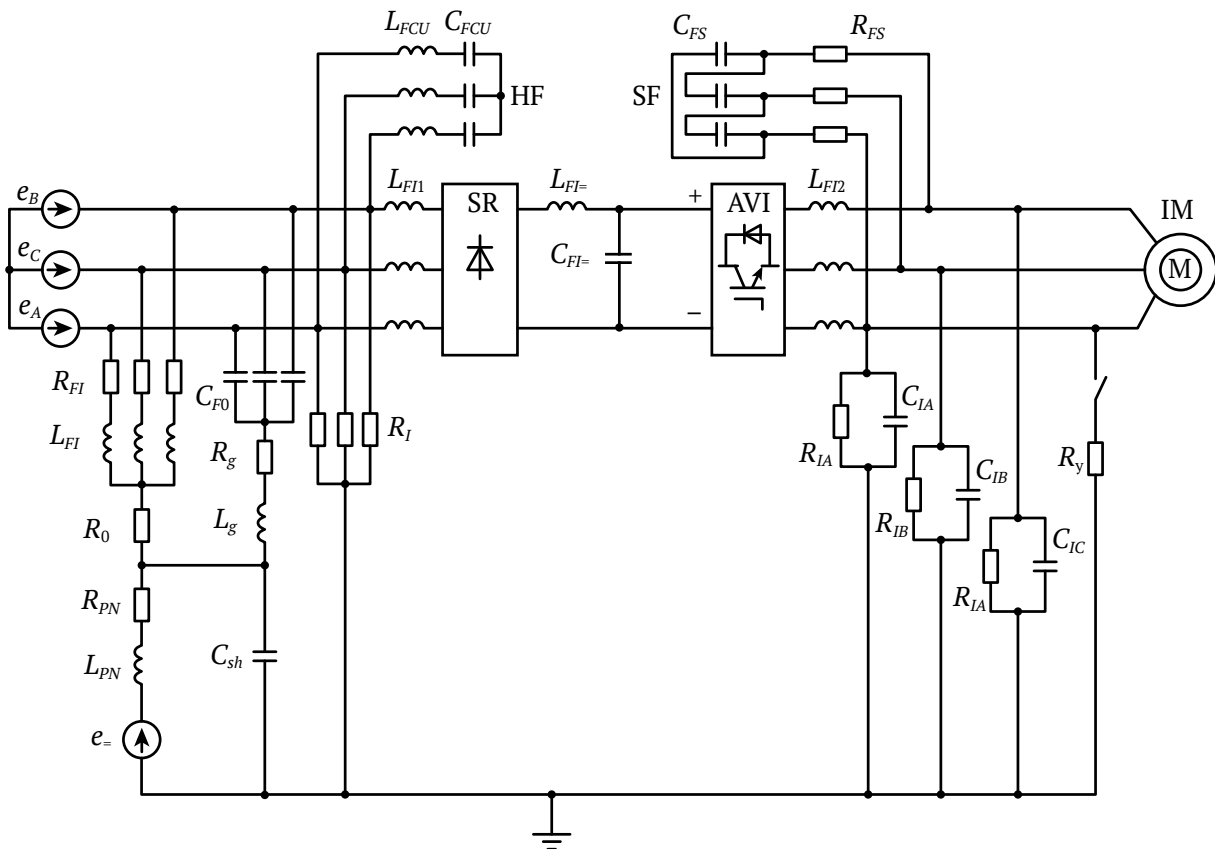


Fig. 1. Equivalent substitution diagram for the MPDS

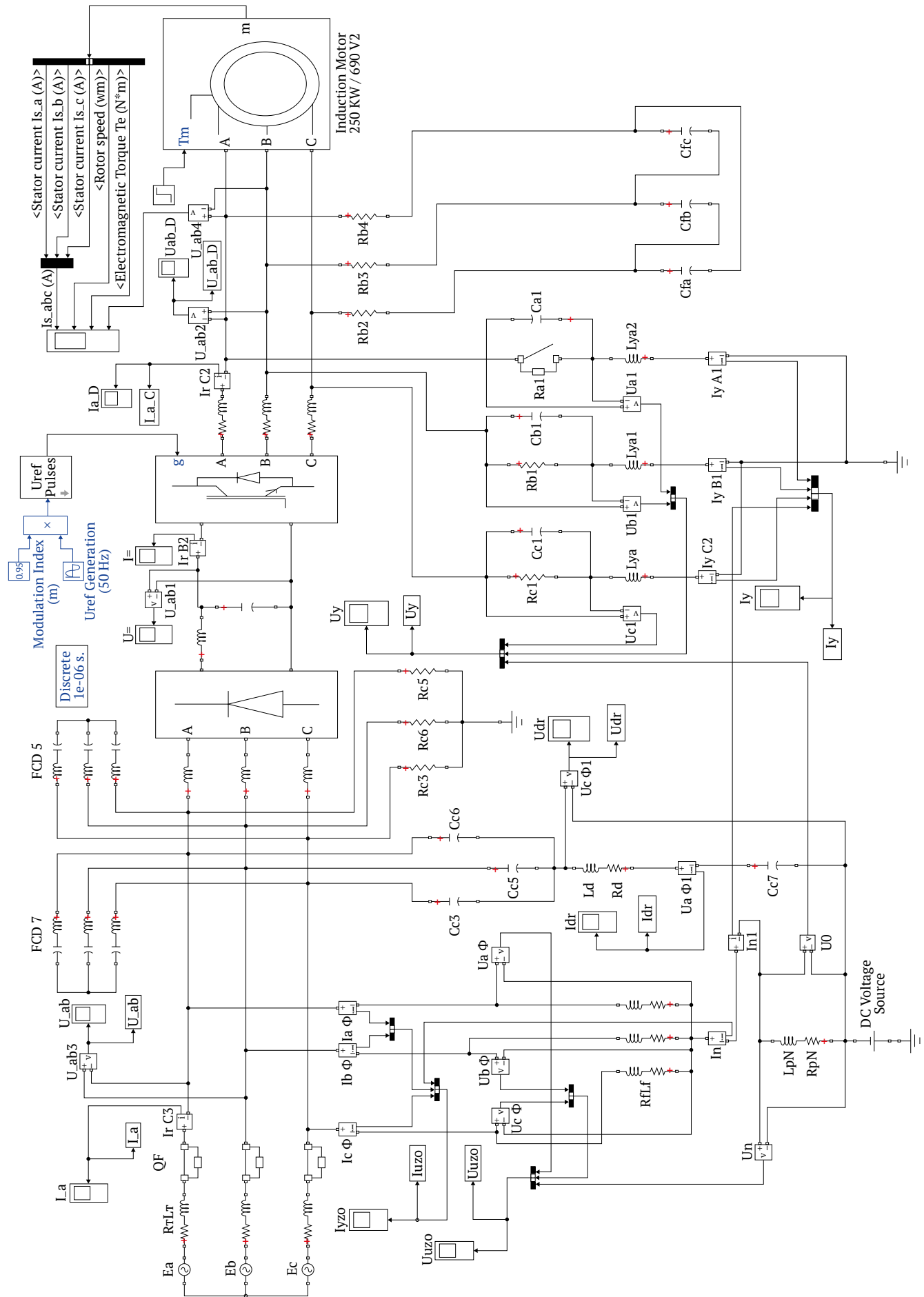


Fig. 2. Simulation model for the MPDS



The drive motors for the scraper conveyor consist of two to four induction motors of SG3-450L-8/4 type, ranging in power from 110 to 400 kW. In the equivalent diagram, an electric motor with a power of 250 kW is assumed in accordance with equivalence rules [15, 16], and its parameters have been calculated following practical recommendations [17]. A frequency converter from WANTAI is used as an equivalent power source for the drive motor. The parameters of throttles L_{FI1} , filter-compensating devices L_{FCU} , C_{FCU} , and sine filters L_{FI2} , L_{FS} , R_{FS} were determined based on Practical tips for selecting output filters³. The PD-SIN-0.5-300 sine filter was used as a prototype.

Fig. 2 illustrates the simulation model of the MPDS with a phase voltage $U_F = 660$ V. This model is equipped with an RCD featuring an R-L filter, a capacitive leakage current compensator, HFs, reactors, and a sine filter. Additionally, it incorporates insulation parameters at both the industrial and regulated frequency sections.

Table 1 provides a summary of the harmonic coefficients of voltage and current components in the power circuit of the MPDS at sections upstream and downstream of the FC.

The analysis of the spectral composition of the voltage and current higher harmonic components in the power circuit of the MPDS revealed the following.

The level of HHC, without considering the parameters of the external power distribution system (from the power source to the PUPP transformer), remains within permissible values according to GOST⁴. The 5th and 7th harmonic components of voltage emerge as the most significant.

Introducing reactors and HFs at the section upstream of the frequency converter, tuned to the 5th and 7th harmonics, proves effective in reducing the total coefficient of harmonic components of voltage $K_U\%$ from 2.81 to 0.51%. The most substantial impact is observed in a significant reduction of the total coefficient of current harmonic components $K_I\%$ from 80.45 to 5.63%. Simultaneously, the HHC indicators of current and voltage at the section downstream of the frequency converter remain practically unchanged ($K_U\% \approx 1,36\%$, $K_I\% \approx 0,3\%$).

³ Practical tips for selecting output filters. URL: <https://drives.ru/stati/prakticheskie-aspekty-po-vyboru-vyhodnyh-filtrov/>

PROMPOWER throttles and sine filters. Technical catalog. URL: https://prompower.ru/docs/inverter-accessories/Chokes_Sinewave-Filters.pdf

⁴ GOST 32144-2013. Quality standard of electric power in power supply systems of general purpose. Moscow: Standartinform, 2014. 39 p.

Table 1

Total coefficients of harmonic components in voltage and current

MPDS structure	Upstream of FC with AVI		Downstream of FC with AVI	
	$K_U\%$	$K_I\%$	$K_U\%$	$K_I\%$
Without compensation means	2.81/2.77	80.45/80.89	2.81/1.35	0.29/0.28
Reactors	2.20/2.19	64.67/65.49	1.39/1.39	0.30/0.29
Reactors, SF	5.68/5.67	26.25/26.26	1.77/1.77	0.25/0.26
Reactors, HF-5	1.31/1.25	21.00/19.30	1.36/1.36	0.30/0.26
Reactors, HF-5, HF-7	0.51/0.31	5.63/3.46	1.35/1.35	0.29/0.28
Reactors, HF-5, HF-7, SF	0.40/0.37	1.89/1.08	1.69/1.69	0.25/0.26

Note. Mode of insulation leakage current (symmetrical, single-phase).

The inclusion of a sine filter downstream of the frequency converter (in the absence of a HF in the diagram) results to an increase of $K_U\%$ up to 5.68 %. This elevation could be attributed to potential factors such as inaccuracies in selecting the sine filter and adjusting reactor parameters or the introduction of HHC to the external power system through circuits of current leakage in insulation. Conversely, using only a sine filter as a compensator enables a fourfold reduction in the total coefficient of harmonic current components compared to the maximum distortion level (in the absence of a HF).

The combined application of reactors, HFs and SFs allows for achieving the maximum level of compensation for voltage and current HHC. However, the rationale for their use, considering the initially low values of the total coefficient of harmonic components, should be justified by the technical necessity to ensure the quality of electric energy at the section downstream of the frequency converter.

An additional noteworthy finding from the study is that the level of HHC and their harmonic composition is practically unaffected by the mode of current leakage through insulation (symmetrical/single-phase leakage). This is attributed to the substantial difference in magnitude (3–4 orders of magnitude) between the power distribution system parameters and the insulation parameters of the current leakage circuit (secondary circuits).

Fig. 3 presents characteristic oscillograms and spectrograms of current and voltage in the circuits of leakage through insulation at the FC-IM section. This is observed in the presence of reactors and HFs tuned to the 5th and 7th harmonics within the power distribution system.

The harmonic composition of current and voltage in the phase insulation of the power distribution system at the FC-IM section, with reactors, HF-5, HF-7 activated at the TR-FC section, is presented in Table 2.

It is important to note that the coefficients of the n -th harmonic component of voltage $K_{U(n)}$ and the total coefficient of harmonic components of voltage K_U , induced in insulation leakage current circuits, in

the RCD filter branches, and capacitive leakage current compensator, are not addressed by GOST⁵. This is because GOST refers to the quality standard indicators of electric energy in general-purpose power supply systems.

⁵ GOST 32144–2013. Quality standard of electric power in power supply systems of general purpose. Moscow: Standartinform, 2014. 39 p.

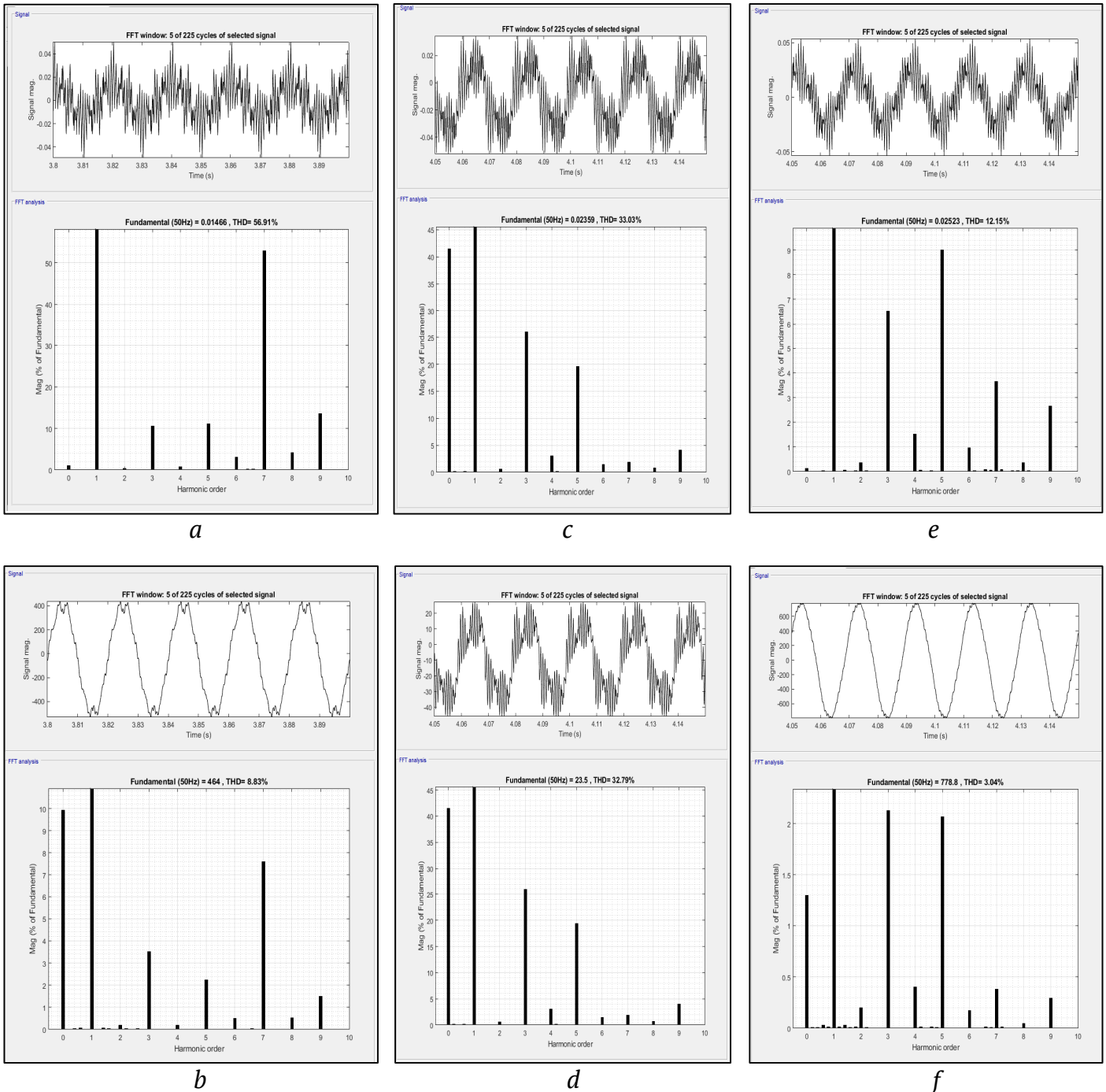


Fig. 3. Oscillograms and spectrograms of current and voltage in insulation leakage circuits with HF at FC-IM section: symmetrical mode – leakage current (a), voltage (b); single-phase leakage mode – current in the damaged phase (c), voltage in the damaged phase (d), current in the undamaged phase (e), voltage in the undamaged phase (f)



Table 2

Harmonic composition of current and voltage in phase insulation

Harmonic number	Leakage mode $I_y^{(3)}$		Leakage mode $I_y^{(1)}$	
	$K_{I(n)}\%$	$K_{U(n)}\%$	$K_{I(n)}\%$	$K_{U(n)}\%$
0	1.05	9.92	41.43	41.45
2	0.4	0.2	0.57	0.57
3	10.5	3.52	25.95	25.85
4	0.75	0.19	3.07	3.05
5	11.1	2.23	19.6	19.4
6	3.02	0.51	1.45	1.43
7	52.58	7.59	1.95	1.87
8	4.16	0.52	0.76	0.74
9	13.49	1.51	4.12	3.96
Total	56.91	8.83	33.03	32.79

The analysis of the harmonic composition revealed that in the symmetrical mode, the 3rd, 5th, 7th, and 9th current harmonics, along with the 0th, 3rd, 5th, 7th, and 9th voltage harmonics, have the highest value. The 7th current harmonic and the 0th and 7th voltage harmonics exhibit the greatest distortion. In the single-phase current leakage mode with an active resistance $R_y = 1 \text{ k}\Omega$, the 0th, 3rd, and 5th current harmonics, as well as the 0th, 3rd, and 5th voltage harmonics, are most pronounced. The 0th and 7th current harmonics, along with the 0th and 3rd voltage harmonics, show the highest distortion.

The presence of the zero-harmonic component of voltage and current is explained by the existence of a rectified current source in the RCD metering device circuit, facilitating the control of insulation resistance in symmetrical leakage modes. Additionally, the flow of zero-sequence current in the single-phase leakage mode, with a spectral composition determined by the modulated voltage signal at the converter output, contributes to this phenomenon.

The study revealed that current leakage through a person induces a broad spectrum of harmonic components, impacting the individual. The 3rd, 5th, 6th, 7th, and 9th harmonics emerge as the most significant. Notably, the coefficient $K_{IH(3)}$ is considerably higher compared to its value with respect to the first harmonic. Such an extensive spectrum may have adverse effects on the human body. For instance, there is an increased likelihood of fibrillation if the peak of current harmonics coincides with the *P*- and *T*-periods of the cardiac cycle.

Fig. 4 presents characteristic oscillograms and spectrograms of zero-sequence current and voltage

in RCD metering circuits in both symmetrical and single-phase leakage modes.

The analysis has revealed a prominent third harmonic in both voltage and current within the metering circuits, connection filter branches, and the RCD capacitive current compensator. Specifically, in the symmetrical leakage mode, the values of $K_{U(3)}$ and $K_{I(3)}$ for the constant component of the third harmonic are significantly compared to those of the first harmonic. In the single-phase leakage mode, the presence of zero-sequence current in the RCD metering circuit results in an increase in $K_{U(0)}$ by up to 25%, $K_{U(3)}$ by up to 16%, and $K_{I(3)}$ by up to 8.5%. To mitigate the impact of the third harmonic component in the leakage current within the metering circuit diagram, a filter was chosen. Its application proved effective in enhancing the performance and efficiency of commercially available RCDs.

Conclusions and recommendations

1. The incorporation of HF, reactors, and SFs has a positive impact on the quality of electric energy supplied to the electric motor through the frequency converter. This approach can be considered for practical implementation, provided that it adheres to the requirements for explosion-proof electrical equipment in mines. A crucial condition is ensuring temperature control within the HF and sine filter housings, maximizing heat dissipation from live parts and insulation.

2. The decision to install a HF directly on the low-voltage supply section of a scraper conveyor should be technically justified. This assessment should consider the need to achieve high electric power quality and economically justify the measure.

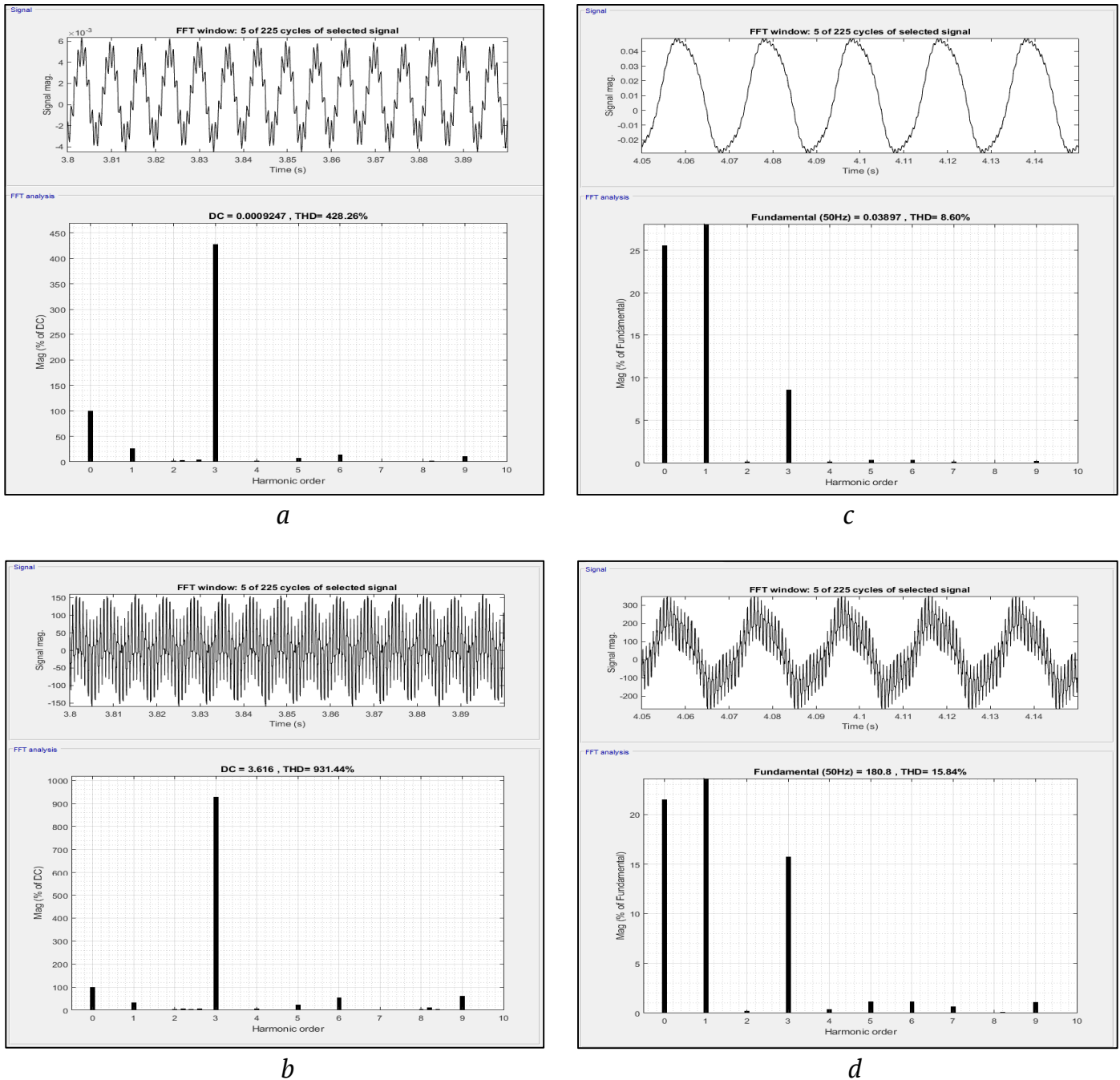


Fig. 4. Oscillograms and spectrograms of current in metering and zero-sequence voltage circuits: symmetrical mode – current (a), voltage (b); single-phase leakage mode – current (c), voltage (d)

It is essential to account for the fact that HF and SFs in explosion-proof version for voltage class up to 1140 V are not manufactured. Additionally, there are limitations on mass and dimensional parameters, along with a requirement for forced ventilation of structural components.

3. The presence of a HF, reactors, and sine filters has minimal impact on either the harmonic composition or the magnitude of coefficients of the harmonic components in the phase voltage of the system relative to the ground and insulation leakage currents.

However, additional filtering of higher harmonic components in the range of 1–1.5 kHz, utilized for forming the modulated AVI voltage, is necessary.

4. The existence of higher harmonic components induced in leakage current circuits in both symmetrical and single-phase leakage current modes can potentially disrupt magnetic compatibility during the operation of the electronic metering circuit, power supply unit, and the RCD capacitive leakage current compensator. This poses a potential hazard in case of contact with live parts of electrical equipment.



References

1. Shi J.G., Mao J., Wei X.H. Research on dynamic tension control theory for heavy scraper conveyor. *Applied Mechanics and Materials*. 2010;34–35:1956–1960. <https://doi.org/10.4028/www.scientific.net/AMM.34-35.1956>
2. Stecula K., Brodny J., Tutak M. Informatics platform as a tool supporting research regarding the effectiveness of the mining machines' work. In: *CBU International Conference on Innovations in Science and Education*. 2017;5:1215–1219. <https://doi.org/10.12955/cbup.v5.1099>
3. Voronin V.A., Nepsha F.S., Ermakov A.N., Kantovich L.I. Analysis of electrical equipment operating modes of the excavation site of a modern coal mine. *Sustainable Development of Mountain Territories*. 2021;(4):599–607. (In Russ.) <https://doi.org/10.21177/1998-4502-2021-13-4-599-607>
4. Klyuev R.V., Bosikov I.I., Gavrina O.A., Lyashenko V.I. Assessment of operational reliability of power supply to developing ore mining areas at a high-altitude mine. *Mining Science and Technology (Russia)*. 2021;6(3):211–220. (In Russ.) <https://doi.org/10.17073/2500-0632-2021-3-211-220>
5. Babokin G.I. Influence of process flow diagram and longwall length on specific energy consumption of shearers. *Mining Informational and Analytical Bulletin*. 2021;(2):139–149. (In Russ.) <https://doi.org/10.25018/0236-1493-2021-2-0-139-149>
6. Boykov I.L., Shestakov V.V., Zaklika M., Ulrich N. Experience in introducing frequency converters to drive face conveyors of the Vorgashorskaya mine. *Gluckauf*. 2010;(1):79–83. (In Russ.)
7. Shevyrev Y.V., Pichuev A.V., Shevyreva N.Y. Improving energy performance in networks with semiconductor converters. In: *2019 International Conference on Industrial Engineering, Applications and Manufacturing, ICIEAM 2019*. Sochi, March 25–29, 2019. Pp. 1–6. <https://doi.org/10.1109/ICIEAM.2019.8743020>
8. Feng D., Lu M., Lan J., Sun L. Research on switching operation transient electromagnetic environment of substations in a coal mine. *IET Generation, Transmission & Distribution*. 2016;10(13):3322–3329. <https://doi.org/10.1049/iet-gtd.2016.0292>
9. Babokin G.I., Shevyrev Yu.V., Shevyreva N.Yu. Power quality in coal longwalls. *Gornyi Zhurnal*. 2021;(7):80–85. (In Russ.) <https://doi.org/10.17580/gzh.2021.07.14>
10. Pustovetov M. Yu. Experience in developing sine-wave filter for power circuit of VVVF-drive with induction motor. *Bulletin of the Tomsk Polytechnic University*. 2014;324(4):84–94. (In Russ.) URL: <http://earchive.tpu.ru/handle/11683/5238>
11. Pichuev A.V., Petrov V.L. Equivalent circuit for mine power distribution systems for the analysis of insulation leakage current. *Mining Science and Technology (Russia)*. 2023;8(1):78–86. <https://doi.org/10.17073/2500-0632-2023-01-72>
12. Babokin G.I., Kunitsky V.G., Shelenev P.I. Protective switching-off on a direct operating current for combined mine networks. *Mining Informational and Analytical Bulletin*. 2009;(S8):285–288. (In Russ.)
13. Shchutsky V.I., Babokin G.I., Lazarev A.I. Experimental study of the operating conditions of protective shutdown devices in a network with a frequency converter. *Elektrobezopasnost'*. 1996;(3–4):31–41. (In Russ.)
14. Pichuev A.V., Petrov V.L. Equivalent circuit for mine power distribution systems for the analysis of insulation leakage current. *Mining Science and Technology (Russia)*. 2023;8(1):78–86. <https://doi.org/10.17073/2500-0632-2023-01-72>
15. Syromyatnikov I.A. *Operating modes of asynchronous and synchronous motors*. Mamikonyants L.G. (Ed.) 4th ed., revised and additional. Moscow: Energoatomizdat; 1984. 240 p. (In Russ.)
16. Pichuev A.V. Information and analytical system for analyzing the reliability and safety of electrical installations at mining enterprises. *Mining Informational and Analytical Bulletin*. 2011;(3):355–359. (In Russ.)
17. Kopylov I.P. *Mathematical modeling of electrical machines*. Moscow: Vysshaya Shkola; 2001. 218 p. (In Russ.)

Information about the authors

Vadim L. Petrov – Dr. Sci. (Eng.), Vice-Rector, Professor of the Department of Energy and Energy Efficiency of Industrial Enterprises, University of Science and Technology MISIS, Moscow, Russian Federation; ORCID [0000-0002-6474-5349](https://orcid.org/0000-0002-6474-5349), Scopus ID [8919065900](https://orcid.org/8919065900); e-mail petrovv@misis.ru

Alexandr V. Pichuev – Cand. Sci. (Eng.), Associate Professor of the Department of Energy and Energy Efficiency of Mining Industry, University of Science and Technology MISIS, Moscow, Russian Federation; ORCID [0000-0001-7457-5702](https://orcid.org/0000-0001-7457-5702), Scopus ID [57209798580](https://orcid.org/57209798580); e-mail allexstone@mail.ru

Received 05.01.2024

Revised 27.01.2024

Accepted 18.02.2024